

Online Measurement of Three-phase AC Power System Impedance in Synchronous Coordinates

Zhiyu Shen

Dissertation submitted to the faculty of the Virginia Polytechnic Institute
and State University in partial fulfillment of the requirements
for the degree of

Doctor of Philosophy
In
Electrical Engineering

Dushan Boroyevich

Douglas K. Lindner

Guo-Quan Lu

John J. Lesko

Paolo Mattavelli

January 23, 2012

Blacksburg, Virginia

Keywords: three-phase AC power system, impedance measurement,
synchronous coordinates, system stability

Online Measurement of Three-phase AC Power System Impedance in Synchronous Coordinates

Zhiyu Shen

Abstract

Over the last two decades there has been an increased use of three-phase AC power systems that may not be connected to the main power grid, such as the power systems on more-electric airplane and all-electric ships. Power-electronic converters are usually a significant part of these systems, which provide excellent performance. But their negative incremental impedance nature increases the possibility of system instability.

A small-signal analysis that uses interface impedances defined in the synchronous frame is developed by Belkhat at Purdue in the mid-90s to assess the system stability. The system impedance varies with the operating point. Thus the impedance has to be obtained online at the desired operating point, on even in situ.

Literature investigates its use with system models, but the lack of equipment to measure such impedance prevents its use in practical systems. Measurement of impedances of each component enables the prediction of system stability before building the real system. The impedance data can also be used to investigate the instability in the system after it is built. The capability of impedance measurement can save the cost and time of system integrators.

After reviewing the state-of-the-art development of impedance measurement systems, the dissertation analyzes several systematic error sources in the system, which includes the signal processing and sampling circuits, the phase estimation for coordinate transformation and the injection device connection, and proposes the solution to reduce their influence.

Improved algorithm and system architecture are proposed to increase the measurement speed and accuracy. Chirp signal is used as an excitation signal to extract impedances at a group of frequencies at one time. The use of both shunt current injection and series voltage injection improves the SNR of measured signal. Oversampling, cross-correlation and frequency domain averaging technique are used to further reduce the influence of noise.

An instrument is built based on the proposed solution. A voltage source inverter is used to generate the perturbation. A PXI computer is used for real-time signal processing. A PC is used for data post processing and measurement process control. Software is developed to fully automate the measurement. The designed unit is tested with various linear and nonlinear load. The test result shows the validity of the proposed solution.

To My Family
My Parents: Chengli Shen and Manfei Jiang
My Wife: Shuwen Duan

Acknowledgement

I am very happy to have a great opportunity to express my gratitude to all the people that helped, influenced and supported my work.

I would like to express my sincere gratitude to my advisor, Dr. Dushan Boroyevich, for his support, guidance and encouragement during my study at the Center for Power Electronics Systems (CPES) - Virginia Tech. His profound knowledge, gentle personality and rigorous attitude toward research will benefit my career as well as my whole personal life.

It is an honor for me to have Dr. Paolo Mattavelli, Dr. Douglas Lindner, Dr. G. Q. Lu and Dr. Jack Lesko as my committee members. I am very thankful to them for all the technical discussions, opinions and suggestions. Thanks to Dr. Rolando Burgos, Dr. Fred Wang, and Dr. Khai Ngo for the technical discussions and valuable suggestions.

I also express my thanks to everyone in the Center for Power Electronics (CPES) who helped me achieve my goal. Thanks to Ms. Marianne Hawthorne, Ms. Teresa Shaw, Ms. Trish Rose, Ms. Linda Long, Ms. Linda Gallagher, Mr. Douglas Sterk, and Mr. David Gilham.

Thanks and appreciation are given to my team members on the Boeing and NNS projects Dr. Jerry Francis, Mr. Bo Wen, Mr. Marko Jaksic, Mr. Igor Cvetkovic, Mr. Bo Zhou, Mr. Justin Walraven, Dr. Dong Dong, and Ms. Sara Ahmed.

I am very grateful to all my colleagues in CPES for their help, mentorship, and friendship. I cherish the wonderful time that we worked together. Many thanks to Dr. Rixin Lai, Dr. Di Zhang, Dr. Puqi Ning, Dr. Dong Jiang, Mr. Daocheng Huang, Mr. Zheng Chen, Dr. Fang Luo, Dr. Jin Li, Dr. Ruxi Wang, Mr. Xuning Zhang, Mr. Jing Xue, Mr. Wei Zhang, Mr. Jiang Li, Mr. Milisav Danilovic, and Mr. Hemant Bishno, Dr. Qiang Li, Dr. Xiao Cao, Dr. David Reusch, Dr. Jian Li, Mr. Zijian Wang, Mr. Pengjie Lai, Mr. Qian Li, Mr. Feng Yu, Mr. Haoran Wu, Mr. Mingkai Mu, Mr. Weiyi Feng, Mr. Yang Jiao, Mr. Shuilin Tian, Ms. Ying Lu, Mr. Chanwit Prasantanakorn, Mr. Zheyuan Tan, Mr. Yingyi Yan Mr. Shu Ji, Mr. Yipeng Su, Mr. Zhemin Zhang, Mr. Bo Zhou, and Mr. Lingxiao Xue

Last but most importantly, I would also like to thank my family for their never-ending support, love, and encouragement that helped me complete this work.

TABLE OF CONTENTS

Chapter 1.	Introduction	1
1.1.	Background	1
1.1.1.	AC Power Electronics Systems	1
1.1.2.	System Stability Analysis in Three-phase AC Power Systems	3
1.2.	Dissertation Motivation and Objective	7
1.2.1.	Challenges in Impedance Extraction in Three-phase AC Systems	7
1.2.2.	Objective.....	11
1.3.	Dissertation Layout	12
Chapter 2.	Impedance Extraction in Three-phase AC Systems	13
2.1.	Impedance Definition in Three-phase Systems.....	13
2.1.1.	Sequence Components in abc Frame and Dq Frame	13
2.1.2.	Impedance Defined per Phase	16
2.1.3.	Impedance Defined Using Sequence Component in abc Frame.....	18
2.1.4.	Impedance Defined in Dq Frame.....	19
2.1.5.	Impedance Selection for Stability Analysis.....	20
2.2.	Impedance Measurement Procedure and Measurement System Architecture	22
2.3.	Perturbation Signal Waveform.....	25
2.3.1.	Periodical Waveforms	25
2.3.2.	Aperiodical Waveforms.....	27
2.4.	Perturbation Generation Method.....	31
2.4.1.	Perturbation Generation Device Connection to System	31
2.4.2.	Perturbation Generation Device	32
2.5.	Impedance Extraction Algorithm	35
2.5.1.	Nonparametric Algorithms	36
2.5.2.	Parametric Algorithms.....	37

Chapter 3.	Measurement Error Analysis	39
3.1.	Error Propagation Path	39
3.2.	Transfer Functions in Abc Frame.....	41
3.3.	Coordinate Transformation	44
3.4.	Perturbation Injection Mode.....	58
3.5.	System Drift during Measurement	61
3.6.	Application to Series Injection	63
3.7.	Conclusion.....	64
Chapter 4.	Improvement Based on Previous System Architecture	66
4.1.	Injection Device Connection	66
4.2.	Measurement Sequence Adjustment	68
4.3.	Other Performance Tuning.....	69
4.4.	Construction of Improved Design	71
4.5.	Experiment Results	73
4.5.1.	Passive Impedance Measurement Result.....	74
4.5.2.	Voltage Source Inverter (VSI) Impedance Measurement Result	75
4.6.	Conclusion.....	76
Chapter 5.	Improved Algorithmic Solution and System Architecture	77
5.1.	Proposed Algorithm	77
5.1.1.	Injection Waveform.....	77
5.1.2.	Impedance Extraction Algorithm	81
5.1.3.	Simulation of Proposed Approach.....	84
5.2.	Measurement System Architecture Design	86
5.2.1.	Measurement System Requirement	86
5.2.2.	Measurement System Partitioning.....	86
5.2.3.	Perturbation Injection Unit	87
5.2.4.	Sensor Selection	91

5.2.5. Signal Interface Unit.....	91
5.2.6. Data Conversion Unit	93
5.2.7. Data Processing Unit	94
5.2.8. Measurement Control Unit	94
5.2.9. Human Interface Unit	95
5.2.10. System Architecture Summary	95
5.3. System Scalability	97
5.3.1. Scaling Up of Perturbation Injection Unit.....	98
5.4. Experimental Results.....	101
5.4.1. Passive Impedance Measurement Result.....	101
5.4.2. Commercial Power Supply Impedance Measurement Result	104
5.4.3. Diode Rectifier Impedance Measurement Results	106
5.5. Conclusion.....	109
Chapter 6. Conclusion and Future Work.....	110
6.1. Summary	110
6.2. Conclusions	111
6.3. Future Work and Improvements	111
6.3.1. High Power High Bandwidth Injection Device Design.....	111
6.3.2. Error Analysis.....	111
References	113
Appendix A. Design and Implementation of the Measurement Equipment	123
A.1. Perturbation Injection Unit.....	123
A.1.1. Power Stage Design	123
A.1.2. Control Loop Design	126
A.1.3. Hardware Characteristics	127
A.2. Signal Interface Unit	128
A.2.1. Analog Input	129

A.2.2. Analog Output	136
A.2.3. Digital Output	138
A.2.4. Digital Input	139
A.2.5. Unit Assembly	140
A.3. Data Conversion Unit	142
A.3.1. Hardware Selection	142
A.3.2. Software Design	145
A.4. Software on Host Computer	154
A.4.1. Introduction of HMI	156
A.4.2. Software Design of Measurement Control	157
A.4.3. Software Design of Data Post Processing	165
A.5. System Assembly	168
A.6. Additional Reference	168

LIST OF FIGURES

FIGURE 1-1: SYSTEM IN ABC COORDINATES	4
FIGURE 1-3: SYSTEM IN DQ COORDINATES.....	6
FIGURE 2-1: EXCITATION AND RESPONSE SEQUENCE COMPONENTS IN BALANCED, SYMMETRIC, LINEAR SYSTEMS	17
FIGURE 2-2: EXCITATION AND RESPONSE SEQUENCE COMPONENTS IN BALANCED, ASYMMETRIC, LINEAR SYSTEMS	18
FIGURE 2-3: EXCITATION AND RESPONSE SEQUENCE COMPONENTS IN BALANCED, SYMMETRIC, QUADRATIC NONLINEAR SYSTEMS	20
FIGURE 2-4: EXCITATION AND RESPONSE SEQUENCE COMPONENTS IN UNBALANCED, ASYMMETRIC, QUADRATIC NONLINEAR SYSTEMS.....	21
FIGURE 2-5: MEASUREMENT SETUP IN [83], USED UNDER FAIR USE, 2013	23
FIGURE 2-6: MEASUREMENT SYSTEM ARCHITECTURE GIVEN IN [93], USED UNDER FAIR USE, 2013	24
FIGURE 2-7: EXAMPLE OF 100HZ SINUSOIDAL WAVEFORM	26
FIGURE 2-8: EXAMPLE OF 100HZ SINUSOIDAL WAVEFORM TRANSFERRED INTO 60HZ ABC FRAME (PHASE A SIGNAL)	26
FIGURE 2-9: EXAMPLE OF 100 HZ SQUARE WAVEFORM.....	27
FIGURE 2-10: EXAMPLE OF 100HZ SQUARE WAVEFORM TRANSFERRED INTO 60HZ ABC FRAME (PHASE A SIGNAL)	27
FIGURE 2-11: EXAMPLE OF A STEP WAVEFORM AT 0.05 s	29
FIGURE 2-12: EXAMPLE OF A STEP WAVEFORM AT 0.05 S TRANSFERRED INTO 60HZ ABC FRAME (PHASE A SIGNAL).....	29
FIGURE 2-13: EXAMPLE OF A WHITE NOISE WAVEFORM	30
FIGURE 2-14: INJECTION CONNECTIONS.....	32
FIGURE 2-15: SHUNT INJECTION USING POWER CONVERTER	33
FIGURE 2-16: SHUNT INJECTION USING CHOPPED IMPEDANCES	34
FIGURE 3-1: PREVIOUS IMPEDANCE MEASUREMENT ANALYZER IN CPES	40
FIGURE 3-2: IMPEDANCE MEASUREMENT SYSTEM WHEN SHUNT INJECTION IS USED	41
FIGURE 3-3: IMPEDANCE MEASUREMENT SETUP IN THREE-PHASE SYSTEMS	45
FIGURE 3-4: TYPICAL D-Q PHASE LOCKED LOOP	46
FIGURE 3-5: SIMULATION CIRCUIT OF LINEAR IMPEDANCE EXTRACTION	51
FIGURE 3-6: EXTRACTED RL IMPEDANCES IN SIMULATION (SOLID LINE: NO PLL; DOTTED LINE: 50 Hz BANDWIDTH; 'X' MARKERS: RESULT BACK CALCULATED FROM 50 Hz RESULT)	52
FIGURE 3-7: EXTRACTED DIODE-RECTIFIER IMPEDANCES (SOLID LINE: NO PLL; DOTTED LINE: 50 Hz BANDWIDTH; 'X' MARKERS: RESULT BACK CALCULATED FROM 50 Hz RESULT)	53
FIGURE 3-8: SIMULATION CIRCUIT OF DIODE RECTIFIER IMPEDANCE EXTRACTION.....	53
FIGURE 3-9: MEASURED RL IMPEDANCES (SOLID LINE: 1Hz PLL; 'X' MARKERS: 50 Hz PLL; 'O' MARKERS: RESULT BACK CALCULATED FROM 50 Hz RESULT)	54
FIGURE 3-10: PERTURBATION INJECTION UNIT BLOCK DIAGRAM WHEN CONTROLLER IS IN ABC FRAME.....	55
FIGURE 3-11: PERTURBATION INJECTION UNIT BLOCK DIAGRAM WHEN CONTROLLER IS IN DQ FRAME.....	56
FIGURE 3-12: SIMULATED PERTURBATION INJECTION CIRCUIT	57
FIGURE 3-13: SIMULATED INJECTION-CIRCUIT TRANSFER FUNCTIONS (SOLID LINE: NO PLL; 'X' MARKERS: 50 Hz BANDWIDTH).....	58
FIGURE 3-14: DIAGRAM OF SHUN INJECTION IN DQ FRAME.....	59
FIGURE 3-15: DIAGRAM OF SERIES INJECTION IN DQ FRAME.....	60
FIGURE 3-16: IMPEDANCE MEASUREMENT SYSTEM WHEN SERIES INJECTION IS USED	64

FIGURE 4-1: INJECTION REFERENCE TO INJECTION CURRENT FOR PHASE A	66
FIGURE 4-2: PERTURBATION INJECTION DEVICES CONNECTION IN PREVIOUS DESIGN	67
FIGURE 4-3: UPDATED PERTURBATION INJECTION DEVICES CONNECTION	68
FIGURE 4-4: DIAGRAM OF OUTPUT STAGE	70
FIGURE 4-5: COMPARISON OF DAC OUTPUT NOISE (ZERO VOLT ADC INPUT COPIED TO DAC OUTPUT).....	70
FIGURE 4-6: FLOW CHART TO IMPROVE NETWORK ANALYZER MEASUREMENT CONSISTENCE	71
FIGURE 4-7: FRONT AND REAR SIDE VIEW OF THE IMPEDANCE ANALYZER	72
FIGURE 4-8: INSIDE VIEW OF CABINET — AMPLIFIER, SENSING AND REAL-CONTROLLER SIGNAL PROCESSING PART	72
FIGURE 4-9: INSIDE VIEW OF CABINET — ZOOM IN TO SENSING AND REAL-CONTROLLER SIGNAL PROCESSING PART	73
FIGURE 4-10: INSIDE VIEW OF CABINET — ANALYZER AND ISOLATION TRANSFORMER PART	73
FIGURE 4-11: RESISTIVE-INDUCTIVE IMPEDANCES MEASUREMENT RESULT (GREEN CURVE) VS. SIMULATION RESULT (BLUE CURVE)	74
FIGURE 4-12: CIRCUIT DIAGRAM OF THE MEASURED VSI.....	75
FIGURE 4-13: VSI OUTPUT IMPEDANCE MEASUREMENT RESULT (GREEN CURVE) VS. SIMULATION RESULT (BLUE CURVE)	76
FIGURE 5-1: COMPARISON OF CHIRP SIGNAL AND WHITE NOISE	78
FIGURE 5-2. COMPARISON OF SIGNALS WAVEFORMS AND SNR.....	80
FIGURE 5-3: MODIFIED SMALL-SIGNAL BLOCK DIAGRAM	82
FIGURE 5-4: SIMULATION CIRCUIT	84
FIGURE 5-5: COMPARISON OF IMPEDANCES EXTRACTED BY DIFFERENT PROCEDURES (BLACK SOLID LINES: SIMULATION RESULT; RED CIRCLES: ANALYTICAL VALUES).....	85
FIGURE 5-6: IMPEDANCE MEASUREMENT SYSTEM.....	87
FIGURE 5-7: SHUNT INJECTION CIRCUIT USING VSI.....	88
FIGURE 5-8: SERIES INJECTION CIRCUIT USING VSI	90
FIGURE 5-9: SIGNAL CONDITIONING CIRCUIT BLOCK DIAGRAM	92
FIGURE 5-10: SYSTEM ARCHITECTURE DIAGRAM.....	96
FIGURE 5-11: SYSTEM SIGNAL FLOW DIAGRAM	97
FIGURE 5-12: TOPOLOGY FOR SHUNT INJECTION AT FULL VOLTAGE	99
FIGURE 5-13: TOPOLOGY FOR SERIES INJECTION AT FULL CURRENT	100
FIGURE 5-14: MEASUREMENT SETUP OF R LOAD.....	101
FIGURE 5-15: RESISTIVE LOAD IMPEDANCE MEASUREMENT RESULT USING DESIGN EQUIPMENT (BLUE CURVE) AND AGILENT EQUIPMENT (GREEN CURVE).....	102
FIGURE 5-16: MEASUREMENT SETUP OF RL LOAD	103
FIGURE 5-17: RESISTIVE AND INDUCTIVE LOAD IMPEDANCE MEASUREMENT RESULT USING DESIGN EQUIPMENT (BLUE CURVE) AND AGILENT EQUIPMENT (GREEN CURVE).....	104
FIGURE 5-18: IMPEDANCE MEASUREMENT OF THE COMMERCIAL POWER SUPPLY (BLUE CURVE: MEASURED WITH RESISTIVE LOAD; GREEN CURVE: MEASURED WITH RESISTIVE-INDUCTIVE LOAD)	105
FIGURE 5-19: DIODE BRIDGE MEASUREMENT SETUP.....	106
FIGURE 5-20: DIODE BRIDGE IMPEDANCE MEASUREMENT (BLUE CURVE) AND SIMULATION (GREEN DOTS) RESULT.....	107
FIGURE 5-21: MEASUREMENT SETUP OF TWELVE-PULSE DIODE RECTIFIER	108
FIGURE 5-22: 12-PULSE DIODE BRIDGE IMPEDANCE MEASUREMENT RESULT	108
FIGURE A-1: COMPLETE SHUNT INJECTION POWER STAGE	124
FIGURE A-2: SERIES INJECTION POWER STAGE	125

FIGURE A-3: PIU CONTROLLER BLOCK DIAGRAM.....	126
FIGURE A-4: D AND Q PERTURBATION CURRENT POWER SPECTRAL DENSITIES AS A RESULT OF A D AND Q PERTURBATION	127
FIGURE A-5: ACHIEVABLE PERTURBATION POWER AS A FUNCTION OF FREQUENCY.....	128
FIGURE A-6: SIGNAL INTERFACE UNIT BLOCK DIAGRAM	129
FIGURE A-7: INPUT STAGE CIRCUIT.....	130
FIGURE A-8: NOTCH FILTER STAGE CIRCUIT	132
FIGURE A-9: TRANSFER FUNCTION OF THE SIGNAL CONDITIONING CARD WITH 60 HZ NOTCH FILTER IN THE PATH	133
FIGURE A-10: ANTI-ALIASING FILTER STAGE CIRCUIT.....	134
FIGURE A-11: OUTPUT STAGE CIRCUIT	135
FIGURE A-12: PICTURE OF THE SIGNAL CONDITIONING CARD.....	136
FIGURE A-13: FUNCTION DIAGRAM OF ANALOG OUTPUT ISOLATION CARD.....	137
FIGURE A-14: PICTURE OF THE ANALOG OUTPUT ISOLATION CARD	137
FIGURE A-15: FUNCTION DIAGRAM OF ONE CHANNEL ON DIGITAL OUTPUT ISOLATION CARD	138
FIGURE A-16: PICTURE OF THE DIGITAL OUTPUT ISOLATION CARD	139
FIGURE A-17: FUNCTION DIAGRAM OF ONE CHANNEL ON DIGITAL INPUT ISOLATION CARD	139
FIGURE A-18: PICTURE OF THE DIGITAL OUTPUT ISOLATION CARD	140
FIGURE A-19: PICTURE OF THE ASSEMBLED SIGNAL INTERFACE UNIT	141
FIGURE A-20: PXI CHASSIS – PXIE-1082	142
FIGURE A-21: REAL TIME CONTROLLER – PXIE-8133.....	143
FIGURE A-22: DATA ACQUISITION CARD – PXIE-6368	144
FIGURE A-23: SOFTWARE FUNCTION BLOCK DIAGRAM OF THE DATA ACQUISITION UNIT.....	146
FIGURE A-24: FIFO DATA BLOCK.....	147
FIGURE A-25: FIFO CIRCULAR BUFFERS	147
FIGURE A-26: CONTROL COMMAND PACKET STRUCTURE.....	150
FIGURE A-27: DATA SERVER PACKET STRUCTURE	151
FIGURE A-28: FLOW CHART OF THE WATCHDOG SERVICE THREAD	153
FIGURE A-29: SOFTWARE ARCHITECTURE ON HOST COMPUTER	155
FIGURE A-30: INTERFACE OF THE MEASUREMENT CONTROL PROGRAM	156
FIGURE A-31: CONTROL MESSAGE STRUCTURE.....	157
FIGURE A-32: PROGRAM FLOW CHART DURING STARTUP	161
FIGURE A-33: PROGRAM FLOW CHART DURING ADVANCE MODE MEASUREMENT.....	163
FIGURE A-34: PROGRAM FLOW CHART DURING PERTURBATION INJECTION	164
FIGURE A-35: THE IMPEDANCE ANALYZER’S FRONT AND BACK VIEWS.....	168

LIST OF TABLES

TABLE 5-1 SIMULATION CIRCUIT PARAMETERS.....	84
TABLE A-1: PERFORMANCE AND HARDWARE SPECIFICATIONS	123
TABLE A-2: SHUNT INJECTION POWER STAGE SCHEMATIC COMPONENT VALUES	124
TABLE A-3: SERIES INJECTION TRANSFORMER SPECIFICATIONS	125

Chapter 1. Introduction

1.1. Background

Power electric technology has infiltrated the power processing and generation fields in contemporary electrical power systems. Power electric technology provides exceptional performance due to its closed-loop control. This means that the output of the power converters can be regulated according to the requirement of the load while the input can usually accommodate a variation of source conditions. It is shown in [1-3] that power electronics converters provide negative incremental impedance characteristics at their input while under regulated output control, which brings in the possibility of system instability.

Because the effect of these converters is small compared to the size of the system, the national power grid can tolerate the various behaviors of many of these converters. However many smaller systems cannot.

1.1.1. AC Power Electronics Systems

An AC power electronics system is defined as an AC power system where a significant portion of system power is processed by power electronic circuits and control [4]. A nearly infinite bus is no longer accessible in such systems. Some of the common AC power electronics systems are reviewed below to show their significant existence today.

A. Independent Power Systems

These systems have their own group of power sources and load, which are not connected to external networks. The power sources only have limited capacity, which is usually close to the total load.

One example of such system is the more-electric aircraft (MEA) power system. In a modern aircraft system, the power is generated by variable frequency generators instead of the traditional maintenance-intensive integrated drive generators, which produce constant 400 Hz AC power [5]. Electric power is used to operate many functions that are traditionally served by mechanical, pneumatic, or hydraulic to improve fuel efficiency and reduce the size and weight of related parts

[6]. A majority of these functions are implemented by electric motors, such as air conditioning, cabin pressure control, fuel pumping, and flight control actuation. All of the motors are controlled by a power-electronics-based motor drive [7]. Although not all of the load are power electronic converters, many of them use power-electronic-based rectifier to provide required power, such as communication, and in-flight entertainment systems [8]. To sum up, it is estimated that more than fifty percent of the electrical power is processed using a power electronic technique.

The power system in all-electric ships (AES) is similar to the MEA. In addition to all the auxiliary loads that are similar to the aircraft case, the propulsion is also powered by electric motors, which are controlled by power-electronic motor drives [9-12].

There are many other systems that fall into this class, such as electrical vehicles [13-15], and data centers or other facilities running on backup power (UPS or generators) etc.

B. Power Systems with Weak Grid Connections

Not all systems connected to the national grid can have a nearly infinite bus. The connection to the grid is sometimes capacity limited. Frequently, the connection is made through a power-electronic converter.

Renewable energy systems and distributed generation systems are examples of this kind. Power-electronic converters are used to interface the power sources with the grid [16, 17]. All the generated energy is processed by power electronics in these applications. With the penetration of distributed generations, nanogrid and microgrid are the trends in the future transmission and distribution system [18, 19]. They group some of the power source and load together then connect them through the energy control centers (ECC) hierarchically to a higher level group, which finally connects to the grid. Power-electronic converters are also highly involved in the internal control of such groups of sources and loads. Many benefits are achieved by this approach, such as decoupled system dynamics, better energy efficiency and power quality

[18, 19]. As the trends continue, the traditional national grid is transforming to a large scale AC power electronics system [20-22].

1.1.2. System Stability Analysis in Three-phase AC Power Systems

Electrical power systems of loads and sources, although stable individually, may become unstable when they are interconnected. The stability of such systems can be analyzed at multiple levels, ranging from power flow analysis to models of the semiconductor devices in the converters. Appropriate models are chosen based on the level of analysis to be performed [23]. Interface impedance is well accepted in the analysis of small-signal stability of interconnected power-electronic converters [24-29].

It has been shown that the small-signal stability of DC power systems can be determined by analyzing the output impedance of the source and the input impedance of the load using an impedance criterion such as the Middlebrook Criteria [1, 2] or other less conservative criteria [26-27]. This approach was essential in the formulation of criteria using the Nyquist stability theorem to study the dynamic interactions introduced by power-electronic converters, and specifically, by studying the loop-gain or return-ratio $Z_{source}(s) / Z_{load}(s)$ of the source and load impedances seen at the interface.

Due to the nonlinear nature of power electronic converters, the system interface impedance varies with the operating point. Thus, the impedance used for analysis has to be obtained online when the measurement target is running at the desired operating point. However, the target can be operated with different sources or loads that are not used in the final systems as long as the operating point is kept the same. In situ measurement in the final system can also be conducted to assess the stability margin. However, it does not require the impedances to be calculated out. The interface voltage or current ratio can be used instead [30]. Such ratio reflects the system return ratio.

A three-phase electrical system usually contains three conductors to deliver power. Figure 1-1 shows a diagram of a three-phase power system.

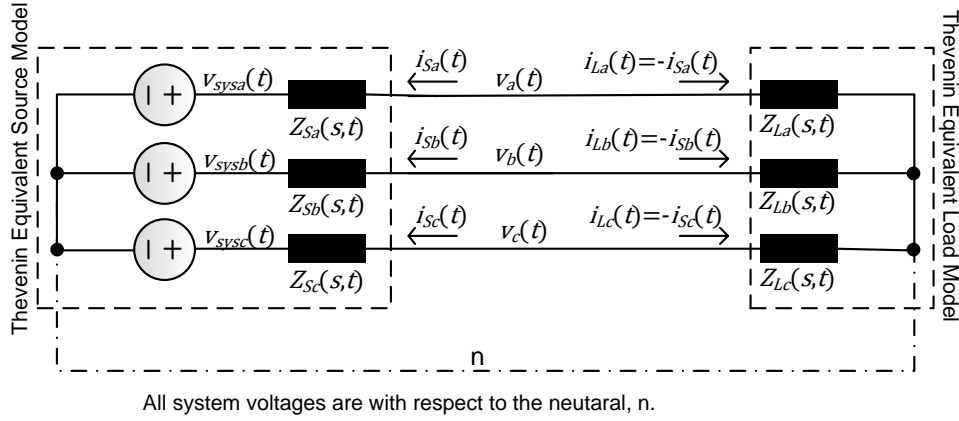


Figure 1-1: System in **abc** coordinates

The voltages and currents at the interfaces of the three-phase AC power system keep changing, which means no operating point can be directly defined by using the interface voltages and currents. The equivalent source and load impedances may also be time variant due to the switching nature of the converters and the closed loop control. However, such non-stationary systems operate on a nominal trajectory in steady-state, nominally given by (1-1), which shows periodic tendencies.

$$\begin{aligned}
 v_a(t) &= V_m \cos(\omega t), \quad i_{Sa}(t) = I_m \cos(\omega t + \varphi) \\
 v_b(t) &= V_m \cos(\omega t - 2\pi/3), \quad i_{Sb}(t) = I_m \cos(\omega t - 2\pi/3 + \varphi) \\
 v_c(t) &= V_m \cos(\omega t + 2\pi/3), \quad i_{Sc}(t) = I_m \cos(\omega t + 2\pi/3 + \varphi)
 \end{aligned} \tag{1-1}$$

One approach in literature is to model the system impedances invariably regardless of alternating voltages and currents in the system. In some of the works, the impedance is defined per phase, and Nyquist stability criteria is directly applied on each phase of the system [31-33]. The other works decouple system voltages and currents into positive and negative sequence components. Self-impedances and coupling-impedances are defined for the two components. Generalized Nyquist criteria (GNC) is used to assess the system stability [34-37], which in turn examines it by looking at the characteristic loci of the return ratio matrix. The GNC was developed by MacFarlane and Postlethwaite in the 1970's [39-41]. It consolidated the frequency-response control methods developed for multivariable linear systems [42-45], and

provided the complete dual development of the classical single-input single-output control theory [46-50] for multivariable systems [51-56].

The other approach tackles the problem by mapping the system from the stationary coordinates into a synchronous coordinates using the **dq** transformation [56]. To transform the system, the three phase variables, such as voltages and currents, can be represented as a vector rotating in three-dimensional space. If the vector follows the trajectory described by (1-1), the vector goes along a circle at a constant frequency of ω . A rotating coordinate system can be defined to match the speed of the vector rotation, making the voltage vector appear stationary in that frame. The transformation matrixes between the two coordinate systems are defined in (1-2) and (1-3):

$$\mathbf{T}_{dq0/abc}(\omega) = \sqrt{\frac{2}{3}} \begin{bmatrix} \cos(\omega t) & \cos\left(\omega t - \frac{2\pi}{3}\right) & \cos\left(\omega t + \frac{2\pi}{3}\right) \\ -\sin(\omega t) & -\sin\left(\omega t - \frac{2\pi}{3}\right) & -\sin\left(\omega t + \frac{2\pi}{3}\right) \\ \frac{1}{\sqrt{2}} & \frac{1}{\sqrt{2}} & \frac{1}{\sqrt{2}} \end{bmatrix} \quad (1-2)$$

$$\mathbf{T}_{abc/dq0}(\omega) = \mathbf{T}_{dq0/abc}^{-1}(\omega) \quad (1-3)$$

The voltage and current vectors shown in Figure 1-1 can be transferred into the synchronous coordinates rotating at angular speed ω as shown in (1-4)

$$\begin{aligned} \begin{bmatrix} v_d(t) \\ v_q(t) \\ v_0(t) \end{bmatrix} &= \mathbf{T}_{dq0/abc}(\omega) \begin{bmatrix} v_a(t) \\ v_b(t) \\ v_c(t) \end{bmatrix} \\ \begin{bmatrix} i_{sd}(t) \\ i_{sq}(t) \\ i_{s0}(t) \end{bmatrix} &= \mathbf{T}_{dq0/abc}(\omega) \begin{bmatrix} i_{sa}(t) \\ i_{sb}(t) \\ i_{sc}(t) \end{bmatrix} \\ \begin{bmatrix} i_{Ld}(t) \\ i_{Lq}(t) \\ i_{L0}(t) \end{bmatrix} &= \mathbf{T}_{dq0/abc}(\omega) \begin{bmatrix} i_{La}(t) \\ i_{Lb}(t) \\ i_{Lc}(t) \end{bmatrix} \end{aligned} \quad (1-4)$$

When the stability of the system is studied, this approach focuses on balanced and symmetric three-phase systems, in which θ -axis components are always zero. Therefore, only the d -axis and q -axis components are used. The transformation matrixes become:

$$\mathbf{T}_{dq/abc}(\omega) = \sqrt{\frac{2}{3}} \begin{bmatrix} \cos(\omega t) & \cos\left(\omega t - \frac{2\pi}{3}\right) & \cos\left(\omega t + \frac{2\pi}{3}\right) \\ -\sin(\omega t) & -\sin\left(\omega t - \frac{2\pi}{3}\right) & -\sin\left(\omega t + \frac{2\pi}{3}\right) \end{bmatrix} \quad (1-5)$$

$$\mathbf{T}_{abc/dq}(\omega) = \sqrt{\frac{2}{3}} \begin{bmatrix} \cos(\omega t) & -\sin(\omega t) \\ \cos\left(\omega t - \frac{2\pi}{3}\right) & -\sin\left(\omega t - \frac{2\pi}{3}\right) \\ \cos\left(\omega t + \frac{2\pi}{3}\right) & -\sin\left(\omega t + \frac{2\pi}{3}\right) \end{bmatrix} \quad (1-6)$$

By applying the dq transformation, a common three-phase system like that shown in Figure 1-1 can be transferred to an equivalent representation, as shown in Figure 1-2.

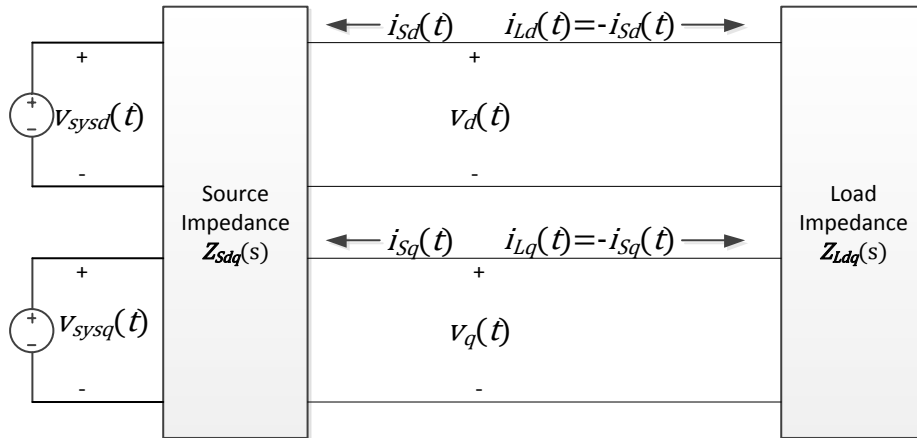


Figure 1-2: System in dq coordinates

The voltages and currents at the interface become a constant in the synchronous coordinates if they follow (1-1) in the stationary coordinates. A steady-state operating point is obtained, and the small signal impedance can be obtained by linearizing the system around the operating point. The interface voltages and currents are related by the impedances as shown in (1-7):

$$\begin{bmatrix} v_d(s) \\ v_q(s) \end{bmatrix} = \mathbf{Z}_{sdq}(s) \begin{bmatrix} i_{sd}(s) \\ i_{sq}(s) \end{bmatrix}, \quad \begin{bmatrix} v_d(s) \\ v_q(s) \end{bmatrix} = \mathbf{Z}_{Ldq}(s) \begin{bmatrix} i_{Ld}(s) \\ i_{Lq}(s) \end{bmatrix} \quad (1-7)$$

where

$$\mathbf{Z}_{sdq}(s) = \begin{bmatrix} Z_{Sdd}(s) & Z_{Sdq}(s) \\ Z_{Sqd}(s) & Z_{Sqq}(s) \end{bmatrix}, \mathbf{Z}_{Ldq}(s) = \begin{bmatrix} Z_{Ldd}(s) & Z_{Ldq}(s) \\ Z_{Lqd}(s) & Z_{Lqq}(s) \end{bmatrix} \quad (1-8)$$

Most of the time, the load-side admittance matrix $\mathbf{Y}_{Ldq}(s) = \mathbf{Z}_{Ldq}(s)^{-1}$ is used in the stability analysis instead of the impedance matrix.

In the early 1990's, Hiti et al. proposed the study of the synchronous d - q frame return ratio matrix $\mathbf{Z}_{sdq}(s) \cdot \mathbf{Y}_{Ldq}(s)$ to study the stability of the three-phase AC power system interfaces [57-58]. Belkhat made a breakthrough by introducing the Generalized Nyquist Criterion (GNC) to assess the AC system stability [59]. It is a precise method to assess stability in multi-variable systems. Norm based criteria are derived from GNC in [59] and [60], which reduces mathematical complexity, but they are more conservative. There are also other approaches trying to simplify the GNC to the stability analysis of a single-input single output system in case the load is operating close to unity power factor conditions [61, 62].

1.2. Dissertation Motivation and Objective

It is apparent that there is a need to fully characterize the impedances of the various AC and DC interfaces in AC power electronic systems for stability purposes. While DC impedance analyzers are mature and widely available, no commercial equipment exists for AC systems. Despite the pronounced need for a method to measure the impedances in AC systems, the problem has not been fully solved.

1.2.1. Challenges in Impedance Extraction in Three-phase AC Systems

Measuring the impedance in three-phase power systems has a history of more than thirty years [63]. During the early days, the extracted impedances are mainly grid impedances. The impedances are modeled linearly and measured separately on each phase using the techniques that are used in DC power systems [63-81]. This approach is continuously evolving even today.

After the stability criteria is proposed using the impedances defined in the synchronous coordinates, attempts are made to extract the impedances in the dq frame [82-95]. New problems emerge involving the coordinates transformation. Some of the research challenges are highlighted below:

A. Perturbation Injection

When measuring a small-signal impedance at a certain frequency, the voltage and current of such frequency are measured at the interface. In some cases, the components of this frequency may exist in the system, and the impedances can be extracted by analyzing the nature of the voltage and current waveforms of the system [63]. But most of the time, the system does not have any signals at the frequencies to be measured. A small disturbance at that frequency has to be injected into the system. While possible, this is not a small task. There are several challenges to create such a perturbation.

The perturbation needs to be able to cover the whole measurement frequency range, which may start close to DC and end at a much higher frequency than the system's fundamental frequency. Some uncontrolled waveforms, like pulse [79], and load step [95], are used to simplify the perturbation generation. While controlled waveforms provide better control and ease the measurement task. Different perturbation waveforms are studied in literature, such as sinusoidal pattern [94], square pattern [91], and white noise [86, 87].

The power rating of three-phase AC power systems is usually much larger when compared to the DC systems. To create a measurable disturbance in such a system requires significant amount of power. Injecting the power with the desired disturbance waveform is even challenging. Power converters [70, 74, 77, 89], motors [89][96], switched impedances [91], and applying perturbation on some accessible control signals [81] are used in the literature.

B. Signal Processing and Impedance Extraction Algorithm

Only the voltages and currents are measured directly from the system. Then the impedance of the system is calculated from the measured data. A proper algorithm needs to be designed to achieve a good extraction.

The algorithms can be classified as parametric [73, 75, 95] or nonparametric [74, 83, 93]. The parametric ones describe the system using a certain model, and use the measurement data to fit the model parameters. The nonparametric ones just describe the impedance as transfer functions with no predefined limitation. While the parametric approaches usually produce better measurement results by taking advantage of the knowledge of the system, the nonparametric methods are more flexible.

However, both approaches have to deal with signals that have a low signal-to-noise ratio (SNR). The disturbance signal is small compared to the fundamental frequency components in the system. Since all the sensing, signal conditioning, and data acquisition circuits are designed to be able to process the full fundamental frequency signals, the noise floor of these circuits are usually close to the small disturbance signal to be measured. Even a large magnitude perturbation can be injected into the system when the system is considered to be linear, the power density spectrum over the frequency range is still very low due to the transient waveforms that are used [79].

C. Measurement Speed

Fast measurement speed is always a desired feature. At least two measurements of voltages and currents need to be taken for the measurement of a single impedance point. The system to be measured has to stay at a certain operating point during both measurements. In a complicated power system used in MEA and AES, it is not easy to hold the system at the operating point for an extended time. When the measurement frequency range reaches the sub-hertz range, the commonly used frequency sweeping methods may take an extremely long time to obtain the results. Faster approaches are proposed using transient perturbation waveforms. However, the

works studied in the literature review all involve perturbation of large magnitude, which may introduce unexpected nonlinear response from the system [69, 76, 95].

D. Dq Frame Alignment

When the impedance to be measured is defined in the synchronous coordinates, the alignment of the frame is an important issue. The alignment of axes defines the frame. Most work aligns either the d -axis or the q -axis to the rotating voltage vector. The impedance may change if the dq frame is aligned differently [97].

The frame can be aligned during post-processing using frequency and initial phase, which are obtained via the FFT technique. The system phase drifting during measurement and tiny system frequency estimation error during data processing can generate a large phase error. A low-pass filtered line voltage is used as the phase information in [83]. But it contains low-frequency perturbation signals. A phase locked loop (PLL) is used to solve these problems in [94]. However, the low bandwidth PLL used to filter out the perturbation signals weakens the capability of the tracking system phase drift.

E. Measurement System Characterization

As a measurement system, the influence of system characteristics on the measurement result should be considered. But most work in literature just treats all the sensing, signal conditioning, analog-to-digital conversion and calculation ideally. Reference [93] discusses the system characterization by looking at the transfer functions of each stage in the system. But some phenomena are still not modeled in the discussion, such as the different characteristics of three-phase signal processing circuits and the dynamic of coordinate transformation.

Besides the systematical errors, the random error is also a very important factor in the characterization of the system. The random errors are generated at each stage of measurement. As the coordinate transformation provides a frequency shift, and the multi-input, multi-output nature of the system allows opportunities for these errors to cross-couple between channels,

tracking the propagation of these errors and analyzing their effect on the measurement result become a challenging task.

F. Measurement Result Validation

The validation of the measured result is another challenge. In the case of linear networks, the impedances can be measured in the stationary coordinates and transferred into synchronous coordinates analytically for comparison [93].

When the measured object contains power-electronic devices, there is no proven independent measurement result that can be used for verification. Simulation models can be used to compare with the measurement result [92, 98]. However, the models are created with approximations and under certain assumptions. Some nonlinear behaviors that are commonly ignored when modeling small-signal behaviors, such as dead time, can cause significant impedance change from the real one [99, 100].

1.2.2. Objective

The main objective of this work is to produce an approach on extracting the frequency-dependent impedances of three phase AC systems that is useful to access the system stability down to the frequency range of a few hertz from both source and load side. The impedance defined in synchronous coordinates is selected, because the approach in synchronous coordinates handles the alternating voltage and current better than the approach in stationary coordinates, which ignores their effects.

Several basic system characteristics that affect the measurement speed and accuracy are first analyzed. To increase the measurement speed, a wide bandwidth perturbation signal is used in the impedance extraction. With the analysis result of system characteristics, a measurement system architecture will be designed and implemented. The equipment built using the proposed approach is to be tested with both linear and nonlinear loads to verify its usability in practical configurations.

1.3. Dissertation Layout

Chapter 2 of this dissertation give a comprehensive review of state-of-the-art impedance extraction approaches used in three-phase AC systems.

Chapter 3 analyzes several systematical errors in the measurement system and proposes solutions to reduce some of these errors.

Chapter 4 addresses the efforts made based on the previous equipment architecture to improve the measurement accuracy.

Chapter 5 shows an improved measurement system architecture and the algorithm used in the new system design. The new design overcomes some of the inherent issues of the previous design and further improves the system performance.

The last chapter summarizes the work and discusses possible future improvement.

Chapter 2. Impedance Extraction in Three-phase AC Systems

This chapter first describes the relationship, including the differences between the three types of impedances that are used in literature for stability analysis of three-phase AC power systems, It also explains the reason why impedance as defined in synchronous coordinates is used in this research.

Then the state-of-the-art technique for impedance extraction in a three-phase system is reviewed, with an emphasis on extracting impedance as defined in synchronous coordinates. The overall measurement procedure and measurement system architecture is recapped. Then more detail is discussed from the following aspects: perturbation signal waveform, perturbation generation method, and data processing techniques.

2.1. Impedance Definition in Three-phase Systems

There are three types of impedances used in the stability analysis of three-phase systems. They are all transfer functions from current to voltage at the same interface, or complex a ratio of the voltage to current at a frequency. The difference between the three definitions is the representations of voltages and currents.

2.1.1. Sequence Components in *Abc* Frame and *Dq* Frame

To help with describing the relationship between the impedance definitions, the sequence component is explained in this section.

Sequence component decomposition is commonly used in the power system analysis. A three-phase signal vector of certain angular frequency ω can be expressed as:

$$\mathbf{x}_{abc}(\omega, t) = \begin{bmatrix} x_a(\omega, t) \\ x_b(\omega, t) \\ x_c(\omega, t) \end{bmatrix} = \begin{bmatrix} X_a \cdot \cos(\omega t + \phi_a) \\ X_b \cdot \cos(\omega t + \phi_b) \\ X_c \cdot \cos(\omega t + \phi_c) \end{bmatrix} \quad (2-1)$$

where ϕ_a , ϕ_b and ϕ_c are initial phases of the three-phase signals X_a , X_b and X_c are magnitudes of the signals. In a common three-phase power systems, for the fundament frequency signals, the initial phases have the relation of:

$$\begin{aligned}\phi_b &= \phi_a - \frac{2\pi}{3}, \phi_c = \phi_a + \frac{2\pi}{3} \\ X_a &= X_b = X_c\end{aligned}\tag{2-2}$$

The vector \mathbf{x}_{abc} can be either voltage or current. It can be decomposed into the combination of a positive-sequence component, a negative-sequence component and a zero-sequence component as:

$$\mathbf{x}_{abc}(\omega, t) = \mathbf{x}_{abc_p}(\omega, X_p, \phi_p, t) + \mathbf{x}_{abc_n}(\omega, X_n, \phi_n, t) + \mathbf{x}_{abc_o}(\omega, X_o, \phi_o, t)\tag{2-3}$$

where the positive sequence-component $\mathbf{x}_{abc_p}(\omega, X_p, \phi_p, t)$, the negative-sequence component $\mathbf{x}_{abc_n}(\omega, X_n, \phi_n, t)$ and the zero-sequence component $\mathbf{x}_{abc_o}(\omega, X_o, \phi_o, t)$ are:

$$\begin{aligned}\mathbf{x}_{abc_p}(\omega, X_p, \phi_p, t) &= X_p \left[\cos(\omega t + \phi_p) \quad \cos\left(\omega t + \phi_p - \frac{2\pi}{3}\right) \quad \cos\left(\omega t + \phi_p + \frac{2\pi}{3}\right) \right]^T \\ \mathbf{x}_{abc_n}(\omega, X_n, \phi_n, t) &= X_n \left[\cos(\omega t + \phi_n) \quad \cos\left(\omega t + \phi_n + \frac{2\pi}{3}\right) \quad \cos\left(\omega t + \phi_n - \frac{2\pi}{3}\right) \right]^T \\ \mathbf{x}_{abc_o}(\omega, X_o, \phi_o, t) &= X_o [\cos(\omega t + \phi_o) \quad \cos(\omega t + \phi_o) \quad \cos(\omega t + \phi_o)]^T\end{aligned}\tag{2-4}$$

The zero-sequence component is always zero in the three wire three-phase system that is studied. Thus it is ignored in the analysis.

In a common balanced three-phase system following (2-2), at fundamental frequency, the negative-sequence component $\mathbf{x}_{abc_n}(\omega_s, X_n, \phi_n, t)$ is also zero, where ω_s is the fundament angular frequency.

It can be easily seen from (2-4) that a general negative-sequence component can be rewritten in the positive-sequence component format with a negative frequency value as:

$$\mathbf{x}_{abc_n}(\omega, X, \phi, t) = \mathbf{x}_{abc_p}(-\omega, X, -\phi, t) \quad (2-5)$$

Both positive-sequence and negative-sequence components can be written in the same format:

$$\mathbf{x}_{abc_pn}(\omega, X, \phi, t) = X \left[\cos(\omega t + \phi) \quad \cos\left(\omega t + \phi - \frac{2\pi}{3}\right) \quad \cos\left(\omega t + \phi + \frac{2\pi}{3}\right) \right]^T \quad (2-6)$$

A positive-sequence component has a positive angular frequency, while a negative-sequence component has a negative angular frequency.

A signal vector of certain angular frequency ω in **dq** frame is in the form of:

$$\mathbf{x}_{dq}(\omega, t) = \begin{bmatrix} x_d(\omega, t) \\ x_q(\omega, t) \end{bmatrix} = \begin{bmatrix} X_d \cdot \cos(\omega t + \phi_d) \\ X_q \cdot \cos(\omega t + \phi_q) \end{bmatrix} \quad (2-7)$$

It can be decomposed to a positive-sequence component and a negative-sequence component, which is similar as the **abc** frame case:

$$\mathbf{x}_{dq}(\omega, t) = \mathbf{x}_{dq_pn}(\omega, X_p, \phi_p, t) + \mathbf{x}_{dq_pn}(-\omega, X_n, -\phi_n, t) \quad (2-8)$$

where

$$\mathbf{x}_{dq_pn}(\omega, X, \phi, t) = X \cdot \left[\cos(\omega t + \phi) \quad \cos\left(\omega t + \phi - \frac{\pi}{2}\right) \right]^T \quad (2-9)$$

When transferring signals between the *abc* frame and the *dq* frame, the signal that has a single frequency in one frame is mapped into the other frequency on two frequency points. By defining the sequence component in both frames, one sequence component in one frame is mapped into the other frame as a single sequence component as shown in:

$$\begin{aligned}
 T_{dq/abc}(\omega_s) \cdot x_{abc_{pn}}(\omega, X, \phi, t) &= x_{dq_{pn}}\left(\omega - \omega_s, \sqrt{\frac{3}{2}}X, \phi, t\right) \\
 T_{abc/dq}(\omega_s) \cdot x_{dq_{pn}}\left(\omega - \omega_s, \sqrt{\frac{3}{2}}X, \phi, t\right) &= x_{abc_{pn}}(\omega, X, \phi, t)
 \end{aligned} \tag{2-10}$$

where ω_s is the three-phase system line frequency, which is the rotating speed of the *dq* frame. The transformation from the *abc* frame to the *dq* frame just scales the magnitude of the component and shifts the frequency of the component by $-\omega_s$, and vice versa.

2.1.2. Impedance Defined per Phase

When the per-phase impedance is used for stability analysis, the impedances of all three phases are considered to be the same, and there is no coupling between different phases. The impedance matrix is in the form of:

$$\mathbf{Z}_{abc}(s) = \begin{bmatrix} Z(s) & 0 & 0 \\ 0 & Z(s) & 0 \\ 0 & 0 & Z(s) \end{bmatrix} \tag{2-11}$$

where $Z(s) = V_a(s)/I_a(s) = V_b(s)/I_b(s) = V_c(s)/I_c(s)$.

The system voltages and currents are related by the impedance matrix as:

$$\mathbf{V}_{abc}(s) = \mathbf{Z}_{abc}(s) \cdot \mathbf{I}_{abc}(s) \tag{2-12}$$

When a current $\mathbf{i}_{abc}(t) = \mathbf{x}_{abc_pn}(\omega, I, \phi, t)$, is applied on the impedance, the voltage response is $\mathbf{v}_{abc}(t) = \mathbf{x}_{abc_pn}(\omega, |Z| \cdot I, \phi + \angle Z, t)$, where $|Z|$ is the magnitude of the impedance and $\angle Z$ is the phase of the impedance at angular frequency ω .

The response has only one phase sequence component at the same frequency as the current excitation's. When transferring the excitation and response into the dq frame, they stay as a single frequency point. Figure 2-1 illustrates the relation of the excitation and response components.

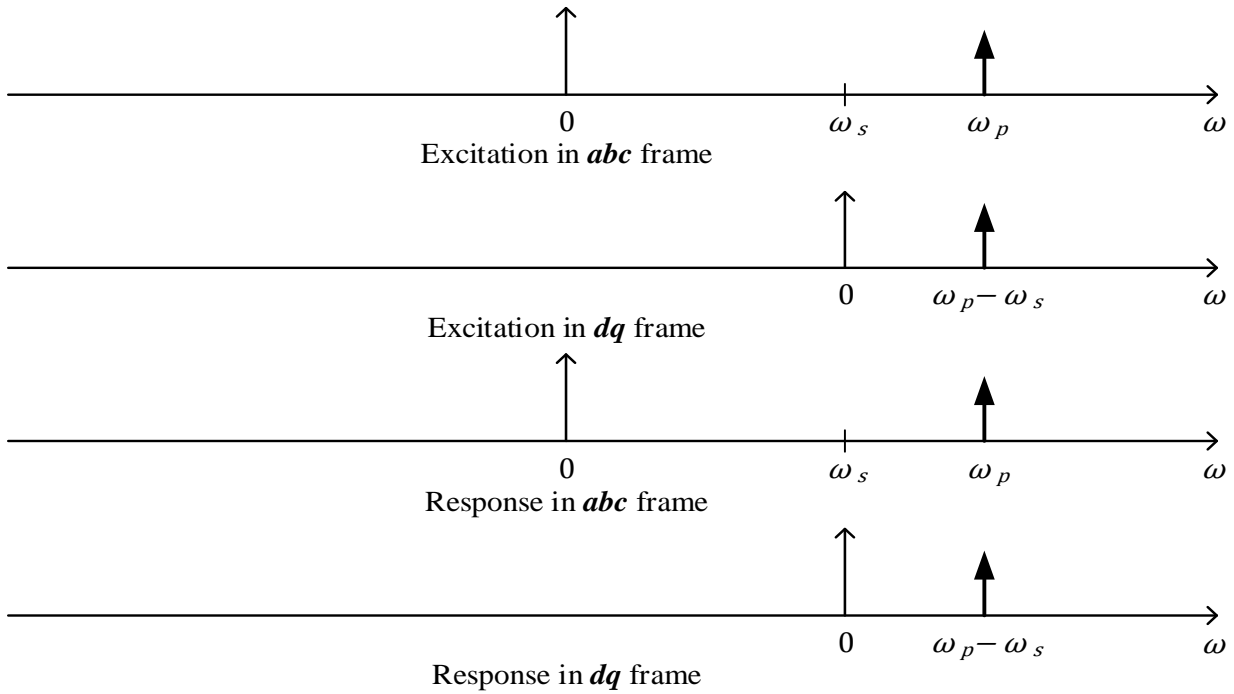


Figure 2-1: Excitation and response sequence components in balanced, symmetric, linear systems

The excitation-response relationship is applicable to not only the impedance matrix of the form (2-11), but also to all the symmetric impedance matrixes which are in the form of:

$$\mathbf{Z}_{abc}(s) = \begin{bmatrix} Z(s) & M(s) & M(s) \\ M(s) & Z(s) & M(s) \\ M(s) & M(s) & Z(s) \end{bmatrix} \quad (2-13)$$

Such a system is also linear in the dq frame. The impedance can be transferred into the dq frame as described in [93].

2.1.3. Impedance Defined Using Sequence Component in abc Frame

A generic linear three-phase system's impedance matrix is:

$$\mathbf{Z}_{abc}(s) = \begin{bmatrix} Z_a(s) & M_{ab}(s) & M_{ac}(s) \\ M_{ba}(s) & Z_b(s) & M_{bc}(s) \\ M_{ca}(s) & M_{cb}(s) & Z_c(s) \end{bmatrix} \quad (2-14)$$

The system is asymmetric if all the self-impedances are not the same or all the coupling-impedances is not equal. When a current excitation of a single phase sequence component is applied on such an impedance matrix, the response is no longer a single phase sequence component. Both a positive sequence component and negative sequence component are generated. The frequency mapping of the excitation and response are shown in Figure 2-2.

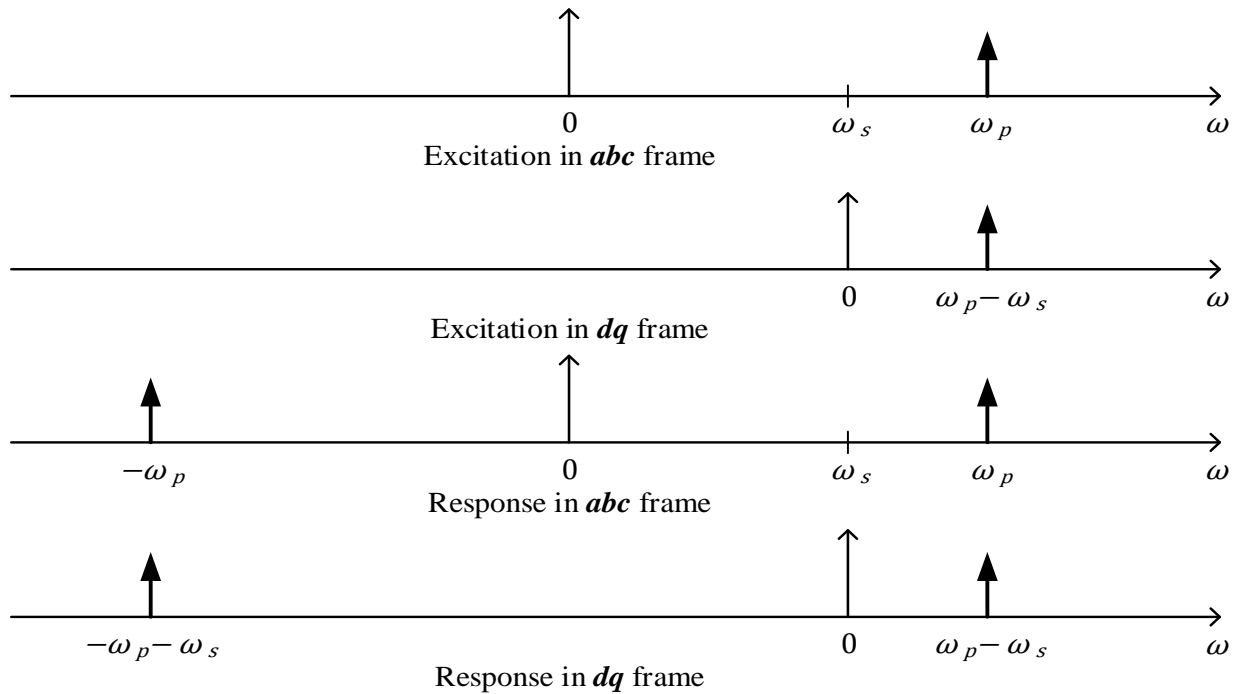


Figure 2-2: Excitation and response sequence components in balanced, asymmetric, linear systems

Reference [34] defines a 2x2 impedance matrix (2-15) to model this behavior.

$$\mathbf{Z}_{pn}(s) = \begin{bmatrix} Z_{pp}(s) & Z_{pn}(s) \\ Z_{np}(s) & Z_{nn}(s) \end{bmatrix} \quad (2-15)$$

The diagonal terms are the self-impedances describing the relationship between the excitation and the response phase-sequence components of the same frequency. The off-diagonal terms model the relationship between the response phase-sequence component at the negative frequency of the excitation signal and the excitation signal.

This kind of systems is not linear in the dq frame. As shown in Figure 2-2, the two response phase-sequence components are not at the same frequency in the dq frame.

2.1.4. Impedance Defined in Dq Frame

A three-phase system can be transferred into the dq frame using (1-5). A steady state operating point is obtained by this transformation. Thus, the system can be linearized at this operating point to get the impedance matrix (1-8). In a balanced, symmetric, and linear system, the impedance matrix has the property:

$$\begin{aligned} Z_{dd}(s) &= Z_{qq}(s) \\ Z_{dq}(s) &= -Z_{qd}(s) \end{aligned} \quad (2-16)$$

By having the relation of (2-16), the frequencies of excitation and response phase-sequence components have the same relation described in section 2.1.2. But for many power electronic converters, the relation in (2-16) does not hold [97], an additional response phase-sequence component is generated at the negative frequency of the excitation phase-sequence component. When transferred back into the abc frame, this component is at a different frequency from the excitation signal. The relation between excitation and response frequencies is illustrated in

Figure 2-3. The impedance defined in the dq frame the quadratic nonlinear behavior in three-phase systems.

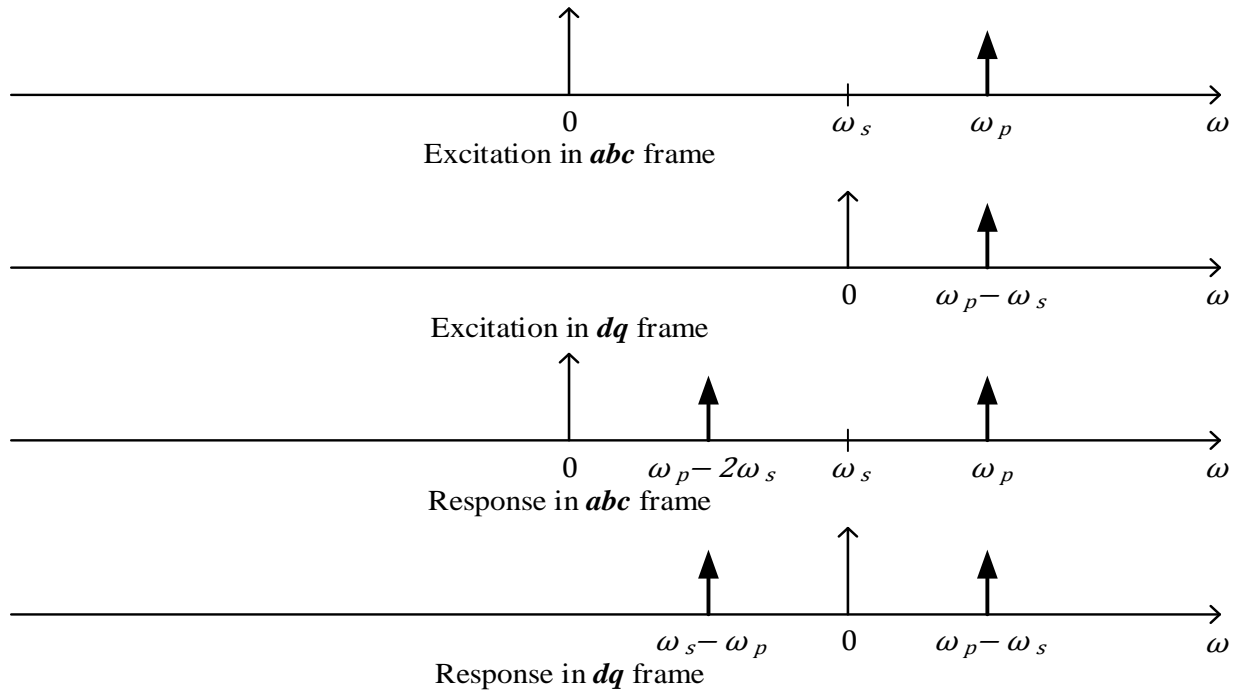


Figure 2-3: Excitation and response sequence components in balanced, symmetric, quadratic nonlinear systems

2.1.5. Impedance Selection for Stability Analysis

Figure 2-4 shows that in a three-phase system that is asymmetric and has quadratic nonlinearity, excitation at one frequency ω_p generates response at infinite frequencies, which are at $2n\omega_s \pm \omega_p$ in the abc frame and $(2n + 1)\omega_s \pm \omega_p$ in the dq frame, where n is an integral number, and ω_s is the system line frequency. This behavior cannot be modeled by linear impedances. Simplification to one of the cases described in the previous sections is usually made in the analysis.

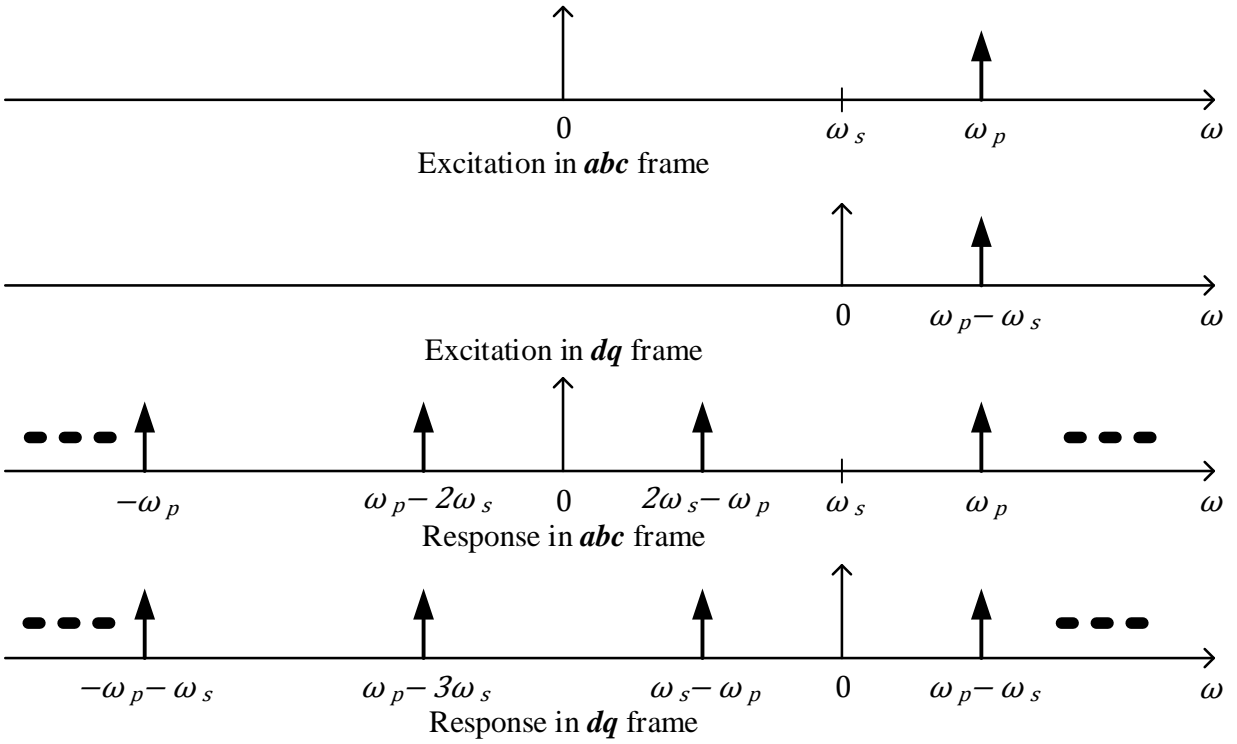


Figure 2-4: Excitation and response sequence components in unbalanced, asymmetric, quadratic nonlinear systems

The quadratic nonlinearity is caused by the control and operation of the converters, which is unavoidable. The impedance defined by the phase-sequence component in the *abc* frame does not model this important effect. However, a normal three-phase system is designed to be balanced and symmetric. When the system is excited by a phase-sequence component, the response at negative excitation frequency is usually less than a few percentages of the one at the excitation frequency. Therefore, the assumption to use the *dq* impedance can be met. Out of the three impedance definitions in literature, the *dq* impedance is the most suitable one for stability analysis and is selected for the rest of the research.

2.2. Impedance Measurement Procedure and Measurement System Architecture

The basic idea of online small signal impedance extraction is to collect the circuit voltage and current information at the frequency of interest on the interface to be measured, and then calculate the corresponding impedances base on the acquired information.

The systems' working voltages and currents can be used if they contain the components of the interested frequencies and these components are "small signal" when compared to the system operating point. Most of the time, the systems' working voltages and currents do not have all the frequency components of interest. To measure such a system, some perturbation has to be injected into the system to disturb the system in order to generate useful voltage and current information at the desired frequencies. This is a common approach used in much of the literature we see on this topic. To identify the full 2x2 impedance matrix, four equations are needed. A single perturbation can generate only two equations as shown in (1-7). Therefore, at least two independent perturbations are required. The voltages and currents at the interface where the impedance is measured are collected and fed to the impedance extraction algorithm to obtain the impedance result. The impedance matrix is then calculated from the measured response data as:

$$\begin{aligned} \mathbf{Z}_{sdq}(s) &= \begin{bmatrix} \tilde{v}_{d1}(s) & \tilde{v}_{d2}(s) \\ \tilde{v}_{q1}(s) & \tilde{v}_{q2}(s) \end{bmatrix} \begin{bmatrix} \tilde{i}_{sd1}(s) & \tilde{i}_{sd2}(s) \\ \tilde{i}_{sq1}(s) & \tilde{i}_{sq2}(s) \end{bmatrix}^{-1} \\ \mathbf{Z}_{ldq}(s) &= \begin{bmatrix} \tilde{v}_{d1}(s) & \tilde{v}_{d2}(s) \\ \tilde{v}_{q1}(s) & \tilde{v}_{q2}(s) \end{bmatrix} \begin{bmatrix} \tilde{i}_{ld1}(s) & \tilde{i}_{ld2}(s) \\ \tilde{i}_{lq1}(s) & \tilde{i}_{lq2}(s) \end{bmatrix}^{-1} \end{aligned} \quad (2-17)$$

Having the algorithm, a measurement system needs to be setup to measure real impedances. Dissertation [83] presents a measurement setup as shown in Figure 2-5:

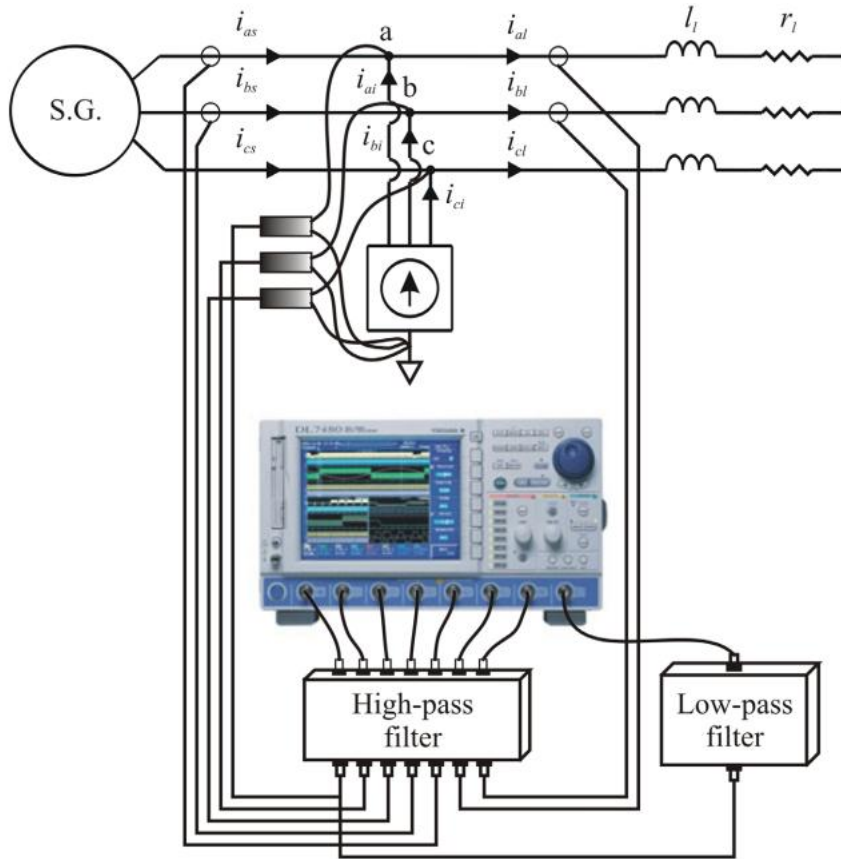


Figure 2-5: Measurement setup in [83], used under fair use, 2013

In this arrangement, the perturbation is generated by an independent unit connected in shunt with the system. The perturbation reference information is not used. The voltage and current responses and one phase of system voltage information are recorded by a scope. The analog signals are passed through some filters to fully utilize the analog-to-digital converter (ADC) resolution. The responses are post processed in a host computer to calculate the impedance. A spectrum analysis method using FFT is implemented. The phase information used for dq transformation is extracted from the recorded single phase information by using the zero-crossing method. A similar test set up is used in many other papers [82-92]: independent perturbation injection device connected in shunt, perturbation reference is not used; response data is recorded by a scope and post-processed.

In [93], a measurement instrument is implemented. The architecture of the system is shown in Figure 2-6

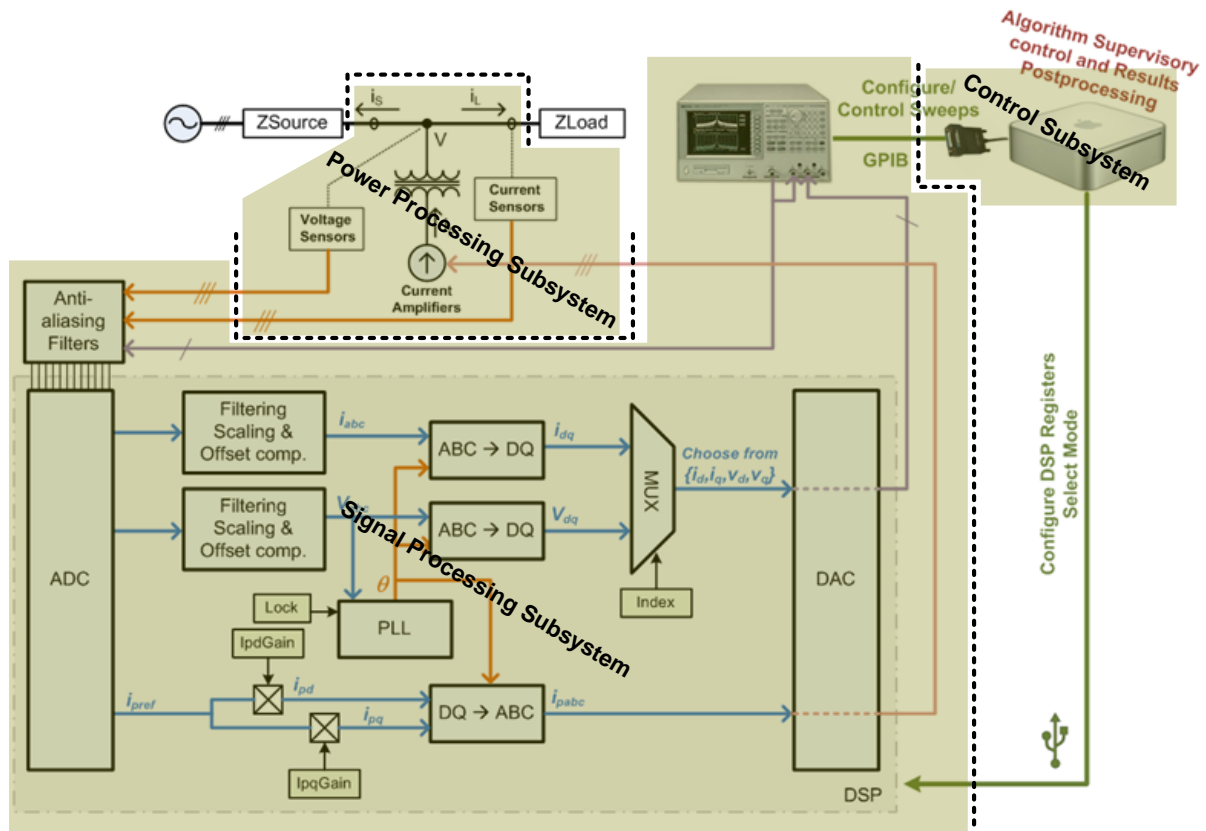


Figure 2-6: Measurement system architecture given in [93], used under fair use, 2013

The system is divided into three subsystems: a power processing subsystem, a signal processing subsystem, and a control subsystem.

The power subsystem takes reference signal from the signal processing subsystem and injects the perturbation into the system in shunt at the measurement point. Then the voltages and currents at the interface are converted into low power signals and sent back to the signal processing system.

The signal processing subsystem takes the perturbation reference in the dq frame and transfers it into the abc frame for use in the power subsystem. The sensed voltages and currents are transferred from the abc frame to the dq frame to identify their phase and gain information. The gain and phase identification in this design is processed by a network analyzer. The original

perturbation reference is also generated by the same network analyzer. The system voltage phase used by the dq transformation is obtained through a three-phase phase locked loop (PLL) in a real-time processor.

The identified gain and phase information is collected by the control subsystem. The system impedances are calculated using this information. The control subsystem also controls the measurement parameters, such as injection power, measured frequency points, etc., through the communication to the signal processing subsystem.

Compared to the setup in Figure 2-5, this architecture improves two aspects. A PLL is used to find the system voltage phase. The PLL usually outperforms the zero-crossing method on phase identification especially when the waveform is distorted. The perturbation reference is used in the gain and phase identification, which helps to remove non-correlated noise. To take advantage of having a perturbation reference signal, the transformation between the dq frame and the abc frame is calculated in real time instead of only during the post-processing phase.

The patent [96] has a similar architecture as [93]. Only the PLL and coordinate transformation part is replaced by the nature of a wound rotor induction machine.

2.3. Perturbation Signal Waveform

Different perturbation waveforms can be used to excite the system at the interested frequencies. They result in a different signal-to-noise ratio (SNR), measurement time and noise immunity, etc.

2.3.1. Periodical Waveforms

Periodical signals' spectrums are discreet. The perturbation is only generated at its fundamental frequency and harmonic frequencies. Thus, a frequency sweep is usually required to get impedance at all frequencies of interest or 'continuous' impedance in the frequency domain. Although the signal self is periodical, when applied to the system, the signal has to be truncated into a limited time period. In addition, after the perturbation is applied, a certain time has to lapse until the system to be measured reaches its steady state. Otherwise, the obtained response

spectrum contains the components coming from the system transient. This requirement further extends the measurement time.

A. Sinusoidal Waveform

Sine signal is the basic periodical signal. Figure 2-7 gives an example of 100 Hz sinusoidal waveform. A sine signal creates a disturbance only one frequency at a time. The response is measured only at this frequency. The harmonics caused by the nonlinearity of the system are filtered out during the measurement. The impedance measured is free of nonlinear distortion, which should be the same as the result obtained from the linearization of the system.

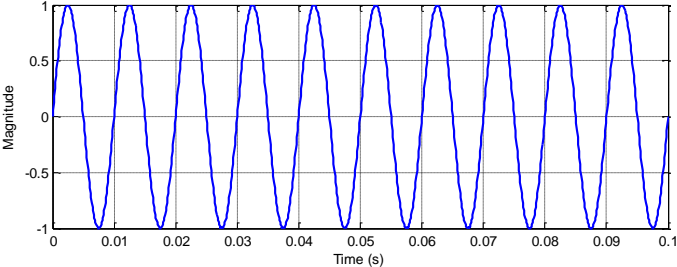


Figure 2-7: Example of 100Hz sinusoidal waveform

It should be mentioned that because the transformations using (1-2) and (1-3) between the *dq* frame and the *abc* frame cause frequency shift, a sinusoidal perturbation in one frame causes two frequencies in the other frame [96]. For example, Figure 2-8 is the result of transferring the waveform in Figure 2-7 into the *abc* frame with a fundamental frequency of 60 Hz.

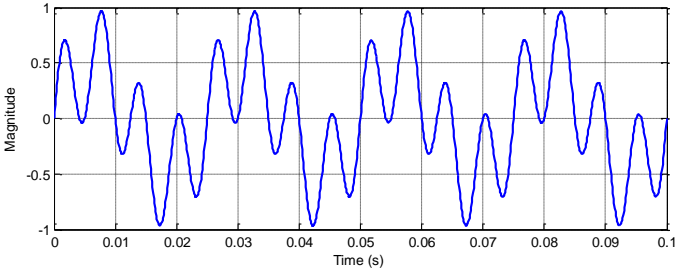


Figure 2-8: Example of 100Hz sinusoidal waveform transferred into 60Hz *abc* frame (Phase A signal)

B. Square Waveform

A square is another example of periodical signals. A 100 Hz example is given in Figure 2-9. The signal contains infinite orders of harmonics. But in the measurement, usually only the signals of fundamental frequency are used [91]. Thus, it still measures impedance one frequency at a time. Although its harmonic could also be used for measurement, the response to harmonic perturbation and the harmonic response of its fundamental mix together and are hard to separate. Thus the use of harmonics is not recommended except if the system is known to be linear, which means that there is no harmonic response.

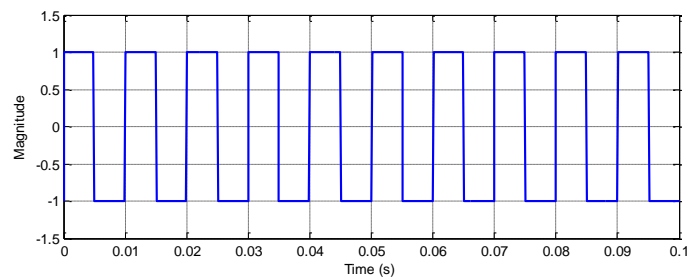


Figure 2-9: Example of 100 Hz square waveform

A square waveform in a dq frame generates a sinusoidal waveform in the abc frame with sharp phase changes which look like the example in Figure 2-10.

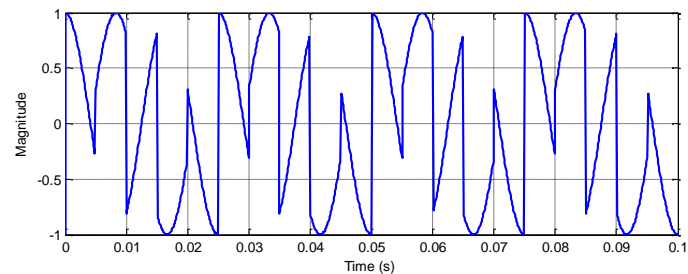


Figure 2-10: Example of 100Hz square waveform transferred into 60Hz abc frame (Phase A signal)

2.3.2. Aperiodical Waveforms

Aperiodical signals have continuous spectrums. If used properly, they can be used to measure the impedance at all interested frequencies simultaneously and in a shorter time compared to the

frequency sweep method. But they suffer the same problem as the square waveform, the response to harmonic perturbation and the harmonic response of its fundamental mix together, if there is no way to separate them.

A. Impulse Waveform

An impulse is a waveform with zero width and infinite magnitude. It has a white spectrum which perturbs the system at the same level for all the frequencies. Thus the impedances at all frequencies can be measured with the same impulse disturbance. The impulse signal is still impulse after it is transferred into the stationary coordinates and keeps its white spectrum.

Because a real impulse with zero width and infinite magnitude does not exist in reality, some other signals are generated to emulate it. It can be a controlled waveform, such as triangular pulse shown in [79], or an uncontrolled pulse [65], which is a broadband signal where the response can be collected and analyzed.

Ideally, an impulse has an infinite response time. All of the response should be measured to obtain an accurate result. In reality, the response usually settles down to the operating point. Thus, the measurement just needs to continue until the response signal falls into the system background noise [101].

The impulse signal has a high crest factor (the ratio of peak value to rms value of a signal). Ideally, it is infinitely high. In a real system, the signals used to emulate the impulse do not have an infinite crest factor. But it is still much higher than the basic sine signal. To keep the disturbance small enough to not cause a server nonlinear response from the system, the peak value of the pulse should be kept within a certain range. The total energy injected into the system is limited by the high crest factor and the limit of the acceptable peak value. The result is that the energy density over the frequency is very small, which lowers the signal to noise ratio (SNR).

B. Step Waveform

Step is easy to generate. A voltage source, a current source or a set of load is switched into or out of the system to create a step. A step waveform example is shown in Figure 2-11. The

waveform becomes the one shown in Figure 2-12 after being transferred into the *abc* frame. In [92, 98] load steps are used for the measurement of output impedances of a voltage source inverter (VSI). The load steps create current steps as shown in Figure 2-11 in the *dq* frame.

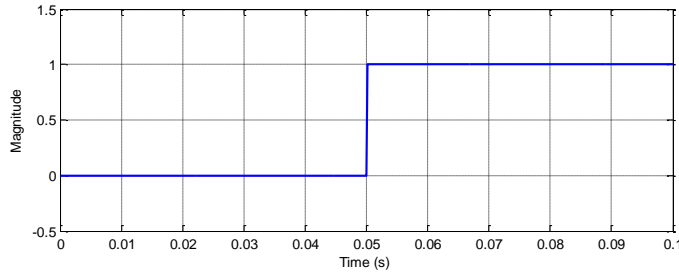


Figure 2-11: Example of a step waveform at 0.05 s

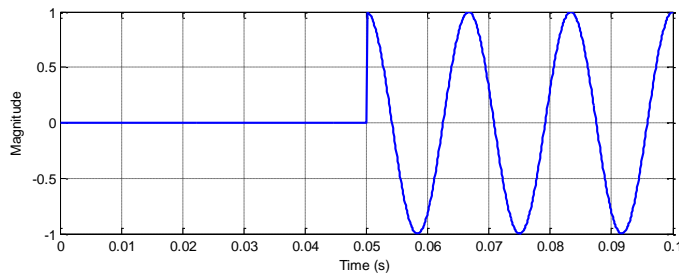


Figure 2-12: Example of a step waveform at 0.05 s transferred into 60Hz *abc* frame (Phase A signal)

Step disturbance changes the operating point of the system. The system state does not go back to the original one before the steps. The measurement should last until the system is considered to be in a new steady state. Also, the steps' magnitude should be controlled so that it is low enough to not change the linearization result for the impedance measurement.

In [92, 98], the converter to be measured is considered to be a black box and is represented using an output error model of given orders. The measured transient waveforms are used to fit the parameters of the dynamic system that is modeled with two polynomials.

It should be mentioned that the impedance in the *dq* frame is a matrix, which is a multi-input multi-output (MIMO) system. As mentioned above, by applying a certain type of load steps, the author considers the system decoupled so that the impedance can extract one by one as a single input single output (SISO) system. The examples in this paper may be satisfactory, but in a more

complex system, the perturbation distribution between the source and load needs to be carefully controlled to decouple the measurement of the impedances or the fitting of the model should be done for the MIMO system instead of the decoupled SISO system.

C. Noise

Noise is another group of broad bandwidth signals. It has a random magnitude and/or a random phase. Figure 2-13 shows an example of white Gaussian noise. In reality, the noise signal is usually obtained using a pseudo random number generation algorithm [81] and is set to conform to a certain spectrum.

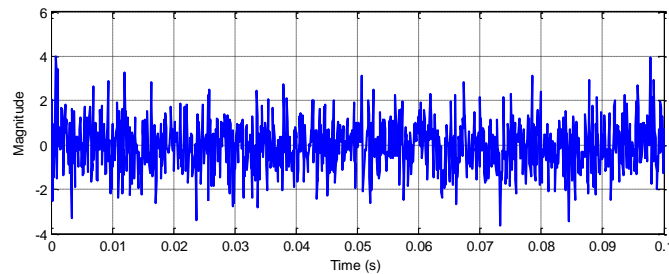


Figure 2-13: Example of a white noise waveform

The crest factor used to be low for commonly seen noise, such as the one shown in Figure 2-13. But by keeping the magnitude of the noise constant, a crest factor as low as unity can be achieved. One example is the maximum length sequence (MLS) [102]. It is a binary sequence, which has a unit magnitude and pseudo-random phase in frequency domain. The signal can be treated as a band limited white noise. When convoluted to itself, it gives the impulse. This property makes it immune to the noise of fixed frequency and phase so it can spread a spike noise's effect all over the frequency range as a background noise that does not affect the measurement much [102]. In reality, due to the limited bandwidth of the perturbation injector, the ideal 0 dB crest factor cannot be achieved. Also, to avoid a huge nonlinearity in a perturbation generation device, the noise signal is usually 5~8 dB lower than the full scale, which limits the disturbance energy [101].

When used to measure the impedances, the spectrum of the noise is usually controlled to be white within the frequency range to be measured, as in [87]. But it can also be shaped to meet certain measurement circumstances. For example, the noise can be shaped ‘blue’ to enhance the perturbation at higher frequencies [103]. The noise still looks like Figure 2-13 even after being transferred into the *abc* frame. But the spectrum may change a little due to the frequency shifting effect of the transformation.

2.4. Perturbation Generation Method

To create the disturbance in a real system, a significant power signal should be injected into the system. Usually the required disturbance power level is proportional to the system power. Because the injection signal bandwidth is supposed to cover all the range of the impedance measurement, which is usually much higher than the system control loop, it is challenging when the system power is high because this means the injection power is high.

2.4.1. Perturbation Generation Device Connection to System

To inject the perturbation into a system, the perturbation generation device has to be electrically connected to the system. The connection can be made at any convenient point. But most of the time, it is made at the interface to be measured. The sensors however need to be connected at this point.

A. *Series vs. Shunt*

To create a disturbance in the system, the perturbation source can be connected either in series in the system as shown in Figure 2-14(a) or shunt to the system as shown in Figure 2-14(b). For series connection, voltage sources are commonly used. Current sources are usually of the choice for shunt connections [82]. If the sources are controlled as power source, they can be connected either in series or in shunt. Other than using sources, controlled impedances can also be used as a perturbation source [83]. They can also be put in both series and shunt.

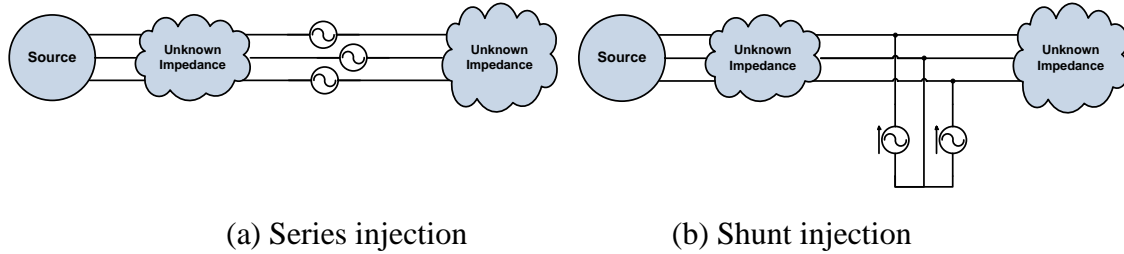


Figure 2-14: Injection connections

B. Balance vs. unbalance

When talking about a three phase system, it is often assumed to be balanced. In most of the papers, disturbance is also balanced to measure a three phase system. A creative way that injects unbalanced signals into the system is proposed in [91]. Unlike the other injection methods, unbalance injection does not make use of a three-phase symmetrical injection. It only creates disturbance between two phases. Although a simplifying injection circuit can be used for this technique, the total injection power may not be lower than the three-phase injection equipment when the same response level is anticipated.

This method is creative for a three wire system. But for a three-phase-four-wire system in which the neutrals of the source and load are connected together, its validity is not proven yet.

2.4.2. Perturbation Generation Device

The perturbation generation device generates a three-phase or a single-phase disturbance depending on the selection between balanced injection and unbalanced injection. The device behaves as a controlled voltage source, current source, power source or just some impedance.

A. Power Amplifier

In reference [93], linear power amplifiers are used to inject the perturbation into the system. The amplifiers are set to current mode. They follow the perturbation references and generated the required currents. The outputs of the amplifiers are isolated from each other to avoid forming unexpected current loop from the power supply side.

B. Power Converter

Power converters are a commonly used perturbation source. For high power perturbation, a switching converter is preferred due to their lower losses.

In [83], a power converter was used to generate a perturbation into the system on all three phases. The converter is connected to the system as shown in Figure 2-15. The voltage source inverter is powered from the DC side using an external power supply. Activating the converter switches allows the converter to inject current into the system. The paper also mentioned that the technique may be performed using an active filter technique, but did not demonstrate it.

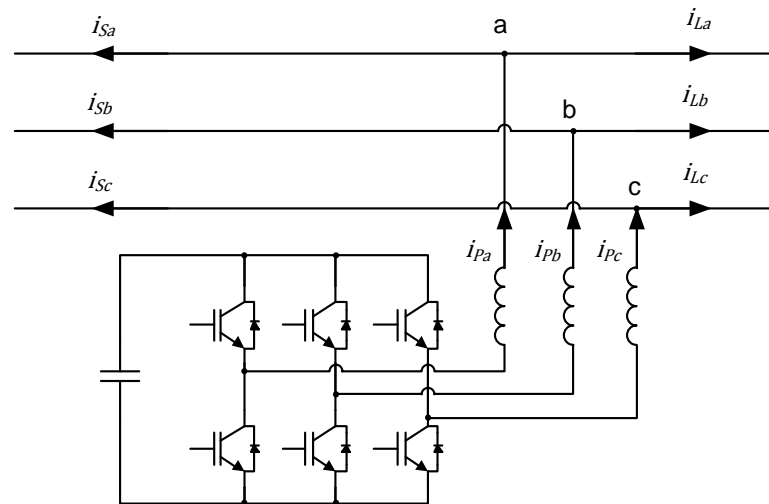


Figure 2-15: Shunt injection using power converter

To generate a sine waveform with a low distortion usually requires the switching frequency to be much higher than the injection frequency. But the switching frequency can be as low as the injection frequency when using the square disturbance waveform.

C. Chopped Impedances

Another technique used to generate disturbance is connecting modulated impedances into the system. A three-phase shunt-connected impedance is used in [82] (done with a three phase chopper circuit). Figure 2-16 shows the circuit used in [82]. Power semiconductor switches are

used to switch in and out some resistors continuously to create the perturbation. The injection is made smoother by using the additional series inductors.

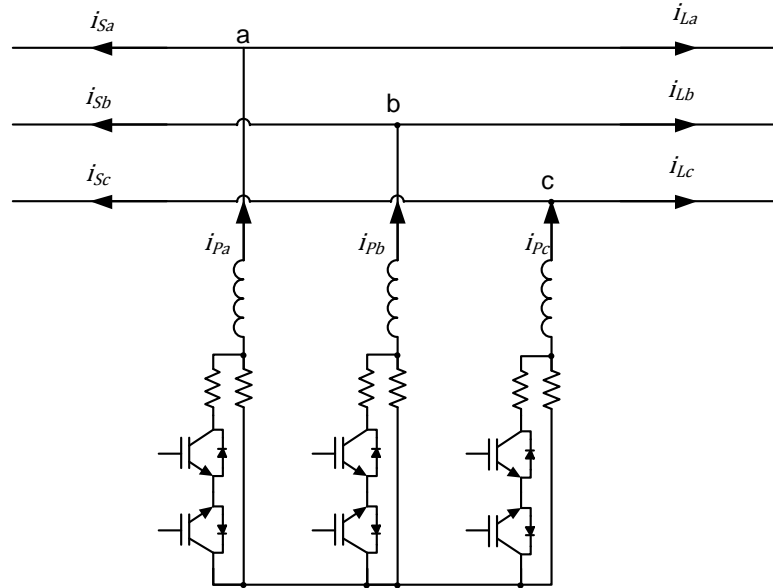


Figure 2-16: Shunt injection using chopped impedances

The switches are controlled open loop in [82] to follow some pattern. It results in time-variant impedances being connected into the system. The impedance variation repeats in a fixed frequency, creating the disturbance at that frequency. The chopper circuit can also be controlled to force the injected current following certain references. But the current injecting capability is not as flexible as the power converter's.

Depending on the modulation scheme used, the required switching frequency is similar to the power converters.

D. Wound rotor induction machine

Reference [89] also describes a case where a wound-rotor induction machine is used to inject a perturbation into the system. In this dissertation, a DC current is injected into the machine rotor winding and the machine is allowed to spin up to speed and synchronize with the system, after

which the perturbation can be injected on top of the DC signal. A disadvantage mentioned in this paper is that the induction machine must be sized for each application and power level. The machine injects onto all three phases as it rotates.

E. Load bank switched in or out

Switching a load bank in or out of a system is a simple way to create a step disturbance. The technique requires no high frequency switching, and is widely available for high power systems since similar equipment is used in the power system for reactive power compensation. The equipment can even be used directly as a disturbance source if the measurement target is the power system [69].

The problem with this method is that the disturbance magnitude is only controlled by the load bank itself. No other control can be involved. Thus adjustable load banks or many load banks are necessary to measure different power level systems.

F. Existing Power Converters in the System

Reference [81] generates perturbation using the existing converter in the system. This work injects the perturbation signal on the control signal of the converter which is directly connected to the interface to be measured. This approach requires no additional power device. By utilizing the sensing circuit of the converter, it requires no extra components. However, this approach requires intensive access to the control of the components in the system, which is unachievable in commercial systems.

2.5. Impedance Extraction Algorithm

After collecting the perturbation and voltage and current response, the impedance needs to be extracted via a certain algorithm. There are two approaches in literature to find the impedances: spectrum analysis and the model fitting.

2.5.1. Nonparametric Algorithms

Nonparametric algorithms have no assumption on the system, which introduce no limit on the transfer function to be identified. The algorithms used in literature are solving impedance from (1-7). As mentioned previously in this chapter, two independent perturbations are made to gather enough information to solve the impedance matrix. The result is (2-18), which is repeated at each frequency point using the data from two perturbations.

$$\begin{bmatrix} Z_{dd}(s) & Z_{dq}(s) \\ Z_{qd}(s) & Z_{qq}(s) \end{bmatrix} = \begin{bmatrix} v_{d1}(s) & v_{d2}(s) \\ v_{q1}(s) & v_{q2}(s) \end{bmatrix} \begin{bmatrix} i_{d1}(s) & i_{d2}(s) \\ i_{q1}(s) & i_{q2}(s) \end{bmatrix}^{-1} \quad (2-18)$$

This requires obtaining the magnitude and phase information at the measuring frequency. They can be obtained by the following ways.

A. Simply Convolution

A simple convolution is calculated in the way shown in (2-19). It extracts the signal at the injection frequency ω that is known before processing, and filters out all the other frequencies. It is effective, but works at a single frequency.

$$cs = LPF \left(\int_0^{\frac{k2\pi}{\omega}} f(t) \sin(\omega t) \right), cc = LPF \left(\int_0^{\frac{k2\pi}{\omega}} f(t) \cos(\omega t) \right) \quad (2-19)$$

$$\text{Amp} = \frac{\omega}{\pi} \sqrt{cs^2 + cc^2}, \text{Phase} = \arctan \left(\frac{cc}{cs} \right)$$

The method is used in [83]. It is also likely to be used if a commercial gain/phase analyzer is used.

B. Fast Fourier Transformation (FFT)

FFT is a fast way of doing discrete Fourier Transformation, which can be treated as parallel convolution. It reveals the information on all frequencies at a time, which is fast and efficient. But if non-integral periods of the signal are sampled, the leakage effect may change the obtained spectrum from the actual one. Extra caution should be taken when it is used. There are several

ways to reduce the leakage effect such as windowing. However, when wide-bandwidth excitation is used, it is the most common choice of spectrum [83, 91].

2.5.2. Parametric Algorithms

Nonparametric algorithms assume no knowledge about the system to be measured. If there is some knowledge about the system model, the system can also be represented using a model with certain parameters. Then these parameters are fitted using the acquired voltage and current information. The impedance information can later be obtained from the model.

A. Time Domain System Identification

The system model can be obtained through a time domain system identification approach. There are many algorithms on the topic. Usually, an impedance term is modeled as a division of two polynomials with a limit order. The impedance matrixes in (1-8) model a MIMO system. But up to now, the system is only identified as a single-input single-output system in [95]. The paper assumes the perturbation to the source can be concentrated on one channel and the other channel is kept zero. Thus the impedances are decoupled, and mature model fitting technology can be used. Some commercial tools such as MatLAB provide the toolbox to simplify the fitting work. The orders of polynomials should be high enough to capture the dynamics of the system. Although this model is just an approximation of the real system, it looks like a good match between the simulation using a frequency sweep and experiment using this method in [95].

B. Neural Network

A neural network is another good method to model a system when the system internal details are not known. In [86-88], recurrent neural networks are used to model the system. A pseudo-random PWM pattern is used to generate a nearly white noise to train the network. After the training, the network behaves similar to the system to be measured, and can be treated as a model of the physical system. Although this is a good way to model the system, it does not

directly reveal the impedance of the system. So there is an additional step: a frequency sweep using a sine wave and the FFT technique to obtain the impedance from the model.

Chapter 3. Measurement Error Analysis

Measurement error is an important topic for measurement equipment. So far, no paper has been published which investigates error analysis for the impedance measurement in three-phase systems, although in [104] the repeatability of the measurements was briefly discussed, providing error bands based on statistical variation of 30 repeated measurements.

In this chapter, the main systematical error sources are analyzed. Solution to reduce the influence of some of the error sources are discussed.

3.1. Error Propagation Path

The impedance measurement system is a complex system. The measurement starts at the sensors and analog signal processing circuits before the signal get digitalized. These sensing related components have their own transfer characteristics, which can reflect in the measurement result. There is quantification error when the signal gets digitalized. The computation techniques used in all the approaches can also produce unexpected errors. These errors may not be obvious, as the transformation to rotating coordinates generates a frequency shift, and the multi-input, multi-output nature of the system allows opportunities for these errors to cross-couple between channels, further complicating the analysis.

It still remains an open question as to how much error is in the computed impedance based on what is measured in the actual system. The only way to improve such systems and to analyze their correctness is to systematically identify the sources of error and their effect on the reported measurement results.

Figure 3-1 illustrates the impedance analyzer previously built by our group. Perturbation references are generated in dq frame, then transferred into abc frame. The linear power amplifiers inject the perturbation current into the system in shunt following the references. The interface voltages and currents are acquired in abc frame then transferred into dq frame. The dq frame voltages and currents signals are sent to a network analyzer to identify the magnitude and phase of signals. A host computer collect these then calculate the system impedances from them.

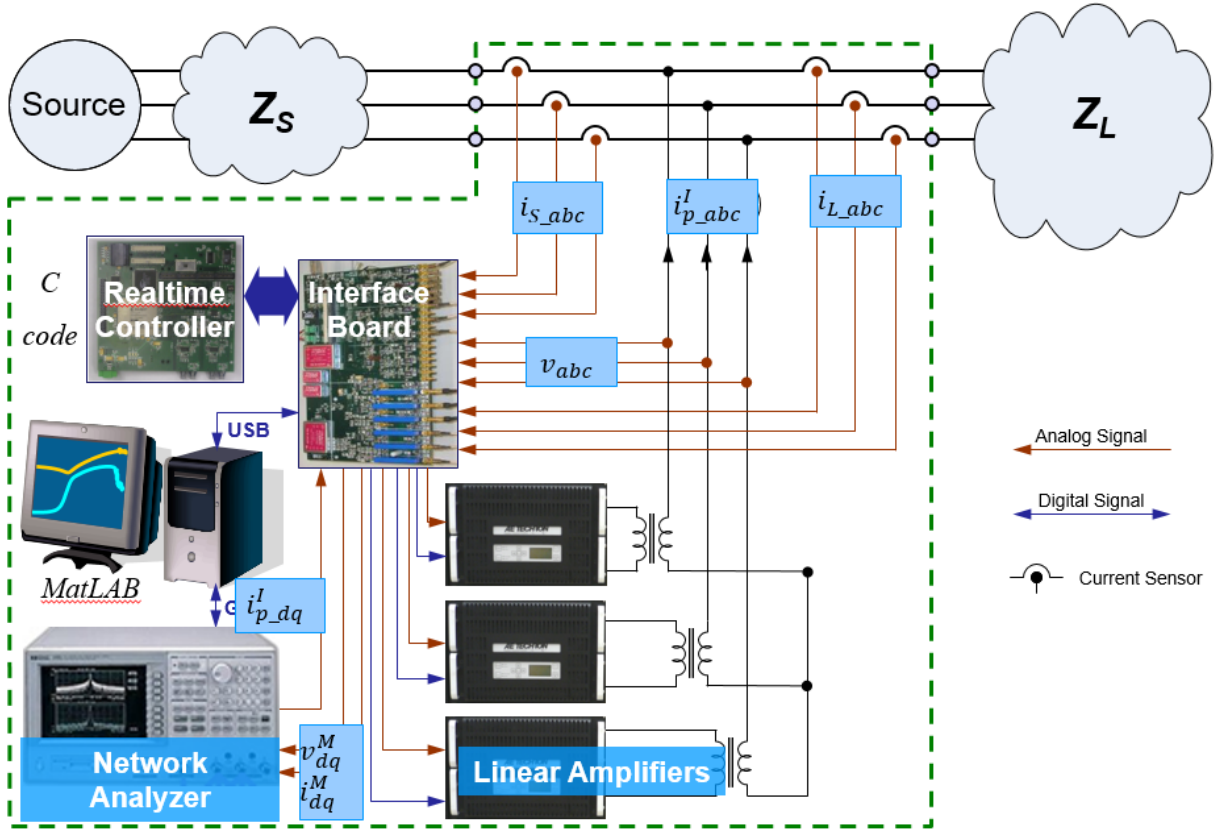


Figure 3-1: Previous impedance measurement analyzer in CPES

Figure 3-2 shows the system diagram of this measurement setup. The setup is divided into three subsystems. The system under test is modeled in the dq frame. Z_s and Y_L are source side impedance and load side admittance. There is no dq frame in physical systems, the interface to the measurement equipment is done in the abc frame. The dq frame model is transferred into the abc frame using the system phase θ^s , which is an independent variable determined only by the system operation. The processing in measurement subsystem is aggregated into three steps. The transfer functions H_x describes the processing in the abc frame, which includes the sensor transfer functions, the transfer functions of signal conditioning circuit, and the analog to digital conversion. The next step is to transform the coordinates from the abc frame to the dq frame. The phase θ^M used for the transformation is estimated by a phase detection model from the interface voltage. Then the transfer functions G_x represent all the processing happening in the dq frame. Each of these steps can generate errors. The output of the measurement subsystem is the interface voltages and currents in the dq frame. Further calculation is required to produce the impedance result. The algorithm used produces additional errors.

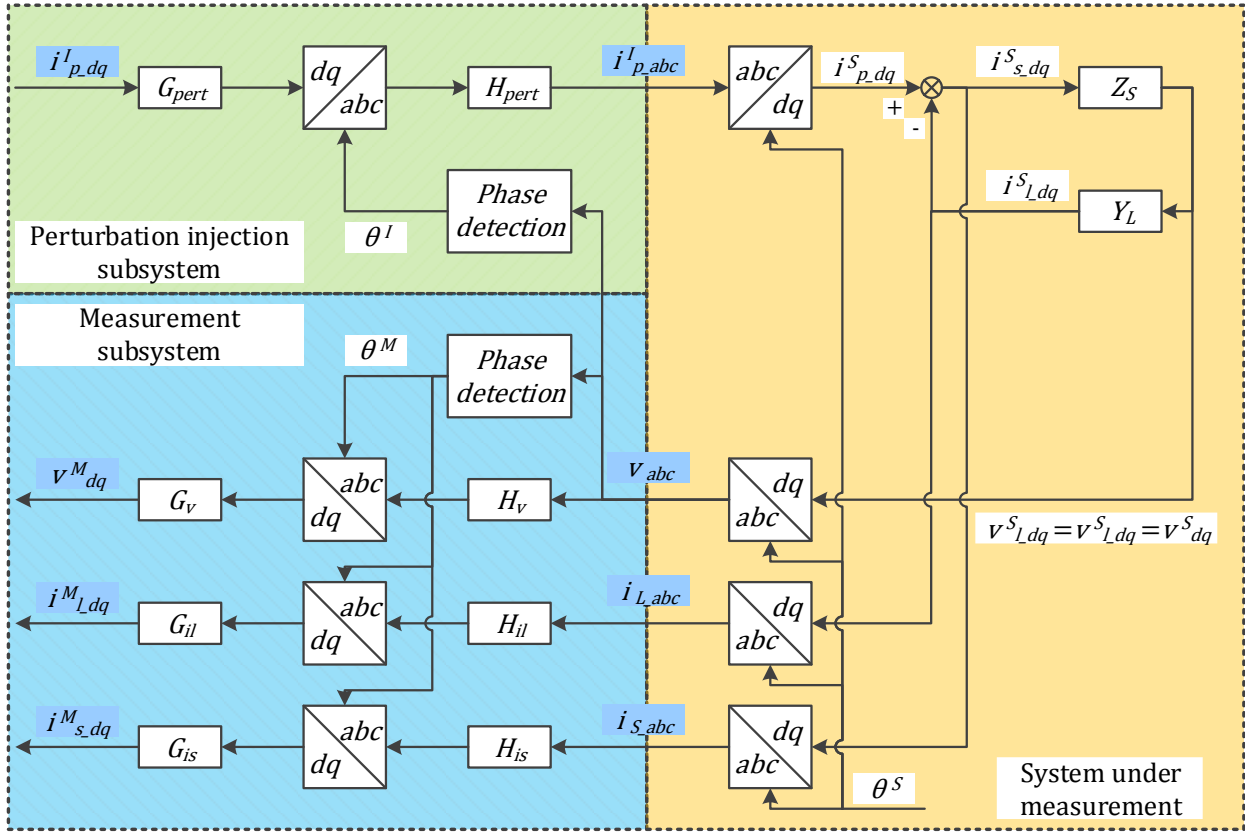


Figure 3-2: Impedance measurement system when shunt injection is used

As described in [93], the impedance can be correctly measured only if all the transfer functions are characterized. However, these transfer functions are usually ideally treated in literature as simple gains.

The perturbation injection subsystem is also a mandatory part of the measurement setup. It does not directly generate any error on the measurement result. But the quality of generated perturbation affects the signal-to-noise ratio of the measured signal, which influences the measurement result.

3.2. Transfer Functions in Abc Frame

The impedances are defined using dq frame variables. The systems are modeled in the dq frame. Thus all the blocks in Figure 3-2 and Figure 3-16 should be transferred into the dq frame for analysis. However, the voltages and currents can only be measured in the abc frame. The

transfer functions of the measuring components and processing procedures in the *abc* frame aggregate in to a single one in the figures. These components and procedures include sensors, signal conditioning circuits, analog-to-digital convertors and the digital signal processing that is carried in the *abc* frame.

If the transfer functions of all three phases are the same, the transfer function matrix can be transferred into the *dq* frame as described in [93]. The transfer functions can be written in matrix form as:

$$\mathbf{H}_{abc}(s) = \begin{bmatrix} H_a(s) & 0 & 0 \\ 0 & H_b(s) & 0 \\ 0 & 0 & H_c(s) \end{bmatrix} \quad (3-1)$$

where $H_a(s) = H_b(s) = H_c(s) = H(s)$ is the transfer function of one phase of the system.

Defining the two operators **CMOD** and **SMOD** as:

$$\mathbf{CMOD}(H(s), \omega) \equiv \frac{1}{2} (H(s + j\omega) + H(s - j\omega)) \quad (3-2)$$

$$\mathbf{SMOD}(H(s), \omega) \equiv \frac{1}{2j} (-H(s + j\omega) + H(s - j\omega)) \quad (3-3)$$

So $\mathcal{L}\{h(t) \cos(\omega t)\} = \mathbf{CMOD}(H(s), \omega)$, $\mathcal{L}\{h(t) \sin(\omega t)\} = \mathbf{SMOD}(H(s), \omega)$ where $H(s) = \mathcal{L}\{h(t)\}$.

The system described by (3-1) can be transferred into the *dq* frame using the defined operators as:

$$\mathbf{H}_{dq}(s) = \begin{bmatrix} \mathbf{CMOD}(H(s), \omega) & \mathbf{SMOD}(H(s), \omega) \\ -\mathbf{SMOD}(H(s), \omega) & \mathbf{CMOD}(H(s), \omega) \end{bmatrix} \quad (3-4)$$

As described in section 2.1.3, if the transfer functions $H_a(s)$, $H_b(s)$, $H_c(s)$ are not identical, the system behavior is nonlinear in the *dq* frame. Thus no transfer function exists to

describe the behavior. However, the nonlinear behavior is well defined: one phase-sequence component input in the dq frame generates two phase-sequence components at output.

Let the input be a dq frame phase-sequence component $x_{dq_pn}(\omega, X, \phi, t)$, which is defined by (2-9). For a system with fundamental angular frequency ω_s , it corresponds to the abc frame phase-sequence component $x_{abc_pn}(\omega + \omega_s, \sqrt{\frac{2}{3}}X, \phi, t)$ which is defined by (2-6). The output of system (3-1) is:

$$\mathbf{y}_{abc}(t) = \sqrt{\frac{2}{3}} \begin{bmatrix} |H_a(j\omega + j\omega_s)| \cdot X \cdot \cos[(\omega + \omega_s)t + \phi + \angle H_a(j\omega + j\omega_s)] \\ |H_b(j\omega + j\omega_s)| \cdot X \cdot \cos\left[(\omega + \omega_s)t + \phi - \frac{2\pi}{3} + \angle H_b(j\omega + j\omega_s)\right] \\ |H_c(j\omega + j\omega_s)| \cdot X \cdot \cos\left[(\omega + \omega_s)t + \frac{2\pi}{3} + \phi + \angle H_c(j\omega + j\omega_s)\right] \end{bmatrix} \quad (3-5)$$

$\mathbf{y}_{abc}(t)$ can be decomposed to phase-sequence components:

$$\begin{aligned} \mathbf{y}_{abc}(t) = M_p \begin{bmatrix} X \cdot \cos[(\omega + \omega_s)t + \phi + \theta_p] \\ X \cdot \cos\left[(\omega + \omega_s)t + \phi - \frac{2\pi}{3} + \theta_p\right] \\ X \cdot \cos\left[(\omega + \omega_s)t + \frac{2\pi}{3} + \phi + \theta_p\right] \end{bmatrix} + M_n \begin{bmatrix} X \cdot \cos[(\omega + \omega_s)t + \phi + \theta_n] \\ X \cdot \cos\left[(\omega + \omega_s)t + \phi + \frac{2\pi}{3} + \theta_n\right] \\ X \cdot \cos\left[(\omega + \omega_s)t - \frac{2\pi}{3} + \phi + \theta_n\right] \end{bmatrix} \\ + M_o \begin{bmatrix} X \cdot \cos[(\omega + \omega_s)t + \phi + \theta_o] \\ X \cdot \cos\left[(\omega + \omega_s)t + \phi + \frac{2\pi}{3} + \theta_o\right] \\ X \cdot \cos\left[(\omega + \omega_s)t - \frac{2\pi}{3} + \phi + \theta_o\right] \end{bmatrix} \end{aligned} \quad (3-6)$$

where

$$\begin{aligned} M_p &= \frac{|H_a(j\omega + j\omega_s) + H_b(j\omega + j\omega_s) + H_c(j\omega + j\omega_s)|}{3} \\ M_n &= \frac{|H_a(j\omega + j\omega_s) + H_b(j\omega + j\omega_s) \cdot e^{j\frac{2\pi}{3}} + H_c(j\omega + j\omega_s) \cdot e^{-j\frac{2\pi}{3}}|}{3} \\ M_o &= \frac{|H_a(j\omega + j\omega_s) + H_b(j\omega + j\omega_s) \cdot e^{-j\frac{2\pi}{3}} + H_c(j\omega + j\omega_s)|}{3} \end{aligned} \quad (3-7)$$

$$\begin{aligned}\theta_p &= \angle(H_a(j\omega + j\omega_s) + H_b(j\omega + j\omega_s) + H_c(j\omega + j\omega_s)) \\ \theta_n &= \angle\left(H_a(j\omega + j\omega_s) + H_b(j\omega + j\omega_s) \cdot e^{j\frac{2\pi}{3}} + H_c(j\omega + j\omega_s) \cdot e^{-j\frac{2\pi}{3}}\right) \\ \theta_o &= \angle\left(H_a(j\omega + j\omega_s) + H_b(j\omega + j\omega_s) \cdot e^{-j\frac{2\pi}{3}} + H_c(j\omega + j\omega_s) \cdot e^{j\frac{2\pi}{3}}\right)\end{aligned}$$

As shown by (2-10), the positive-sequence component is mapped to the excitation frequency ω_s in the **dq** frame; the negative-sequence component is mapped to the frequency $-\omega - 2\omega_s$ in the **dq** frame; the zero-sequence component is not mapped into the **dq** frame.

When the frequency sweep method is used, only the component at excitation frequency is measured, which is the positive-sequence component in (3-6). The transfer function matrix (3-1) is equivalent to

$$\begin{bmatrix} \frac{H_a(s) + H_b(s) + H_c(s)}{3} & 0 & 0 \\ 0 & \frac{H_a(s) + H_b(s) + H_c(s)}{3} & 0 \\ 0 & 0 & \frac{H_a(s) + H_b(s) + H_c(s)}{3} \end{bmatrix} \quad (3-8)$$

which can be transferred into the **dq** frame using (3-4). Then the normal calculation in can be used to calculate the impedance matrix.

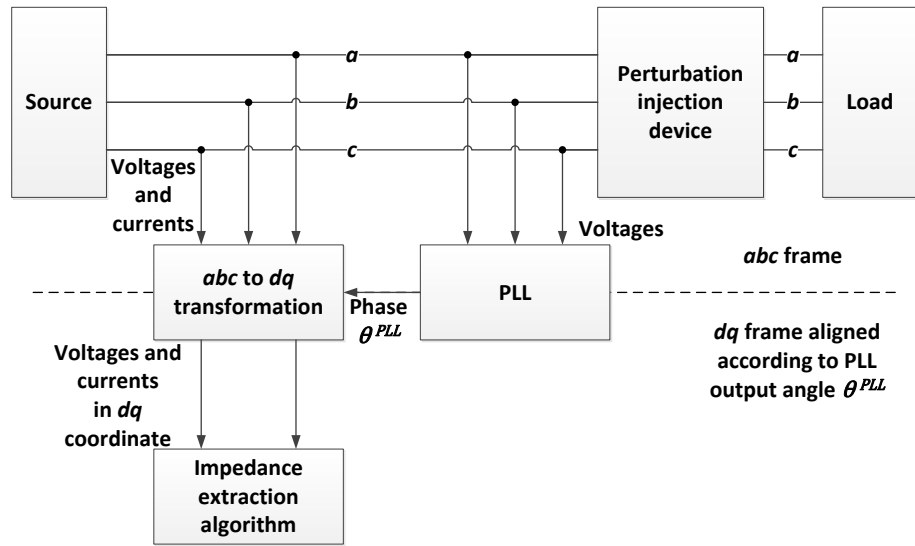
3.3. Coordinate Transformation

When all the measured **abc** frame variables are transferred into then **dq** frame, the phase used is obtained from the measured voltages, which may be different from the system real phase. The phase error is propagated through the system and causes impedance result errors.

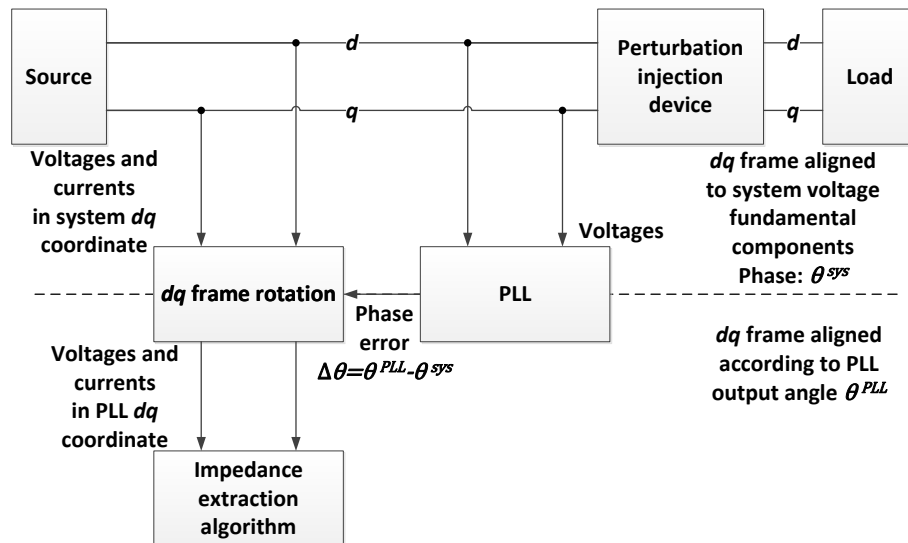
PLL is the preferred method to identify the system voltage phase information to be able to track the system frequency and phase drift during the measurement. But the dynamic of the PLL also shows up in the measurement result. It is stated in [93] that the injected perturbation will cause sinusoidal fluctuations in the observed line frequency by PLL. But no further discussion is made.

Figure 3-3(a) gives the block diagram of a setup measuring source side impedance. Disturbances are created by the perturbation injection device inserted between source and load.

The voltage and current responses at the interface are measured and transferred into a dq frame using the phase θ^p estimated by the PLL. The impedance is calculated using the responses in the dq frame. The system can be also represented in its own dq frame, which is defined by the phase of the system fundamental frequency voltage $\theta^{sys} = \omega^{sys}t$, where ω^{sys} is the system frequency. Figure 3-3 (b) shows the equivalent diagram when the system is represented in the dq frame. The estimated system phase θ^{PLL} usually contains a small error. The measured response in the frame defined by θ^{PLL} can be obtained by rotating the frame by the phase error $\Delta\theta$.



(a) abc coordinates



(b) dq coordinates

Figure 3-3: Impedance measurement setup in three-phase systems

Figure 3-4 shows a typical PLL for three-phase systems [105, 106]. The three-phase voltages are transferred into dq frame. The q -axis voltage contains the phase error information and is fed into the algorithm. The voltage is passed through a loop filter which is usually implemented by a proportional-integral (PI) regulator. The output of the filter is the angular speed. Then it is integrated to obtain the phase information. The value of phase is usually limited within 0 and 2π by adding or subtracting integral times of 2π when it goes outside the range.

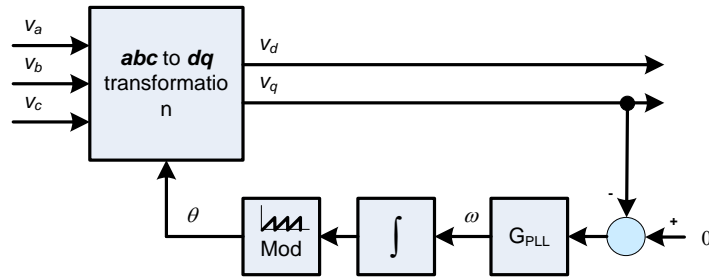


Figure 3-4: Typical D-Q Phase Locked Loop

Going along the loop, the effect of the PLL on the measurement can be analyzed. Accurate, steady phase information is required during the measurement to correctly transfer the variables between the abc frame and the dq frame. The information can be provided by the ideal voltage source shown in Figure 1-1 and Figure 1-2. But these voltages are not accessible practically. Only the voltages at the interface can be measured. The two groups of voltages have a constant phase shift in steady state. Let $\theta^{SYS}(t)$ represent the phase shifted by a constant value and aligned at the phase a voltage of the steady state without any perturbation.

The interface voltage vector at steady state in dq frame is:

$$\mathbf{V}_{dq0.0}^{SYS} = \begin{bmatrix} V_{d.0}^{SYS} \\ V_{q.0}^{SYS} \\ 0 \end{bmatrix} \quad (3-9)$$

which is a constant vector. The superscripts SYS denotes the dq transformation using the phase $\theta^{SYS}(t)$ determined by the equivalent ideal voltage sources.

An additional term is generated when perturbation is injected:

$$\Delta \mathbf{v}_{dqo}^{sys}(t) = \begin{bmatrix} \Delta v_d^{sys}(t) \\ \Delta v_q^{sys}(t) \\ 0 \end{bmatrix} \quad (3-10)$$

The total interface voltage vector is:

$$\mathbf{v}_{dqo}^{sys}(t) = \mathbf{V}_{dqo,0}^{sys} + \Delta \mathbf{v}_{dqo}^{sys}(t) \quad (3-11)$$

Transfer the vector into the **abc** frame to get the voltages at real physical interface:

$$\mathbf{v}_{abc}^{sys}(t) = \mathbf{T}_{abc}(\omega^{sys}t) \mathbf{v}_{dqo}^{sys}(t) \quad (3-12)$$

Let $\theta^{PLL}(t)$ be the phase observed by PLL. The measured voltages in dq frame are:

$$\mathbf{v}_{dqo}^{PLL}(t) = \mathbf{T}_{abc}(\theta^{PLL}(t)) \mathbf{v}_{abc}^{sys}(t) \quad (3-13)$$

In steady state, $\theta^{PLL}(t) = \omega^{sys}t$. Considering PLL to have small phase error $\Delta\theta(t)$ during the perturbation,

$$\begin{aligned} \mathbf{v}_{dqo}^{PLL}(t) &= \mathbf{T}_{abc}(\omega^{sys}t + \Delta\theta(t)) \mathbf{v}_{abc}^{sys}(t) \\ &= \sqrt{\frac{2}{3}} \begin{bmatrix} \cos(\omega^{sys}t + \Delta\theta(t)) & \cos\left(\omega^{sys}t + \Delta\theta(t) - \frac{2\pi}{3}\right) & \cos\left(\omega^{sys}t + \Delta\theta(t) + \frac{2\pi}{3}\right) \\ -\sin(\omega^{sys}t + \Delta\theta(t)) & -\sin\left(\omega^{sys}t + \Delta\theta(t) - \frac{2\pi}{3}\right) & -\sin\left(\omega^{sys}t + \Delta\theta(t) + \frac{2\pi}{3}\right) \\ \frac{\sqrt{2}}{2} & \frac{\sqrt{2}}{2} & \frac{\sqrt{2}}{2} \end{bmatrix} \mathbf{v}_{abc}^{sys}(t) \end{aligned} \quad (3-14)$$

For $\Delta x \approx 0$, $\cos(x + \Delta x) \approx \cos(x) - \Delta x \cdot \sin(x)$, $\sin(x + \Delta x) \approx \sin(x) + \Delta x \cdot \cos(x)$

Thus, if the phase error $\Delta\theta$ is small,

$$\begin{aligned}
\mathbf{v}_{dqo}^{PLL}(t) &\approx \sqrt{\frac{2}{3}} \begin{bmatrix} \cos(\omega^{sys}t) & \cos\left(\omega^{sys}t - \frac{2\pi}{3}\right) & \cos\left(\omega^{sys}t + \frac{2\pi}{3}\right) \\ -\sin(\omega^{sys}t) & -\sin\left(\omega^{sys}t - \frac{2\pi}{3}\right) & -\sin\left(\omega^{sys}t + \frac{2\pi}{3}\right) \\ \frac{\sqrt{2}}{2} & \frac{\sqrt{2}}{2} & \frac{\sqrt{2}}{2} \end{bmatrix} \mathbf{v}_{abc}^{sys}(t) \\
&\quad + \sqrt{\frac{2}{3}} \Delta\theta(t) \begin{bmatrix} -\sin(\omega^{sys}t) & -\sin\left(\omega^{sys}t - \frac{2\pi}{3}\right) & -\sin\left(\omega^{sys}t + \frac{2\pi}{3}\right) \\ -\cos(\omega^{sys}t) & -\cos\left(\omega^{sys}t - \frac{2\pi}{3}\right) & -\cos\left(\omega^{sys}t + \frac{2\pi}{3}\right) \\ \frac{\sqrt{2}}{2} & \frac{\sqrt{2}}{2} & \frac{\sqrt{2}}{2} \end{bmatrix} \mathbf{v}_{abc}^{sys}(t) \quad (3-15) \\
&= \mathbf{v}_{dqo}^{sys}(t) + \Delta\theta(t) \begin{bmatrix} 0 & 1 & 0 \\ -1 & 0 & 0 \\ 0 & 0 & 1 \end{bmatrix} \mathbf{v}_{dqo}^{sys}(t) \\
&= \mathbf{V}_{dqo.0}^{sys} + \Delta\mathbf{v}_{dqo}^{sys}(t) + \Delta\theta(t) \begin{bmatrix} 0 & 1 & 0 \\ -1 & 0 & 0 \\ 0 & 0 & 1 \end{bmatrix} (\mathbf{V}_{dqo.0}^{sys} + \Delta\mathbf{v}_{dqo}^{sys}(t))
\end{aligned}$$

The term $\Delta\theta(t) \begin{bmatrix} 0 & 1 & 0 \\ -1 & 0 & 0 \\ 0 & 0 & 1 \end{bmatrix} \Delta\mathbf{v}_{dqo}^{sys}(t)$ is infinitesimal of higher order and is ignored.

Convert all the rest of the variables into S-domain:

$$\mathbf{V}_{dqo}^{PLL}(s) \approx \mathbf{V}_{dqo.0}^{sys} + \Delta\mathbf{V}_{dqo.inj}^{sys}(s) + \Delta\Theta(s) \begin{bmatrix} 0 & 1 & 0 \\ -1 & 0 & 0 \\ 0 & 0 & 1 \end{bmatrix} \mathbf{V}_{dqo.0}^{sys} \quad (3-16)$$

From the PLL diagram in Figure 3-4, we have:

$$\Delta\Theta(s) = \frac{G_{PLL}(s)}{s} \cdot \tilde{V}_q^{PLL}(s) \quad (3-17)$$

where $\tilde{V}_q^{PLL}(s)$ is the small signal portion of the q -axis voltage calculated using phase from the PLL.

$V_q^{PLL}(s)$ can be solved from (3-16):

$$V_q^{PLL}(s) = V_{q.0}^{sys} + \Delta V_q^{sys}(s) - \Delta\Theta(s) V_{d.0}^{sys} = V_q^{PLL} + \tilde{V}_q^{PLL}(s) \quad (3-18)$$

where V_q^{PLL} is the dc component of $V_q^{PLL}(s)$. Then $\Delta\theta(s)$ can be solved from (3-17) and (3-18) to be:

$$\Delta\theta(s) = \frac{G_{PLL}(s)}{s + V_{d.0}^{sys} \cdot G_{PLL}(s)} \Delta V_q^{sys}(s) \quad (3-19)$$

Define

$$H_{PLL}(s) = \frac{G_{PLL}(s)}{s + V_{d.0}^{sys} \cdot G_{PLL}(s)} \quad (3-20)$$

The observed voltage vector in dq frame can be expressed as:

$$\mathbf{V}_{dqo}^{PLL}(s) \approx \mathbf{V}_{dqo.0}^{sys} + \Delta \mathbf{V}_{dqo}^{sys}(s) + H_{PLL}(s) \Delta V_q^{sys} \begin{bmatrix} 0 & 1 & 0 \\ -1 & 0 & 0 \\ 0 & 0 & 1 \end{bmatrix} \Delta \mathbf{V}_{dqo}^{sys} \quad (3-21)$$

The small signal portion of $\mathbf{V}_{dqo}^{PLL}(s)$, which is used for the impedance calculation, is:

$$\begin{aligned} \tilde{\mathbf{V}}_{dqo}^{PLL}(s) &= \Delta \mathbf{V}_{dqo}^{sys}(s) + H_{PLL}(s) \Delta V_q^{sys} \begin{bmatrix} 0 & 1 & 0 \\ -1 & 0 & 0 \\ 0 & 0 & 1 \end{bmatrix} \mathbf{V}_{dqo.0}^{sys} \\ &= \begin{bmatrix} 1 & V_{q.0}^{sys} H_{PLL}(s) & 0 \\ 0 & 1 - V_{d.0}^{sys} H_{PLL}(s) & 0 \\ 0 & V_{o.0}^{sys} H_{PLL}(s) & 1 \end{bmatrix} \Delta \mathbf{V}_{dqo}^{sys} \end{aligned} \quad (3-22)$$

A similar approach can be followed for the currents. The result is:

$$\begin{aligned}
\tilde{\mathbf{I}}_{dqo}^{PLL}(s) &= \Delta \mathbf{I}_{dqo}^{sys}(s) + H_{PLL}(s) \Delta \mathbf{V}_q^{sys} \begin{bmatrix} 0 & 1 & 0 \\ -1 & 0 & 0 \\ 0 & 0 & 1 \end{bmatrix} \mathbf{I}_{dqo,0}^{sys} \\
&= \Delta \mathbf{I}_{dqo}^{sys}(s) + \begin{bmatrix} 0 & I_{q,0}^{sys} H_{PLL}(s) & 0 \\ 0 & -I_{d,0}^{sys} H_{PLL}(s) & 0 \\ 0 & I_{o,0}^{sys} H_{PLL}(s) & 0 \end{bmatrix} \Delta \mathbf{V}_{dqo}^{sys}
\end{aligned} \tag{3-23}$$

where $\tilde{\mathbf{I}}_{dqo}^{PLL}(s)$ is the small signal part of the observed current vector in the dq frame synchronized using PLL, $\Delta \mathbf{I}_{dqo}^{sys}(s)$ is the perturbation current in the dq frame synchronized with the ideal voltage sources, and $\mathbf{I}_{dqo,0}^{sys}$ is the system operating point current vector.

Ideally, we would like to solve the system impedance matrix $\mathbf{Z}^{sys}(s) = \begin{bmatrix} Z_{dd}^{sys}(s) & Z_{dq}^{sys}(s) \\ Z_{qd}^{sys}(s) & Z_{qq}^{sys}(s) \end{bmatrix}$

from

$$\mathbf{Z}^{sys}(s) = \left[\Delta \mathbf{V}_{dq,1}^{sys}(s), \Delta \mathbf{V}_{dq,2}^{sys}(s) \right] \left[\Delta \mathbf{I}_{dq,1}^{sys}(s), \Delta \mathbf{I}_{dq,2}^{sys}(s) \right]^{-1} \tag{3-24}$$

But instead of the vectors in the frame synchronized with the ideal voltage sources, the vectors which are calculated using the phase information from PLL are obtained. If these vectors are used to directly replace the voltage and current vectors in (3-24), the impedance matrix will be:

$$\begin{aligned}
\mathbf{Z}^{PLL}(s) &= \left[\Delta \mathbf{V}_{dq,1}^{PLL}(s), \Delta \mathbf{V}_{dq,2}^{PLL}(s) \right] \left[\Delta \mathbf{I}_{dq,1}^{PLL}(s), \Delta \mathbf{I}_{dq,2}^{PLL}(s) \right]^{-1} \\
&= \begin{bmatrix} 1 & V_{q,0}^{sys} H_{PLL}(s) \\ 0 & 1 - V_{d,0}^{sys} H_{PLL}(s) \end{bmatrix} \left[\Delta \mathbf{V}_{dq,1}^{sys}(s), \Delta \mathbf{V}_{dq,2}^{sys}(s) \right] \\
&\quad \cdot \left(\left[\Delta \mathbf{I}_{dq,1}^{sys}(s), \Delta \mathbf{I}_{dq,2}^{sys}(s) \right] \right. \\
&\quad \left. + \begin{bmatrix} 0 & I_{q,0}^{sys} H_{PLL}(s) \\ 0 & -I_{d,0}^{sys} H_{PLL}(s) \end{bmatrix} \left[\Delta \mathbf{V}_{dq,1}^{sys}(s), \Delta \mathbf{V}_{dq,2}^{sys}(s) \right] \right)^{-1}
\end{aligned} \tag{3-25}$$

From (3-24) and (3-25), the relation between \mathbf{Z}^{sys} and \mathbf{Z}^{PLL} can be derived:

$$\mathbf{Z}^{PLL}(s) = \begin{bmatrix} 1 & V_{q,0}^{sys} H_{PLL}(s) \\ 0 & 1 - V_{d,0}^{sys} H_{PLL}(s) \end{bmatrix} \left(\mathbf{Z}^{sys}(s)^{-1} + \begin{bmatrix} 0 & I_{q,0}^{sys} H_{PLL}(s) \\ 0 & -I_{d,0}^{sys} H_{PLL}(s) \end{bmatrix} \right)^{-1} \quad (3-26)$$

In (3-26), the transfer function of PLL is known from the design. The operating point voltages and currents can be saved before the measurement starts and are assumed to not change during the measurement. Thus, the actual system impedance $\mathbf{Z}^{sys}(s)$ can be solved:

$$\mathbf{Z}^{SYS}(s) = \left(\mathbf{Z}^{PLL}(s)^{-1} \cdot \begin{bmatrix} 1 & V_{q,0}^{sys} H_{PLL}(s) \\ 0 & 1 - V_{d,0}^{sys} H_{PLL}(s) \end{bmatrix} - \begin{bmatrix} 0 & I_{q,0}^{sys} H_{PLL}(s) \\ 0 & -I_{d,0}^{sys} H_{PLL}(s) \end{bmatrix} \right)^{-1} \quad (3-27)$$

To verify the conclusions, an impedance measurement system shown in Figure 3-5 is simulated. A series injection is used in the impedance measurement unit. The measurement frequency range is from 1 Hz to 200 Hz to show the influence of a PLL with a 50 Hz Bandwidth.

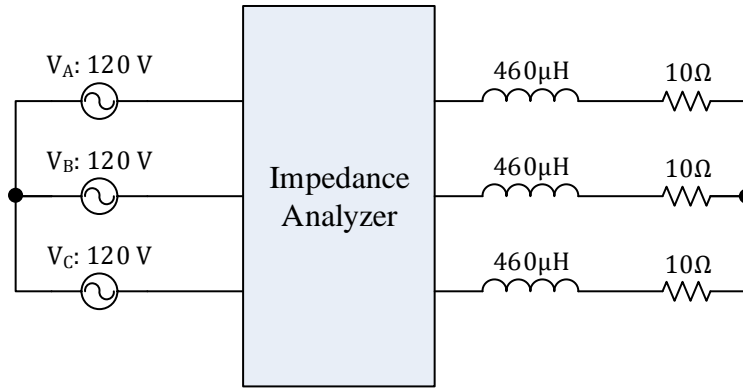


Figure 3-5: Simulation circuit of linear impedance extraction

The impedance is first extracted using the source phase as a known variable. Then the phase estimated by the PLL is used to extract the impedances again. The two results are shown in Figure 3-6 using solid lines and dotted lines correspondingly.

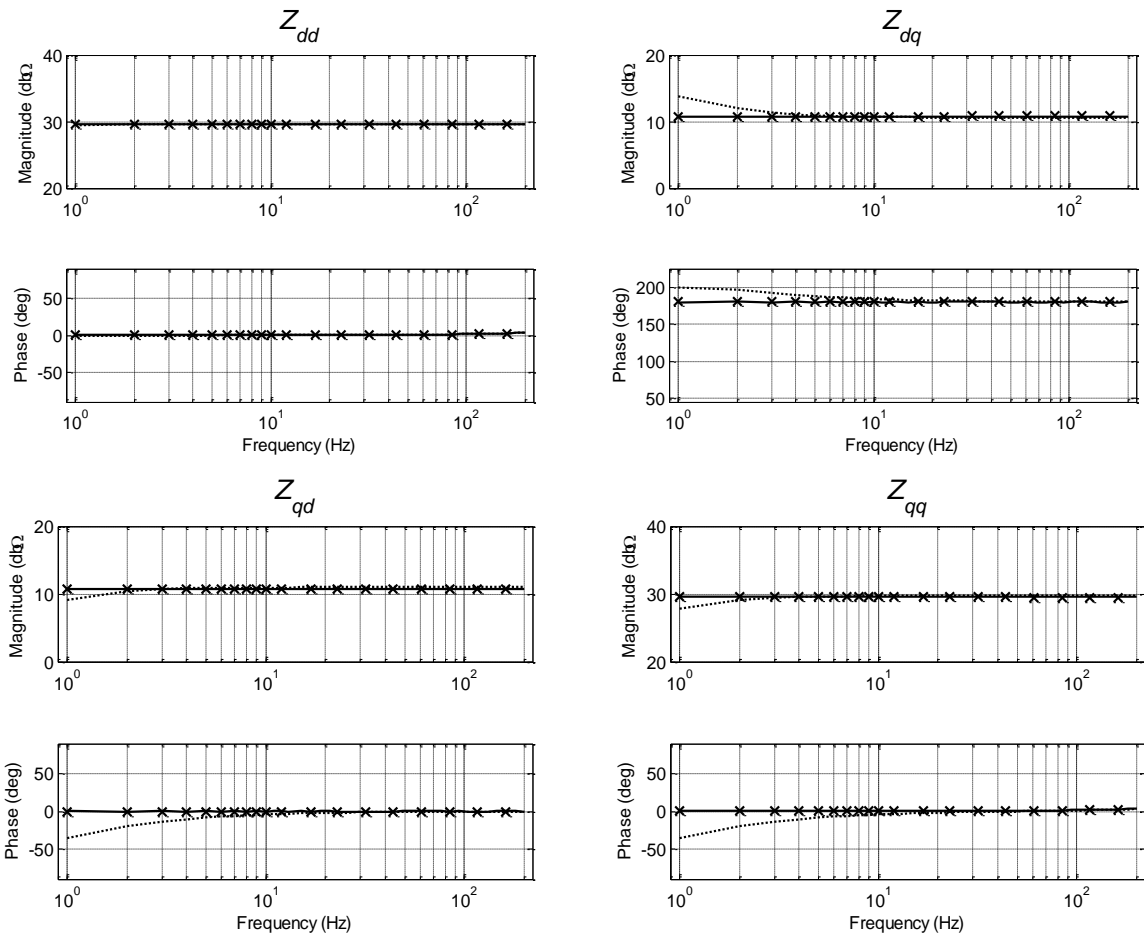


Figure 3-6: Extracted RL impedances in simulation (Solid line: no PLL; dotted line: 50 Hz bandwidth; 'x' markers: result back calculated from 50 Hz result)

It can be seen that using a PLL with a 50 Hz bandwidth, which is at the middle of the measurement frequency range, causes a huge error on the measurement result. However, the error can be significantly reduced by applying (3-27). The corrected points are shown in Figure 3-6. using 'x' markers, which are very close to the measurement results without the use of PLL.

A diode rectifier load is also simulated to verify the derivation under the nonlinear load. The simulation result is shown in Figure 3-7. The diode bridge parameters are shown in Figure 3-8.

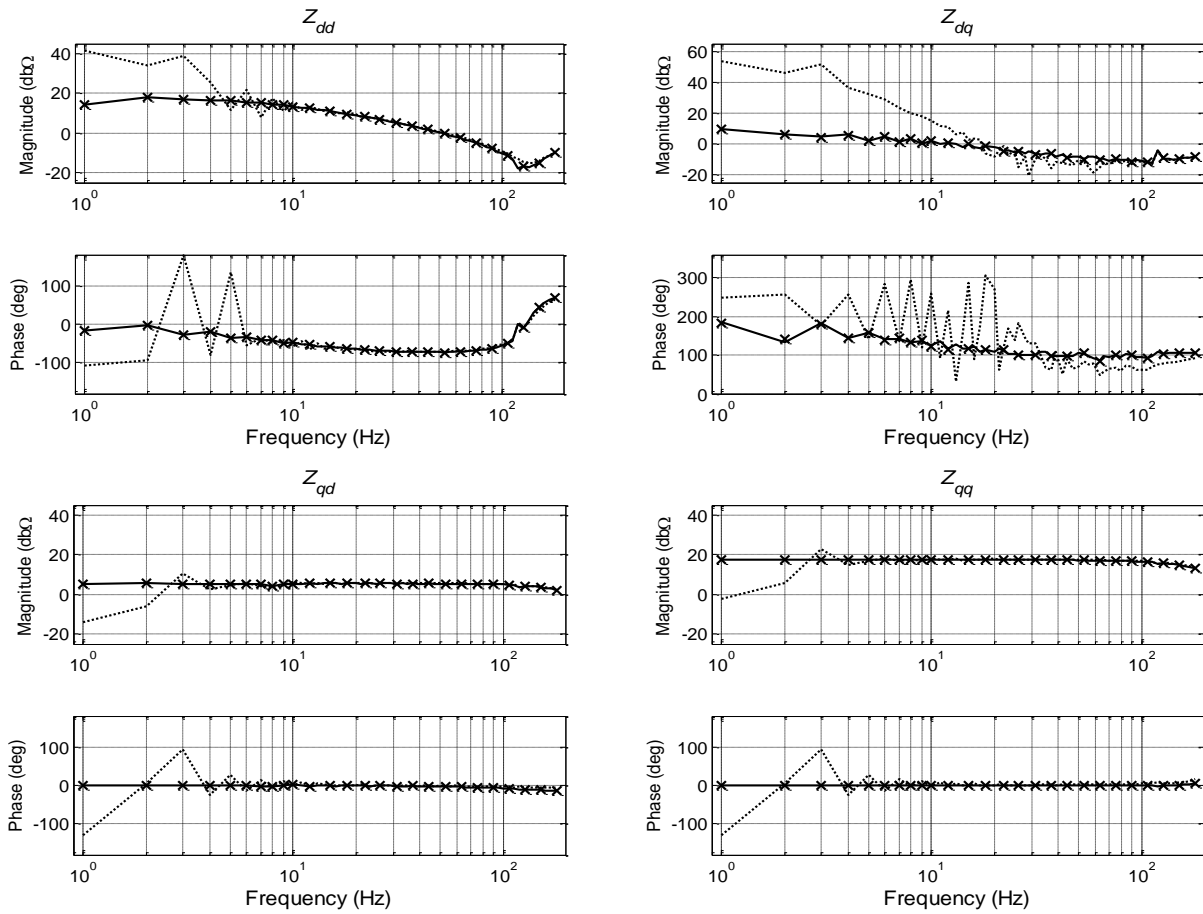


Figure 3-7: Extracted diode-rectifier impedances (Solid line: no PLL; dotted line: 50 Hz bandwidth; 'x' markers: result back calculated from 50 Hz result)

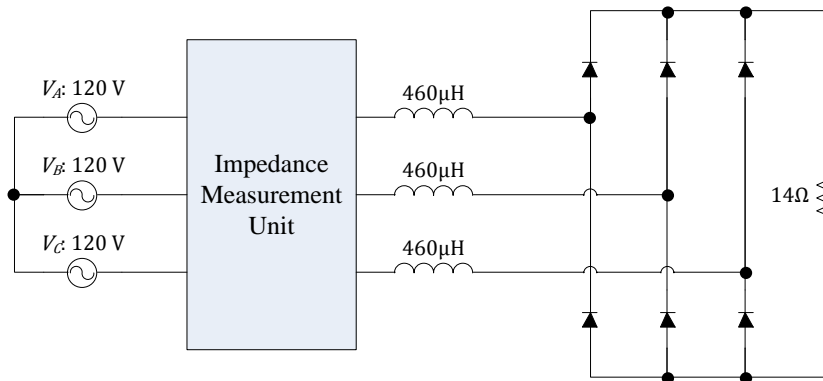


Figure 3-8: Simulation circuit of diode rectifier impedance extraction

The simulation results of the linear impedance extraction are also verified in the experiment. The obtained results are shown in Figure 3-9. Since the phase of the source voltages is unknown

in the experiment, the phase has been estimated by a PLL of 1 Hz bandwidth. Although the correction does not fully eliminate the error as in the simulation, the error is significantly reduced to produce an acceptable measurement result.

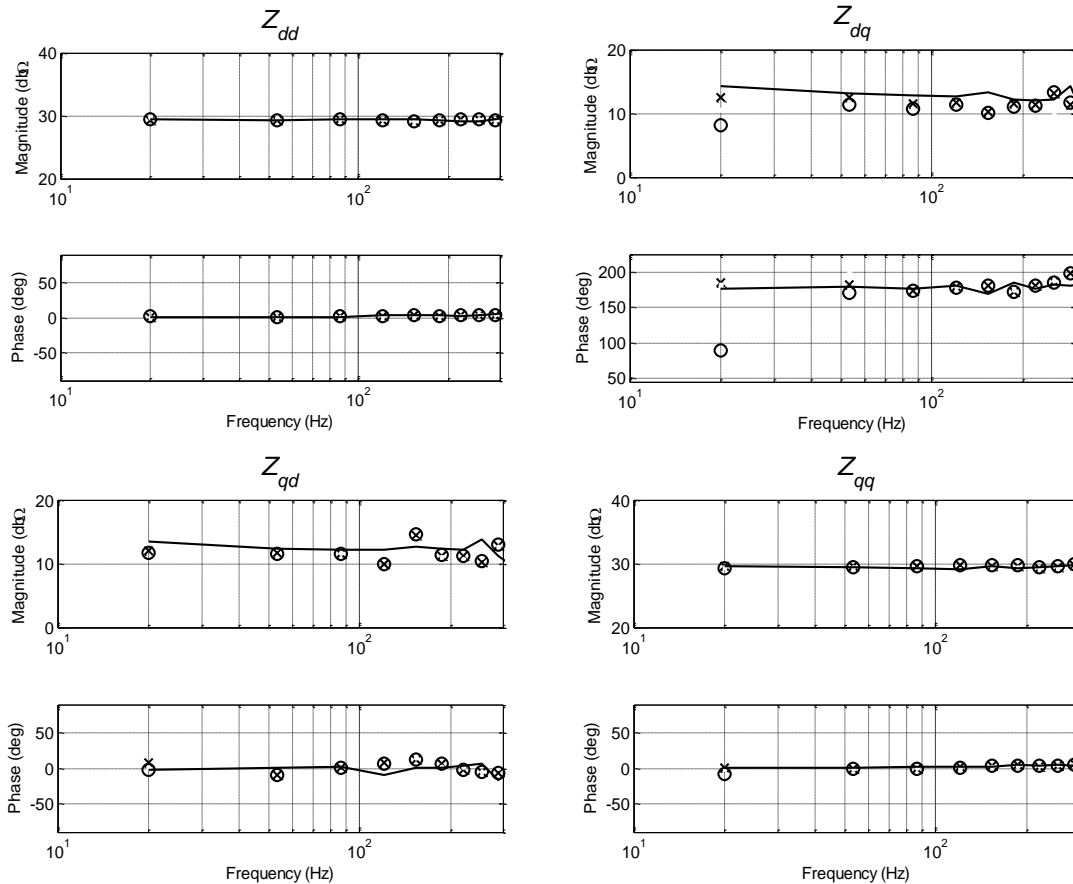


Figure 3-9: Measured RL impedances (Solid line: 1Hz PLL; 'x' markers: 50 Hz PLL; 'O' markers: result back calculated from 50 Hz result)

Besides the measurement path, the dynamics of PLL may also influence the perturbation generation in the measurement. The perturbation reference is usually generated in the dq frame first, and then transferred into the abc frame using the phase information provided by a PLL. The PLL can be the same or different from the PLL used for the measurements.

The influence of PLL depends on whether the controller of the perturbation generation device is implemented in the dq coordinates.

Figure 3-10 shows the block diagram of a perturbation injection device which runs open loop or has a controller in the *abc* coordinates. The system is also represented in the *dq* frame defined by the supply voltages, which is the same as in Figure 3-3(b).

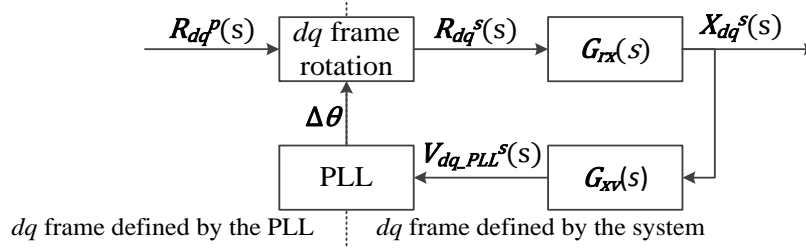


Figure 3-10: Perturbation injection unit block diagram when controller is in *abc* frame

$R_{dq}^p(s)$ is the perturbation reference in the PLL *dq* frame; $R_{dq}^s(s)$ is the reference transferred into the system *dq* frame; $X_{dq}^s(s)$ is the injected voltage or current; and $V_{dq_PLL}^s(s)$ is the voltage used by PLL; $G_{rx}(s)$ is the transfer function modeling the system characteristic and the *abc* frame controller behavior; $G_{xv}(s)$ is the transfer function from the injection to the voltages used by the PLL.

In this configuration, PLL only affects when the reference is transferred into the system *dq* frame. This influence can be derived through the same procedure as described previously for measurement path:

$$R_{dq}^p(s) = R_{dq}^s(s) + H_{PLL}(s) \begin{bmatrix} 0 & R_{q0}^s \\ 0 & -R_{d0}^s \end{bmatrix} V_{dq_PLL}^s(s) \quad (3-28)$$

where R_{d0}^s and R_{q0}^s are DC components of the reference signal.

The measurement frequency range usually does not include DC. Thus, the perturbation reference has no DC component, which makes $R_{dq}^s(s) = R_{dq}^p(s)$. The PLL has no influence on the injection-circuit transfer function.

When the control loop of the injection circuit is closed in the *dq* frame, the block diagram of the system is shown in Figure 3-11:

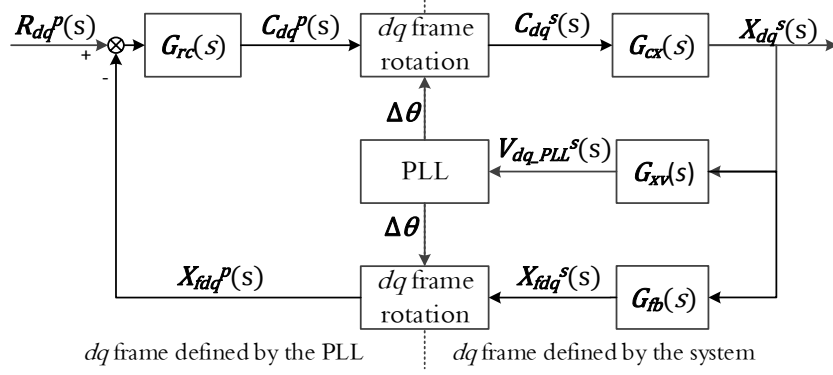


Figure 3-11: Perturbation injection unit block diagram when controller is in dq frame

$X_{fdq}^s(s)$ is feedback signal in system dq frame; $X_{fdq}^p(s)$ is the feedback signal transferred to PLL dq frame; $C_{dq}^p(s)$ is the intermediate control variable which is transferred from the dq frame to abc frame in the controller; $C_{dq}^s(s)$ is the control variable transferred to the system dq frame; $G_{rc}(s)$ is the controller in PLL dq frame; $G_{cx}(s)$ is the transfer function from the intermediate control variable to final output; $G_{fb}(s)$ is the feedback path transfer function; other symbols are the same as in Figure 3-10.

Ideally, the PLL tracks the system phase without any error. $C_{dq}^s(s) = C_{dq}^p(s)$ and $X_{fdq}^p(s) = X_{fdq}^s(s)$. In reality, the variables have similar relations like (3-28):

$$C_{dq}^p(s) = C_{dq}^s(s) + H_{PLL}(s) \begin{bmatrix} 0 & C_{q0}^s \\ 0 & -C_{d0}^s \end{bmatrix} V_{dq_PLL}^s(s) \quad (3-29)$$

$$X_{fdq}^p(s) = X_{fdq}^s(s) + H_{PLL}(s) \begin{bmatrix} 0 & X_{fq0}^s \\ 0 & -X_{fd0}^s \end{bmatrix} V_{dq_PLL}^s(s) \quad (3-30)$$

Since $R_{dq}^p(s)$ has no DC components, both X_{fd0}^s and X_{fq0}^s equal to zero if the controller has zero error in steady state. Although the transfer function from reference to output may change due to non-zero C_{d0}^s and C_{q0}^s , the output still follows the reference within the control bandwidth thanks to the closed loop control.

To summarize, the dynamics of PLL has little effect on the perturbation injection as long as there is no DC component in the reference.

A perturbation injection circuit shown in Figure 3-12 is simulated to verify the conclusion on the injection circuit. The controlled voltage sources with unit gain are used as an injection device. The circuit is expected to have the transfer function of:

$$\mathbf{G}_{rx}^s(s) = \begin{bmatrix} 1 & 0 \\ 0 & 1 \end{bmatrix} \quad (3-31)$$

which is validated using simulation as shown in Figure 3-13 by solid lines. The ‘x’ marks in the figure shows measured transfer function when a 50 Hz bandwidth PLL is used to provide the phase for the coordinate transformation. The result shows that PLL has nearly no effect on the transfer function except for the off-diagonal terms, which are still close to zero and can be ignored.

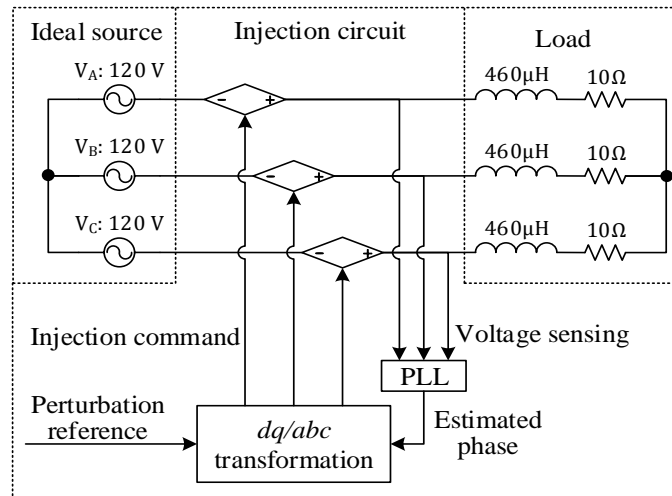


Figure 3-12: Simulated perturbation injection circuit

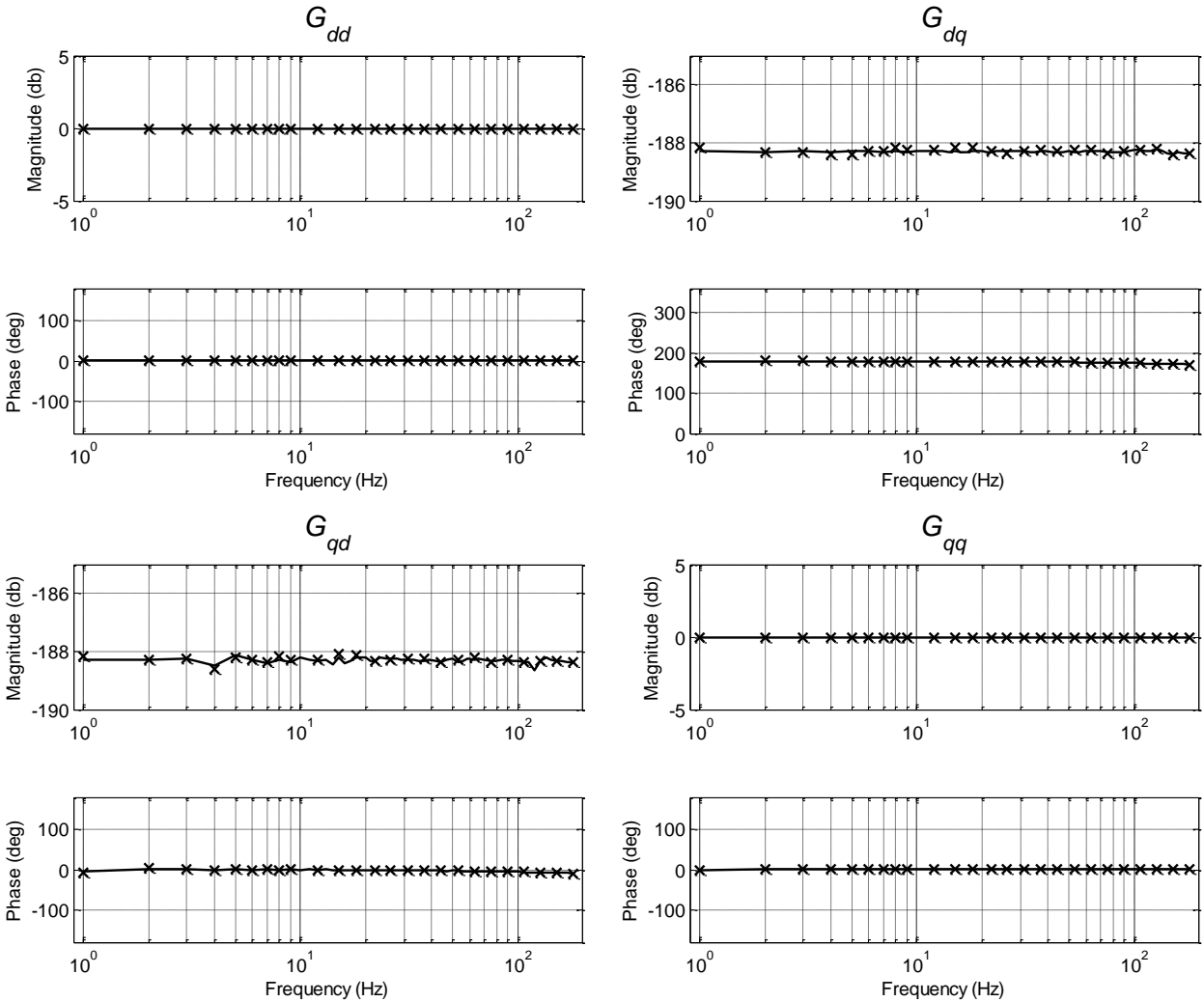


Figure 3-13: Simulated injection-circuit transfer functions (Solid line: no PLL; 'x' markers: 50 Hz bandwidth)

3.4. Perturbation Injection Mode

Signal to noise ratio (SNR) is an important parameter in measurement system. A lower SNR usually means a less accurate measurement. To increase SNR, there are usually two approaches. The first one is to decrease the noise level. In the design of the system, the noise level should be minimized. The suppression of noise is a complex topic, and is not discussed here. The other way to increase SNR is to increase the signal level. The injected perturbation level can be as high as the perturbation generation device is able to produce. But there is another limit. Since the

impedances measured are the small signal impedances at a certain operating point, the perturbation should not be so huge that the operating point is disturbed. This usually limits the injected power to only a few percent of the power of the system to be measured. It is mentioned in [93] that if the response is still too small to measure even the perturbation reaches its maximum allowable level, the system is not measurable. The system is also not measurable if the operating point is moved even with the minimum measurable injection level. Usually, a higher perturbation power within the allowable range generates a better result.

Besides the perturbation power, there is another factor that affects the measured signal level – the perturbation distribution in the system. System impedances are measured at an interface at which the system is divided into a load part and a source part. When a perturbation is injected, the perturbation energy splits into two portions. Either the source or load part of the system only gets one portion of the energy. Therefore, the interested part of the system may not be perturbed enough even when the maximum allowable perturbation level is used. While injecting the perturbation into the system, the distribution between source and load cannot be easily controlled without modifying the system. Take the system with shunt injection shown in Figure 3-14 as an example.

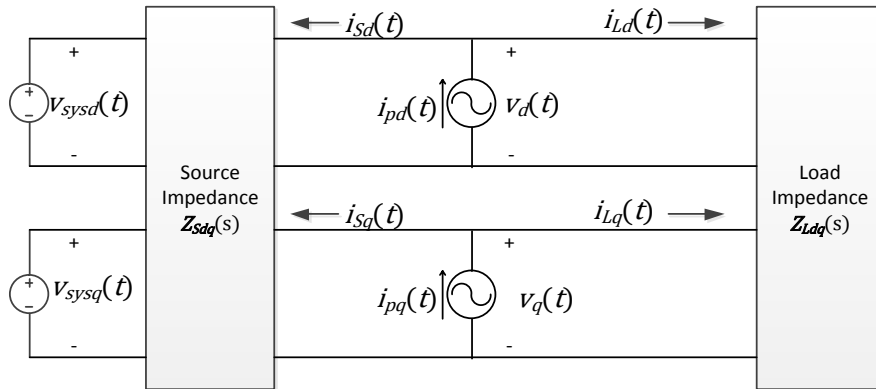


Figure 3-14: Diagram of shunt injection in **dq** frame

The injection currents flow into the source and load side are:

$$\begin{bmatrix} I_{Sd}(s) \\ I_{Sq}(s) \end{bmatrix} = Z_{Ldq}(s) \cdot (Z_{Sdq}(s) + Z_{Ldq}(s))^{-1} \begin{bmatrix} I_{Pd}(s) \\ I_{Pq}(s) \end{bmatrix} \quad (3-32)$$

$$\begin{bmatrix} I_{Ld}(s) \\ I_{Lq}(s) \end{bmatrix} = Z_{Sdq}(s) \cdot (Z_{Sdq}(s) + Z_{Ldq}(s))^{-1} \begin{bmatrix} I_{Pd}(s) \\ I_{Pq}(s) \end{bmatrix} \quad (3-33)$$

It can be seen that the current distribution is determined only by the system impedances. To measure the impedances of a load converter, a power supply with very a small output impedance is usually used to ensure the stability during the measurement. This makes most of the injected current flow into the source side. The load side gets little perturbation.

This can be changed by changing the system configuration. A filter can be installed into the system to block the perturbation energy going into the source side. The filters should not change the system operating point. The filter has to let all the system power flow pass through it at the fundamental frequency while blocking the power at other frequencies. This requires a high-Q notch filter with high a current rating. It is very hard to implement such a filter in normal three-phase AC systems.

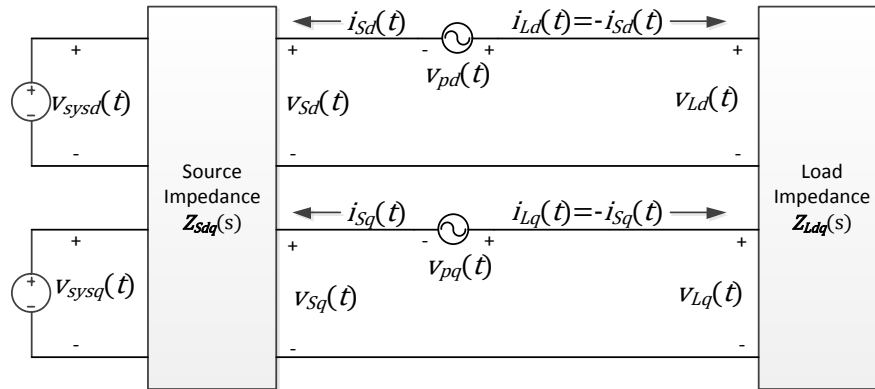


Figure 3-15: Diagram of series injection in **dq** frame

Another way to change the perturbation distribution is to change the injection device connection. If series injection as shown in Figure 3-15 is used, the distribution of injected power is swapped:

$$\begin{bmatrix} V_{Sd}(s) \\ V_{Sq}(s) \end{bmatrix} = Z_{Sdq}(s) \cdot (Z_{Sdq}(s) + Z_{Ldq}(s))^{-1} \begin{bmatrix} V_{Pd}(s) \\ V_{Pq}(s) \end{bmatrix} \quad (3-34)$$

$$\begin{bmatrix} V_{Ld}(s) \\ V_{Lq}(s) \end{bmatrix} = Z_{Ldq}(s) \cdot (Z_{Sdq}(s) + Z_{Ldq}(s))^{-1} \begin{bmatrix} V_{Pd}(s) \\ V_{Pq}(s) \end{bmatrix} \quad (3-35)$$

Most of the perturbation power goes to the load side, which is to be measured. Although the system bus needs to be broken into two parts to insert the injection device, the series injection is more efficient than inserting filtering impedances on changing the perturbation power distributions in this example.

The series injection is better for measurement of the high impedance side of the system. The injector usually carries a low voltage and the full system current, which is usually high. Another requirement for the injection circuit is that isolation is required between the different circuits in different phases. The shunt injection is better for measurement of the low impedance side of the system. It does not need isolation between circuits connected to different phases and it does not need to be disconnected from the source and load to connect to the injector. Only a part of the system full current flows into the circuit, which is much lower when compared to the system. But the circuit needs to work with full system voltage. To be able to measure any combination of source and load impedances, both shunt and series injection should be implemented.

3.5. System Drift during Measurement

As shown in [93], at least two independent perturbations have to be made to extract the impedance matrix. The calculation is based on the assumption that the system stays the same for the two measurements. But the real system usually drifts along with time. The two groups of voltage and current responses may be measured on two different impedance matrixes.

Let the two measurements be described as

$$\begin{bmatrix} v_{d1} \\ v_{q1} \end{bmatrix} = \mathbf{Z}_1 \begin{bmatrix} i_{d1} \\ i_{q1} \end{bmatrix}, \quad \begin{bmatrix} v_{d2} \\ v_{q2} \end{bmatrix} = \mathbf{Z}_2 \begin{bmatrix} i_{d2} \\ i_{q2} \end{bmatrix} \quad (3-36)$$

where $\mathbf{Z}_1 = \begin{bmatrix} Z_{dd1} & Z_{dq1} \\ Z_{qd1} & Z_{qq1} \end{bmatrix}$ is the system impedance matrix during the first measurement and $\mathbf{Z}_2 = \begin{bmatrix} Z_{dd2} & Z_{dq2} \\ Z_{qd2} & Z_{qq2} \end{bmatrix}$ is the system impedance matrix during second measurement. All the

voltages, currents and impedances are in the S-domain. The '(s)' after the variable names is omitted for simplicity.

The impedance matrix can be calculated based on these two measurements as:

$$\mathbf{Z}_m = \begin{bmatrix} Z_{ddm} & Z_{dqm} \\ Z_{qdm} & Z_{qqm} \end{bmatrix} = \begin{bmatrix} v_{d1} & v_{d2} \\ v_{q1} & v_{q2} \end{bmatrix} \begin{bmatrix} i_{d1} & i_{d2} \\ i_{q1} & i_{q2} \end{bmatrix}^{-1} \quad (3-37)$$

The four impedances are solved as:

$$\begin{aligned} Z_{ddm} &= \frac{Z_{dd1}i_{d1}i_{q2} - Z_{dd2}i_{d2}i_{q1} + (Z_{dq1} - Z_{dq2})i_{q1}i_{q2}}{i_{d1}i_{q2} - i_{d2}i_{q1}} \\ &= Z_{dd1} + \frac{-(Z_{dd1} - Z_{dd2})i_{d2}i_{q1} + (Z_{dq1} - Z_{dq2})i_{q1}i_{q2}}{i_{d1}i_{q2} - i_{d2}i_{q1}} \end{aligned} \quad (3-38)$$

$$\begin{aligned} &= Z_{dd2} + \frac{(Z_{dd1} - Z_{dd2})i_{d2}i_{q1} + (Z_{dq1} - Z_{dq2})i_{q1}i_{q2}}{i_{d1}i_{q2} - i_{d2}i_{q1}} \\ Z_{dqm} &= \frac{Z_{dq1}i_{d1}i_{q2} - Z_{dq2}i_{d2}i_{q1} - (Z_{dd1} - Z_{dd2})i_{d1}i_{d2}}{i_{d1}i_{q2} - i_{d2}i_{q1}} \\ &= Z_{dq1} + \frac{-(Z_{dq1} - Z_{dq2})i_{d2}i_{q1} - (Z_{dd1} - Z_{dd2})i_{d1}i_{d2}}{i_{d1}i_{q2} - i_{d2}i_{q1}} \end{aligned} \quad (3-39)$$

$$\begin{aligned} &= Z_{dq2} + \frac{(Z_{dq1} - Z_{dq2})i_{d2}i_{q1} - (Z_{dd1} - Z_{dd2})i_{d1}i_{d2}}{i_{d1}i_{q2} - i_{d2}i_{q1}} \\ Z_{qdm} &= \frac{Z_{qd1}i_{d1}i_{q2} - Z_{qd2}i_{d2}i_{q1} + (Z_{qq1} - Z_{qq2})i_{q1}i_{q2}}{i_{d1}i_{q2} - i_{d2}i_{q1}} \end{aligned} \quad (3-40)$$

$$\begin{aligned} &= Z_{qd1} + \frac{-(Z_{qd1} - Z_{qd2})i_{d2}i_{q1} + (Z_{qq1} - Z_{qq2})i_{q1}i_{q2}}{i_{d1}i_{q2} - i_{d2}i_{q1}} \\ &= Z_{qd2} + \frac{(Z_{qd1} - Z_{qd2})i_{d2}i_{q1} + (Z_{qq1} - Z_{qq2})i_{q1}i_{q2}}{i_{d1}i_{q2} - i_{d2}i_{q1}} \end{aligned}$$

$$\begin{aligned} Z_{qqm} &= \frac{Z_{qq1}i_{d1}i_{q2} - Z_{qq2}i_{d2}i_{q1} + (Z_{qd2} - Z_{qd1})i_{q1}i_{q2}}{i_{d1}i_{q2} - i_{d2}i_{q1}} \quad (3-41) \\ &= Z_{qq1} + \frac{-(Z_{qq1} - Z_{qq2})i_{d2}i_{q1} + (Z_{qd2} - Z_{qd1})i_{q1}i_{q2}}{i_{d1}i_{q2} - i_{d2}i_{q1}} \end{aligned}$$

$$= Z_{qq2} + \frac{(Z_{qq1} - Z_{qq2})i_{d2}i_{q1} + (Z_{qd2} - Z_{qd2})i_{q1}i_{q2}}{i_{d1}i_{q2} - i_{d2}i_{q1}}$$

It can be seen from equation (3-38) to (3-41) that if the two impedance matrixes \mathbf{Z}_1 and \mathbf{Z}_2 are close enough, the solved impedance matrix is still a good approximation of either of these two matrixes. But if the system changed too much, the calculated impedance becomes meaningless. Thus the two perturbations should be made as close as possible in order to reduce the influence from the system drift.

3.6. Application to Series Injection

Section 3.4 shows the importance to use series voltage injection. When a series voltage injection is used, source side voltage and load side voltage are different. Since the phase detection requires interface voltages, the voltages used may affect the error. One group of voltages may be used for all the transformation. Or, source and load side voltages are for the impedance measurement of source and load side correspondingly. Figure 3-16 shows an example when source voltages are used for all the transformations. Perturbation distribution is changed as described in Section 3.4. Two groups of interface voltages and the common interface currents are measured instead of two groups of interface currents and the common interface voltages. All the other blocks stays the same as in the shunt injection system. Although all the other analysis are done with the shunt injection system. They are also applicable to the series injection system.

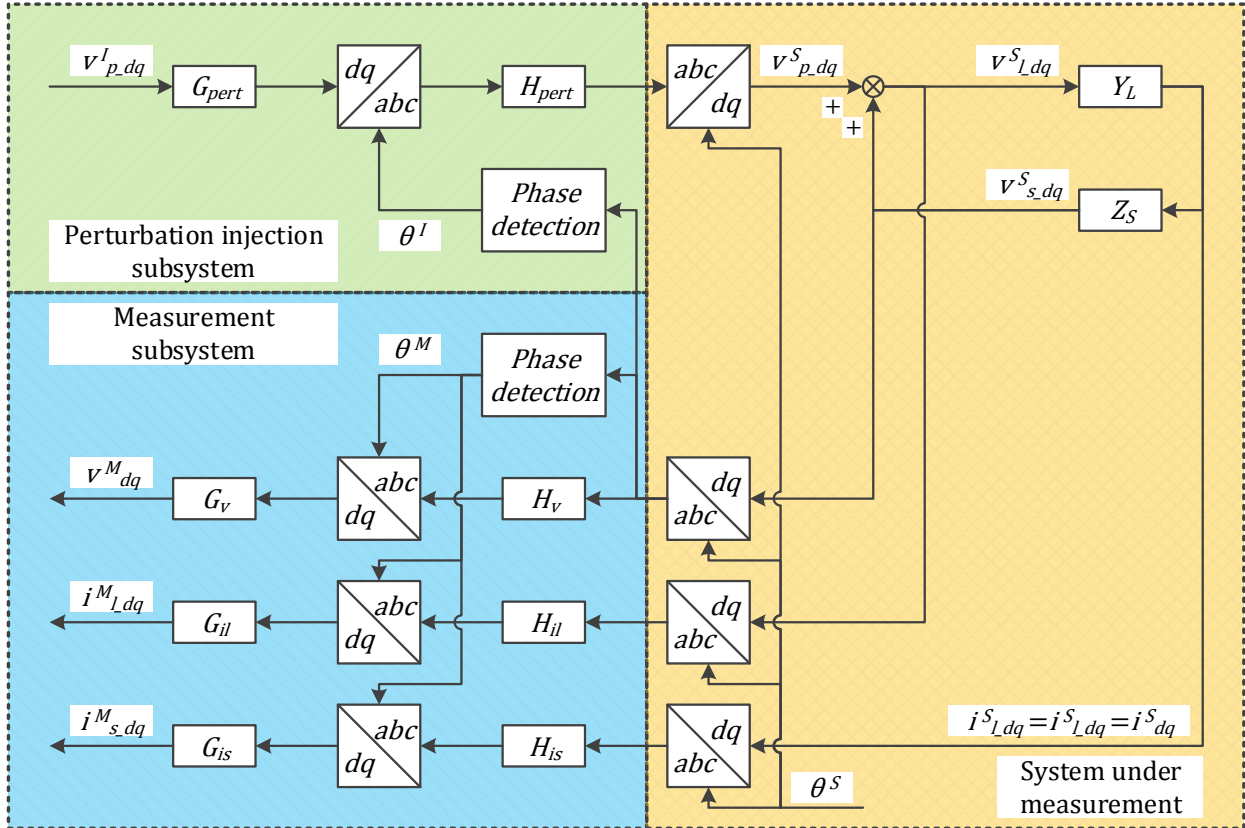


Figure 3-16: Impedance measurement system when series injection is used

3.7. Conclusion

This chapter discusses several systematical error sources and proposes the solution to reduce the influence of some of them.

The influence of different transfer characteristics of the sensors and analog signal processing is first studied. The average of the transfer functions can be used in the measurement to obtain the correct measurement.

The PLL used to estimate the system phase can affect impedance measure by changing the spectrum of voltage and current signals in the dq frame. But the influence can be compensated by post processing. Thus the PLL bandwidth can be increased into the measurement frequency range, which enhances system phase tracking capability can measurement speed. Another PLL is

used to generate the perturbation signal. But the perturbation is not changed by the PLL as long as no active power is injected.

The influence of the perturbation injection connection method is also discussed. Although not generating any error directly, the connection method affected the SNR of the measured signal. The analysis draws the conclusion that both shunt and series connection are required to characterize the source and load impedances at the interface.

Measurement error can be caused by system operating point drift during the measurement. The issue is not solved. However, if the impedance change caused by the system operating point drift is small, the measurement result is a good approximation of the real impedance. Or the system cannot be measured by this approach.

Chapter 4. Improvement Based on Previous System Architecture

After the discussion on measurement errors in the previous chapter, the first attempt to improve system performance is conducted based on the system architecture designed in [93]. The system partition and signal flow are kept the same while both hardware and software design are amended.

4.1. Injection Device Connection

In the previous design, a shunt injection using current sources is used to generate perturbation. A current source is made of a linear amplifier working in a controlled current mode and a transformer. The linear amplifier takes an analog reference signal and outputs a current. The transformer is connected to boost the allowable voltage at the current source. It also provides isolation, so that the current source can be connected into the system flexibly without worry about the potential. Finally, the leakage inductance of the transformer helps the amplifier to stabilize.

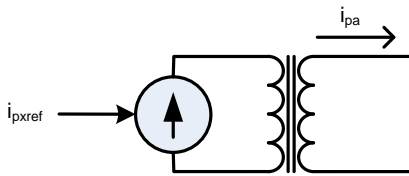


Figure 4-1: Injection reference to injection current for phase a

In the measurement system, three such current sources are connected to the system according to Figure 4-2. The three sources are connected in ‘Y’ shape. The three independent terminals connect to the system in shunt while the common point of the three sources is connected to the neutral point of either source side or load side.

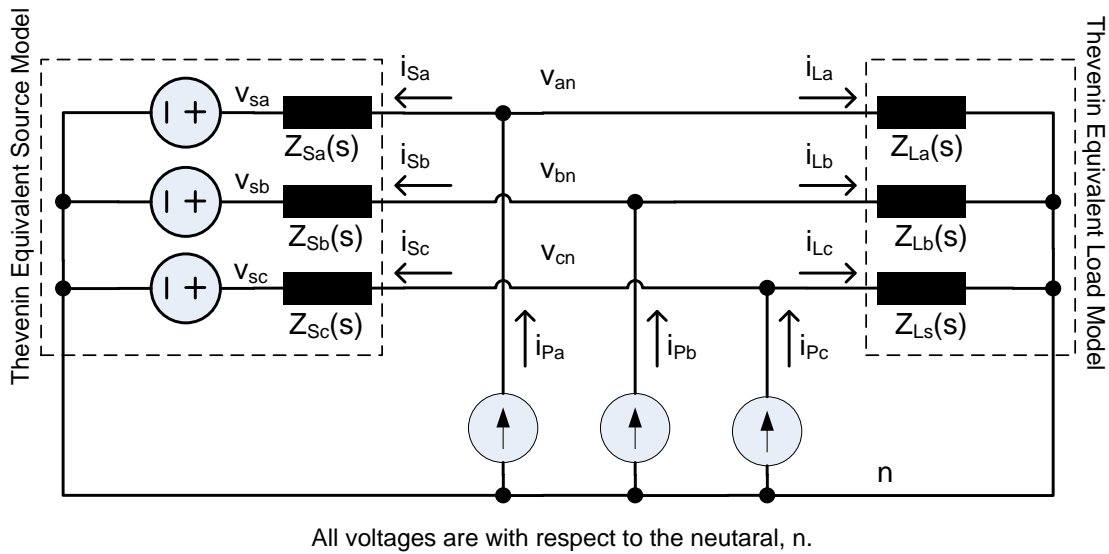


Figure 4-2: Perturbation injection devices connection in previous design

Ideally, the three injection currents add up to zero. There is no current flowing out of or into the common point of the three sources. However, the output currents of the three amplifiers do not add up to zero due to the offsets in the reference signals and the internal controller circuits. A current path must be provided for the ‘Y’ connected current sources to work. That is the role of the neutral point connection. But this connection limits the use of the equipment to the system which has a neutral point to connect. Also the connection brings in the unexpected disturbance on the θ -axis of the system.

To solve the problems, the connection pattern is adjusted as shown in Figure 4-3. Phase *b* current source and the neutral point connection are removed. The neutral points of the source and the load still share the same potential. But they may either be connected as shown by the dotted line or not connected. For a balanced system, there is no current flow through the connection even if they are connected. Although phase *b* current source is removed, the phase *b* injection current is well controlled by the sum of phase *a* and phase *c* currents. Since the total injection power is now provided by two amplifiers instead of the original three, higher power amplifiers are used. The transformer turns ratio is also increased to stand the line-to-line voltages instead of the line-to-neutral voltages.

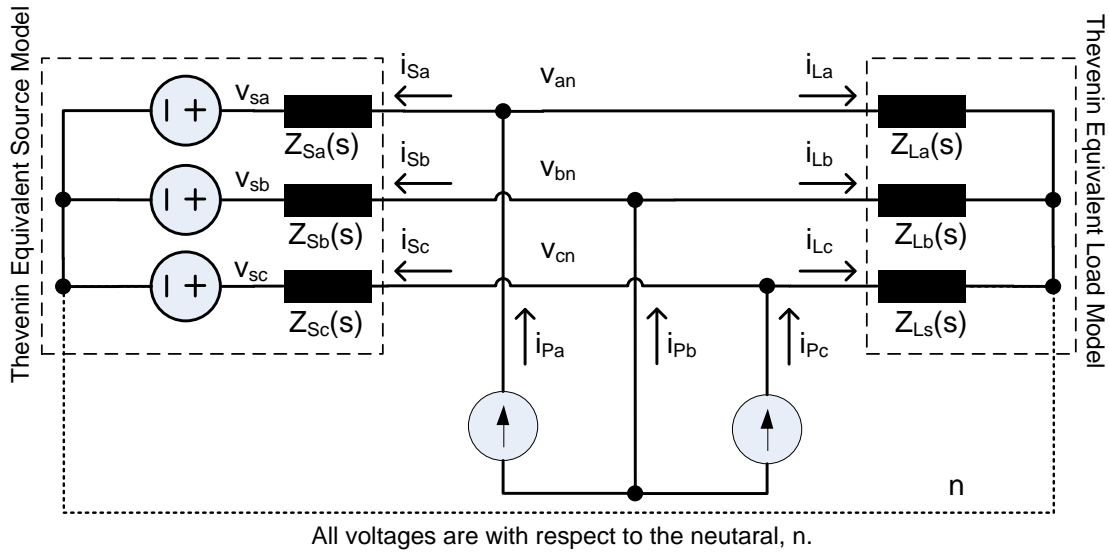


Figure 4-3: Updated perturbation injection devices connection

4.2. Measurement Sequence Adjustment

Another important change of the design is the measurement sequence. As mentioned in Chapter 3, the two perturbations for one measurement should be applied as close to each other as possible to avoid system state change during the measurement.

The old design takes no care of this point. It works under the assumptions that the system state is stable enough during the whole measurement. Due to the limit of the network analyzer, only one variable is measured at a time. The four voltage and current responses are measured in four frequency sweeps. The total measurement takes eight sweeps. The eight frequency sweeps last about twenty to thirty minutes for a sixty-point measurement. The impedance calculation at one frequency takes one data point from each sweep. The measurement of this eight data point spread across tens of minutes in time. The system to measure is very likely to change during this amount of time. The measurement gets meaningless when the state change become large enough.

The sweep sequence is adjusted to reduce the effect of system change. Instead of doing eight frequency sweeps, only one frequency sweep is conducted. But eight data points from two perturbation current vectors are collected one after each other, which usually takes less than half

a minute. It is easier to keep the system in a similar state during this shorter period of time. The measured impedance values reflect more accurately the system state at the measurement moment. There is a disadvantage to this approach because the total measurement time is increased due to the frequently start and stop of the network analyzer measurement.

4.3. Other Performance Tuning

Besides the two important improvements described in the previous two sections, there are also several other small changes made to refine the equipment performance. They are recorded in the section.

A. Noise reduction on signal conditioning circuits

Server DAC output noise is observed on the DAC output which connects to the network analyzer. The measurement result is shown on the left side of Figure 4-5. It is measured with an ADC channel input shorted and the converted value is copied to the DAC output.

The schematic of the circuit output stage is given in Figure 4-4.

The noise is found to couple into the system through power supply rails at points (1) and (2). There are several operational amplifiers which provide buffer to the voltage reference ICs found oscillating. This significant noise is removed after the operational amplifiers are removed. The decoupling capacitors are also moved to just beside the IC pins to reduce the stray inductance which reduces the decoupling effect.

Another noise source is identified as the isolation amplifier. The internal modulation frequency signal is not well attenuated at its output. An additional filter is inserted at point (3).

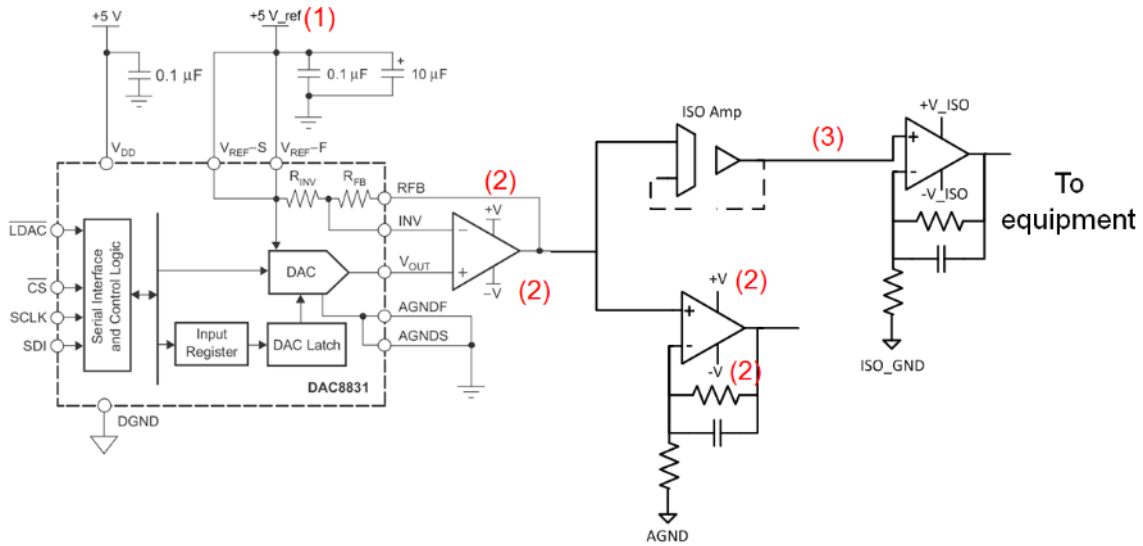


Figure 4-4: Diagram of output stage

After these efforts, the DAC output noise is reduced to the level shown in the right side of Figure 4-5. The measurement condition of this figure is the same as the left one, except that all the ADC channels, instead of only one are tested, although all the output are conducted by the same DAC channel.

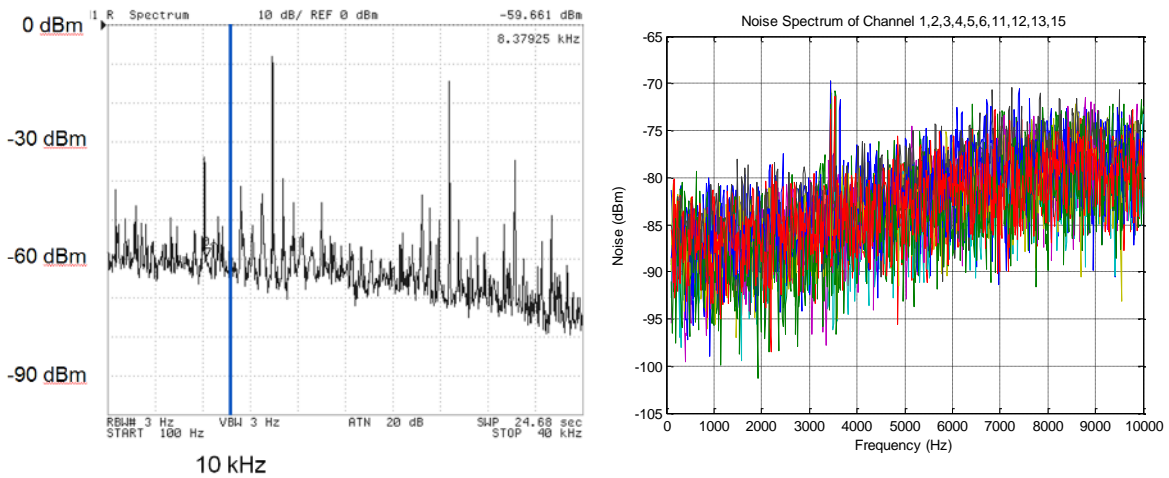


Figure 4-5: Comparison of DAC output noise (zero volt ADC input copied to DAC output)

B. Network analyzer measurement consistence improvement

The input adapter of the network analyzer used is found to be another significant error source. Its transfer function has a big change when the level of input signals changes. A measurement flow is designed to reduce the influence of the adapter. Figure 4-6 shows the detail.

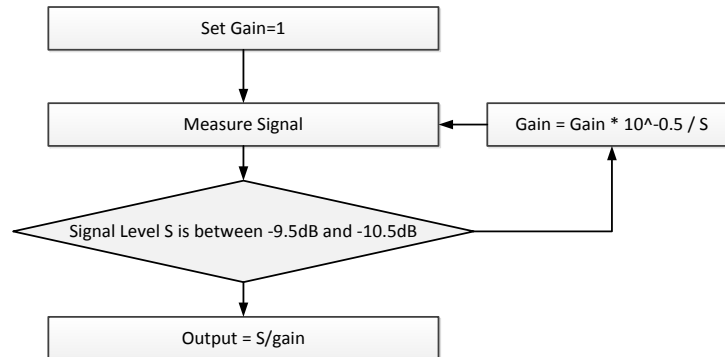


Figure 4-6: Flow chart to improve network analyzer measurement consistence

The procedure ensures the input signal level is between -9.5 dB and -10.5 dB which are around the maximum values that do not introduce significant distortion according to the datasheet, for the final measurement readout. If the signal is not within this range, a gain factor calculated from the measured signal level is multiplied to the DAC output value digitally. Then the DAC output is re-measured. After the measured signal level falls into the given range, the real signal level is calculated from the gain factor and the network analyzer readout.

Since the DAC characteristic is much more linear than the behavior of the input adapter, this approach nearly eliminates the non-linear effect of the network analyzer input adapter.

4.4. Construction of Improved Design

To test the performance of the system adjustment, a new piece of equipment is built. Figure 4-7 shows the exterior of the finished equipment.

The operational interface is cleaned from the previous design to be much more user friendly. Extra protection circuits are added to ensure the equipment safety. The component layout is also

adjusted from the old design. But the whole system architecture is kept the same except the points which are described earlier in this chapter. Figure 4-8 to Figure 4-10 shows the internal components. All the parts shown in Figure 2-6 can be found in these pictures.

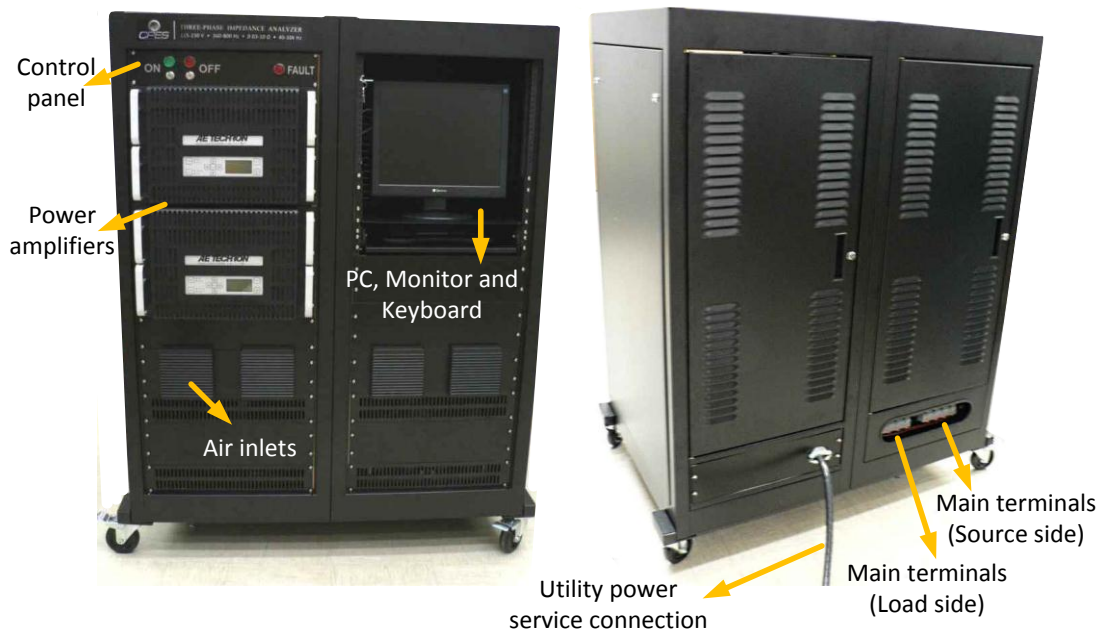


Figure 4-7: Front and rear side view of the impedance analyzer

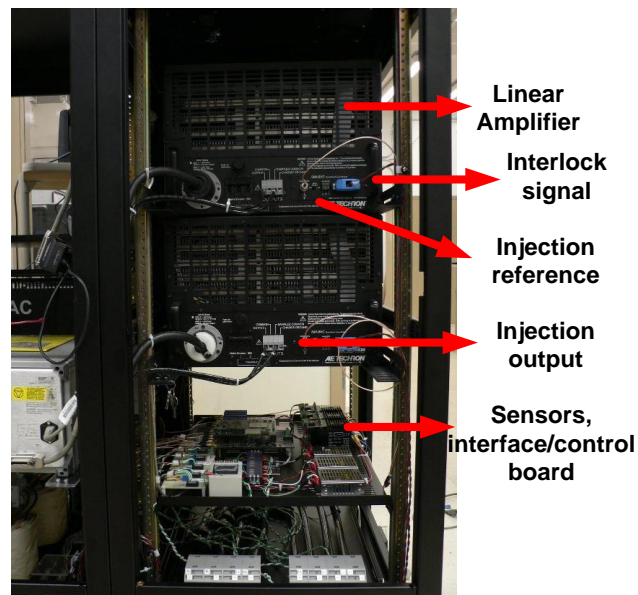


Figure 4-8: Inside view of cabinet —amplifier, sensing and real-controller signal processing part

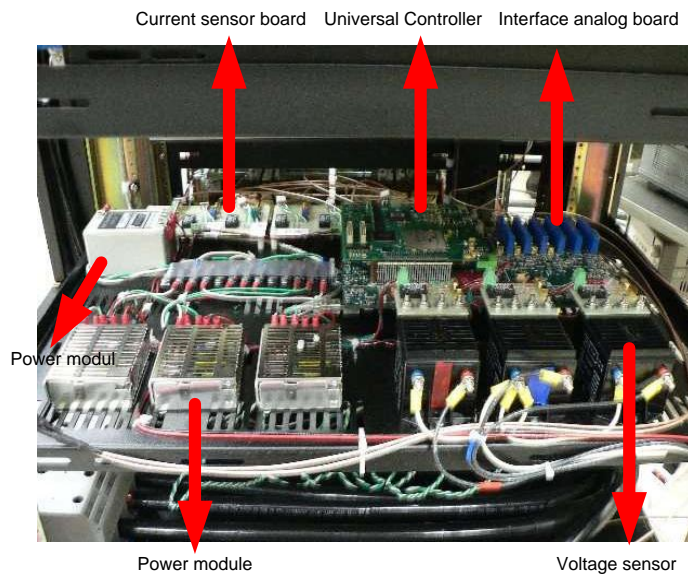


Figure 4-9: Inside view of cabinet — zoom in to sensing and real-controller signal processing part

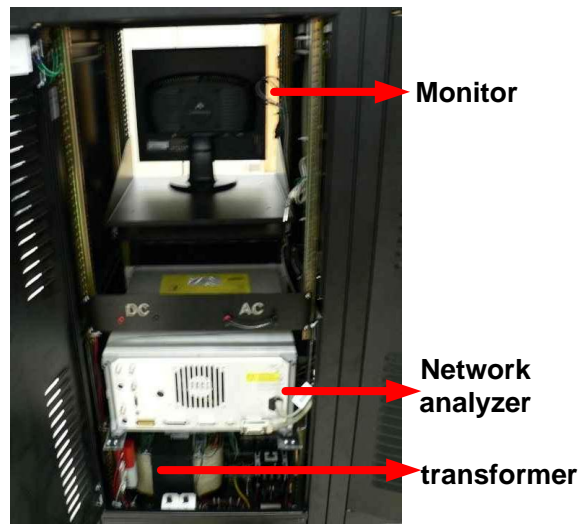


Figure 4-10: Inside view of cabinet — analyzer and isolation transformer part

4.5. Experiment Results

To test the performance of the newly constructed equipment, known passive impedances are measured for comparison. Before showing the measurement result, the transformation from impedances measured by third-party equipment in stationary frame to the impedances in synchronous frame is briefly summarized.

4.5.1. Passive Impedance Measurement Result

In order to compare results of known passive impedances, a mechanism must be in place which can take results measured for linear impedances in the stationary frame and compute their equivalent impedance in dq frame. This approach is derived in [93].

To check the accuracy of the impedance analyzer, a resistive-inductive load bank is measured. When the load bank is directly connected to the source, the measurement shows zigzag results which is away from the reference curve. This is because a shunt injection is used in the equipment. Most of the injection current goes to the source side, which leaves the load side with little to measure. To obtain acceptable results shown in Figure 4-11, a 5% impedance of the load DC value is added to the source side of the system.

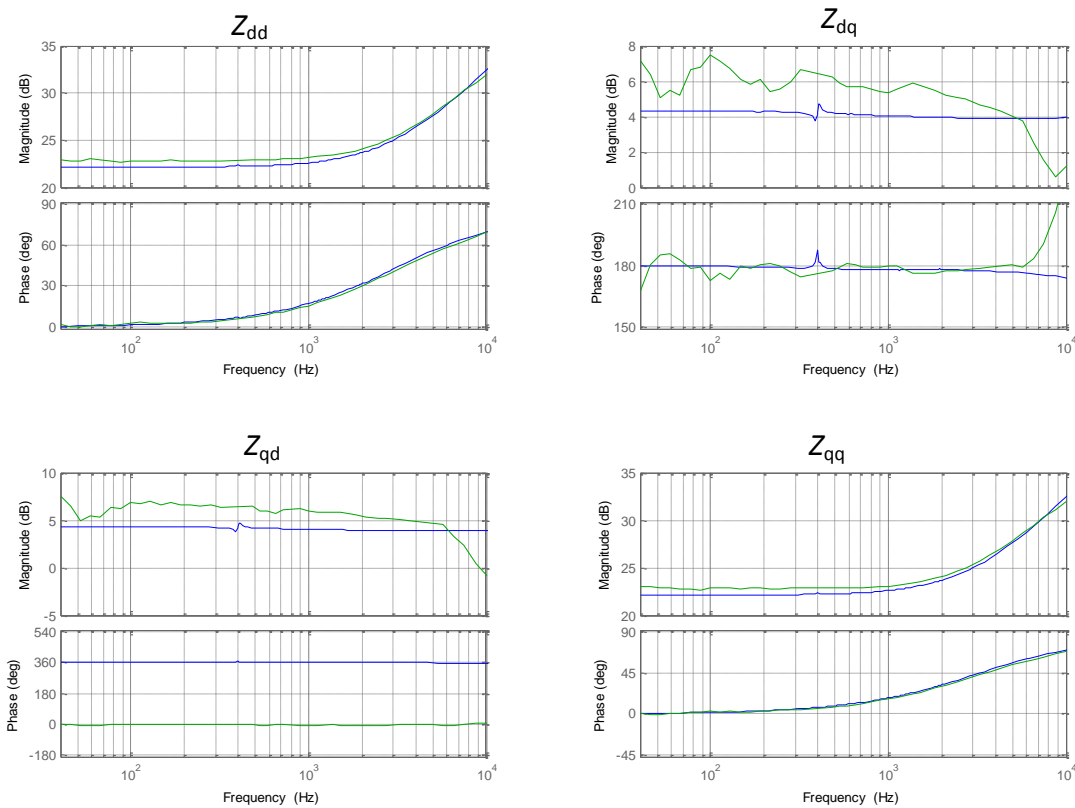


Figure 4-11: Resistive-inductive impedances measurement result (green curve) vs. simulation result (blue curve)

The two curves in the figure shows match within a few dB . The error at higher frequency increase is due to the injection power decrease caused by the transfer function from reference to current output gain attenuation.

4.5.2. Voltage Source Inverter (VSI) Impedance Measurement Result

To verify the equipment performance with switching converters, the output impedances of a VSI are measured. The circuit parameters are shown in Figure 4-12. The impedance is measured before the resistors after the LC filter.

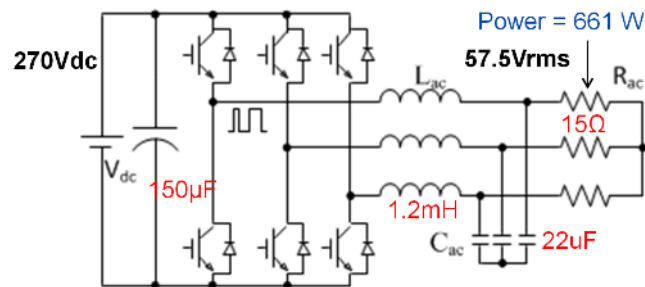


Figure 4-12: Circuit diagram of the measured VSI

Since the traditional VSI small signal model does not model the output impedance accurately [99, 100] and there is no model that has yet to produce a satisfying impedance result, the measurement result is compared with a switching model simulation. The impedances from the simulation model is extracted using the same technique as the equipment. The comparison is shown in Figure 4-13.

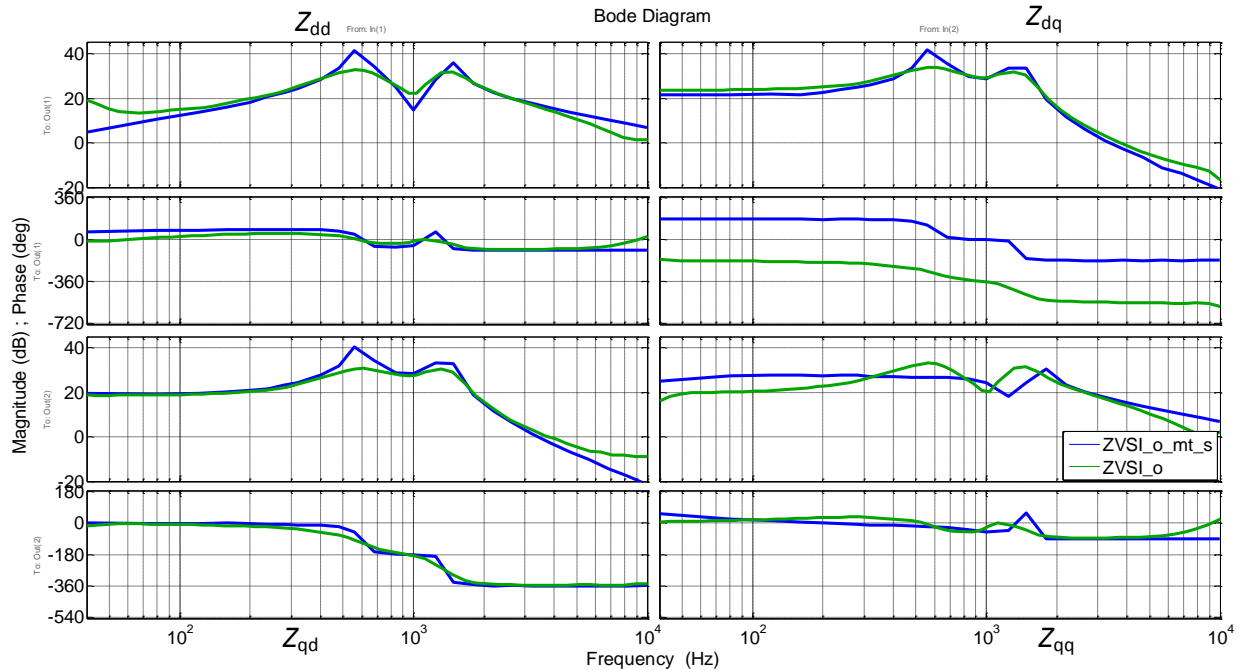


Figure 4-13: VSI output impedance measurement result (green curve) vs. simulation result (blue curve)

The two curves show good agreement within the middle frequency range. The differences at the resonant points are believed to be caused by not modeling some of the damping factor, such as the core loss of the inductors, in the simulation. One reason that the measurement result shows a good trend is that the VSI works as the source, which has lower impedance than the load side. This brings enough perturbation into the converter for the measurement.

4.6. Conclusion

Several approaches to improve the performance of the existing measurement equipment architecture are proposed. An impedance analyzer is built with the improvements. The equipment is tested with both passive and active impedances. Both tests shows acceptable results when the impedance ratio between source side and load side is neither too large nor too small. This limit is due to the shunt injection mode used in the architecture. It cannot be solved without changing the architecture.

Chapter 5. Improved Algorithmic Solution and System Architecture

Limitations in architecture dictate that, not all the problems discussed in Chapter 3 can be solved in Chapter 4. An improved architecture is proposed in this chapter. The algorithm used is also introduced below.

5.1. Proposed Algorithm

The impedance extraction algorithm follows a basic non-parametric analysis procedure described in Chapter 2 except for the changes described below.

5.1.1. Injection Waveform

Due to the interests in the low frequency measurements, wide-bandwidth signals are preferred because of their fast measurement. Although accurate, the sinusoidal excitation may take an extremely long time to measure, which worsens the system drift problem. Among the wide bandwidth-signals, chirp signals are selected instead of the signals listed in Chapter 2 from literature mainly because of its low crest factor, which means a higher power spectrum density for the same peak injection power.

A chirp signal is also called a swept-sine signal. Its instantaneous frequency, which is the derivative of the signal phase, changes as a function of time. The selected excitation signal is the linear chirp:

$$x(t) = \sin(2\pi(f_0 + (f_1 - f_0)t/2T) \cdot t) \quad (5-1)$$

where f_0 is the start frequency, f_1 is the end frequency and T is the duration of the chirp signal. An example of a linear chirp signal is given in Figure 5-1 (a) and (b). The signal increases linearly from 0 Hz to 100 Hz in one second.

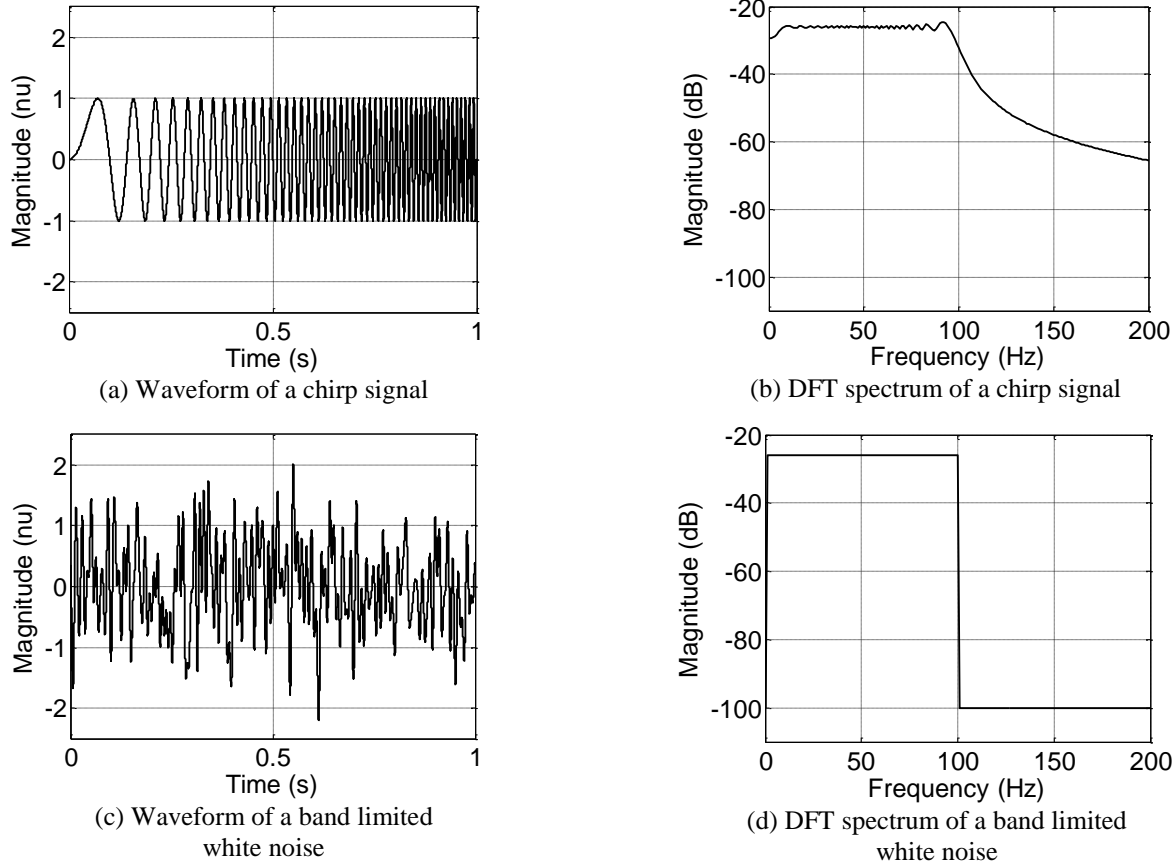


Figure 5-1: Comparison of chirp signal and white noise

Compared to the load step used in [98], the chirp signal has a constant spectrum on the frequency range of interest instead of being attenuated when frequency increases. In order to obtain clean measurements, the load step needs to be 20% of the converter full rating and nearly 100% of the operating point.

The band limited white noise used in [88] also has similar spectrum properties. However, the signal requires higher a peak injection power. A sample noise signal, which displays a similar spectrum as the chirp sample, is created and shown in Figure 5-1 (c) and (d). The peak of the signal is more than twice the peak of the sample chirp signal. Because of the chirp signal's low crest factor, the peak power of the injection circuit can be of smaller design. The operating point of the system to be measured is disturbed less by having less peak injection power.

Background noise always exists in any practical measurement setup. Since the chirp signal spreads the power over a wide frequency range, the signal's power density is decreased, and is more susceptible to the noise. The waveform can be tuned to improve the SNR. Several

approaches are compared. The sample signal shown in in Figure 5-1(a) with additional -6.6 dBW white noise (the power of the signal is calculated by applying the signal on a one ohm resistor) is used as the baseline of the comparison. The time-domain waveform and the spectrum of the base line signal are shown in Figure 5-2 (a) and (b). The first method to increase the SNR is to reduce the frequency span, which can increase the signal power density. Figure 5-2 (c) shows a chirp signal covering only DC to 50 Hz with the same level of noise added. As a result, the signal level is increased by about 3 dB, which is shown in Figure 5-2 (d). Another commonly used approach to increase SNR is to measure for a longer time and take an average of the data. However, this property does not directly apply to a chirp signal. Figure 5-2 (e) and (f) give an example. The chirp signal is extended to last four seconds. Then the signal is cut into four equal segments. The DFT of each segment is calculated. The average of four DFT results is shown in Figure 5-2 (f). Although the noise level is lowered, the signal level is decreased by the same level. No improvement of SNR is gained. This is because the four parts cut from a chirp signal are not correlated to each other. To create the correlation, the chirp signal is repeated instead of extended. In Figure 5-2 (g), the sample signal is repeated four times. The same procedure is repeated. It lowered the noise level by about 6 dB while maintaining a signal level with the same magnitude as the original one shown in Figure 5-2 (h). Both approaches, i.e. limiting bandwidth and frequency domain averaging, are adopted by this paper, as described in the next section.

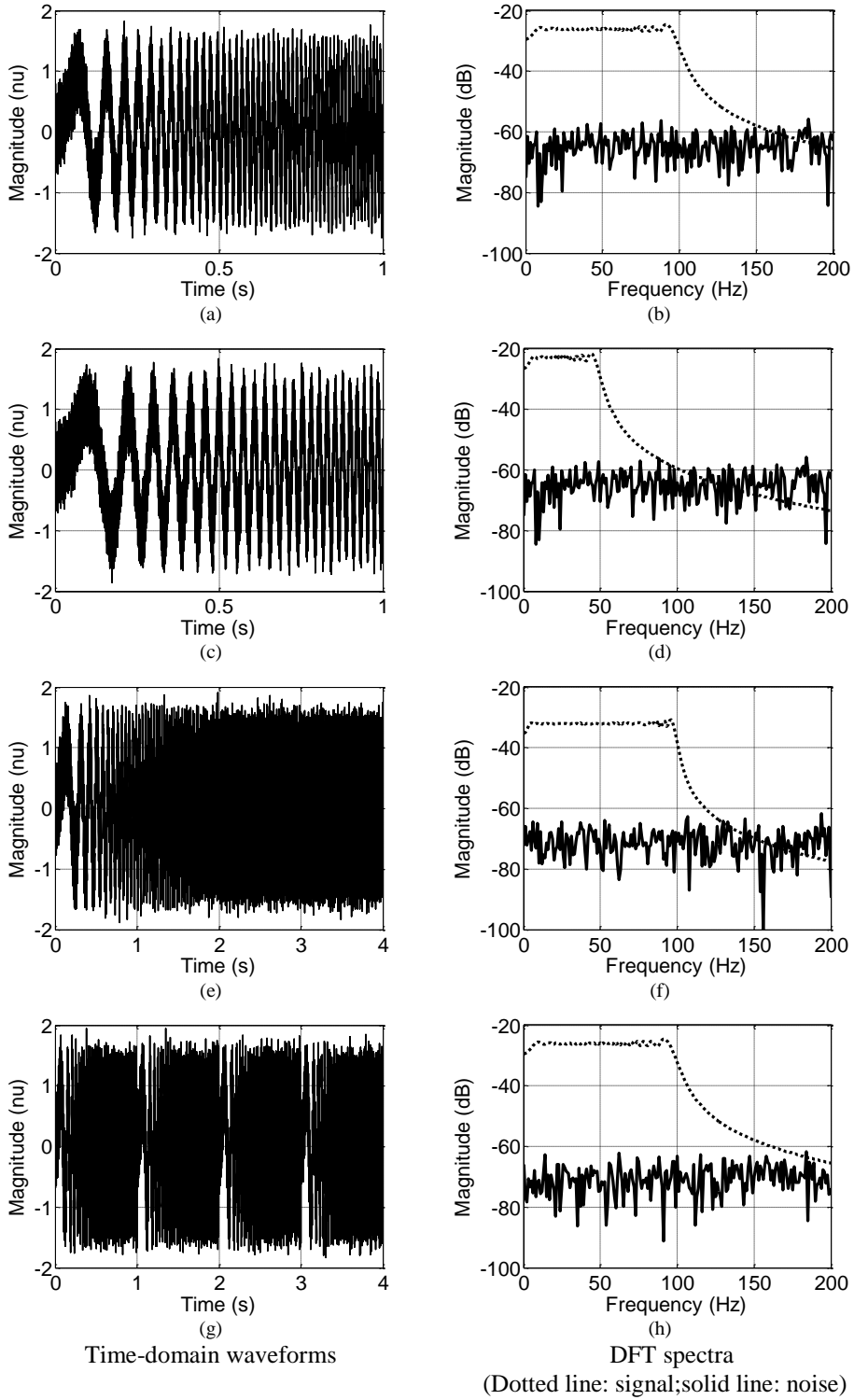


Figure 5-2. Comparison of Signals waveforms and SNR

5.1.2. Impedance Extraction Algorithm

The first step after collecting the circuit responses of the two perturbations is to transfer the voltages and currents from the abc coordinates to the dq coordinates using the phase obtained by a Phase-Locked Loop (PLL) running real-time during the response acquisition. After the coordinate transformation, DFT is traditionally used to obtain the spectra of the voltages and currents [84, 89]. Then impedances are calculated according to (2-17).

The chirp signal spreads the perturbation power over a wide frequency range, which means it is more susceptible to background noise in the system. The impedance results are usually noisier compared to the ones obtained by sinusoidal excitation.

The influence from uncorrelated noise can be reduced by taking into account the perturbation signal using a cross-correlation method [107]. Instead of the spectra of the response signals, the transfer functions from the perturbation signal to the response signals are used in the impedance calculation.

For a generic linear time-invariant discrete-time system described by

$$y(n) = \sum_{k=1}^{\infty} h(k)u(n-k) + v(n) \quad (5-2)$$

where $y(n)$ is the output signal, $u(k)$ is the input signal, $h(k)$ is the system impulse response, and $v(k)$ is the uncorrelated noise in the system.

The method calculates the cross-correlation between the input and output signals. The result is

$$R_{uy}(m) = \sum_{k=1}^{\infty} u(n)y(n+m) = \sum_{k=1}^{\infty} h(n)R_{uu}(m-n) + R_{uv}(m) \quad (5-3)$$

where $R_{uu}(m)$ is the auto-correlation of the input signal and $R_{uv}(m)$ is the cross-correlation between the input signal and the noise which is 0.

The input signal is selected to have $R_{uu}(m) = \delta(m)$ in [107]. Then the transfer function $H(j\omega)$ is calculated by applying DFT to $R_{uy}(m)$.

For a chirp excitation signal, the $R_{uu}(m)$ is not equal to $\delta(m)$, thus the transfer function should be calculated by:

$$H(j\omega) = \frac{\text{DFT}(R_{uy}(m))}{\text{DFT}(R_{uu}(m))} \quad (5-4)$$

where $\text{DFT}(x)$ means applying DFT on signal x .

If the perturbation signals on the d channel and q channel are used separately, the transfer functions from the perturbation signals to the response signals form a two-by-two matrix, which cannot be obtained by a single perturbation. The system block diagram is modified as shown in Figure 5-3 to create single-input-single-output (SISO) transfer functions that can be solved from the data of one perturbation. In Figure 5-3 $G_{con}(s)$ is the transfer function of injection circuit. The perturbations on the d channel and the q channel are no longer considered independent. In fact, they are generated from a single virtual perturbation signal through the transfer function matrix $G_{inj}(s)$, which is given by

$$G_{inj}(s) = \begin{bmatrix} G_{inj d}(s) \\ G_{inj q}(s) \end{bmatrix} \quad (5-5)$$

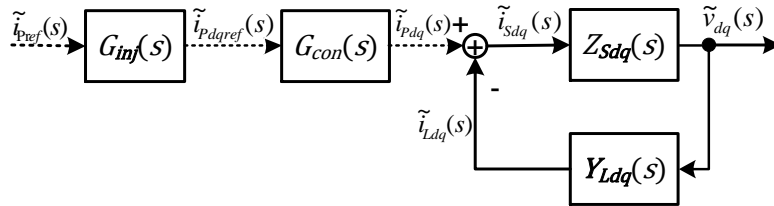


Figure 5-3: Modified small-signal block diagram

To generate two independent perturbations, $\tilde{i}_p(s)$ is kept the same for the two perturbations and two different transfer function matrices $G_{inj}(s)$ are used, i.e.:

$$\begin{aligned} G_{inj1}(s) &= [A_1 \quad B_1]^T \\ G_{inj2}(s) &= [A_2 \quad B_2]^T \end{aligned} \quad (5-6)$$

where $[A_1 \ B_1]^T$ and $[A_2 \ B_2]^T$ are two independent constant vectors. In this way, when a chirp signal is applied as the virtual perturbation signal, the actual perturbations on both the d channel and the q channel are still chirp signals.

The system becomes Single-Input-Multiple-Output (SIMO). With only one excitation at the input port, all the desired transfer functions can be found. Figure 5-3 shows that the transfer functions from the input to the voltages and the transfer functions from the input to the currents are still linked by the system impedances, as shown in the following expression:

$$\begin{bmatrix} \frac{\tilde{v}_d(s)}{\tilde{i}_p(s)} \\ \frac{\tilde{v}_q(s)}{\tilde{i}_p(s)} \end{bmatrix} = \mathbf{Z}_{sdq}(s) \begin{bmatrix} \frac{\tilde{i}_{sd}(s)}{\tilde{i}_p(s)} \\ \frac{\tilde{i}_{sq}(s)}{\tilde{i}_p(s)} \end{bmatrix} \quad (5-7)$$

$$\begin{bmatrix} \frac{\tilde{v}_d(s)}{\tilde{i}_p(s)} \\ \frac{\tilde{v}_q(s)}{\tilde{i}_p(s)} \end{bmatrix} = \mathbf{Z}_{Ldq}(s) \begin{bmatrix} \frac{\tilde{i}_{Ld}(s)}{\tilde{i}_p(s)} \\ \frac{\tilde{i}_{Lq}(s)}{\tilde{i}_p(s)} \end{bmatrix}$$

As in (2-17), the transfer function vectors from two perturbations can be used to calculate the impedance matrices, as follows:

$$\mathbf{Z}_{sdq}(s) = \begin{bmatrix} \frac{\tilde{v}_{d1}(s)}{\tilde{i}_p(s)} & \frac{\tilde{v}_{d2}(s)}{\tilde{i}_p(s)} \\ \frac{\tilde{v}_{q1}(s)}{\tilde{i}_p(s)} & \frac{\tilde{v}_{q2}(s)}{\tilde{i}_p(s)} \end{bmatrix} \begin{bmatrix} \frac{\tilde{i}_{sd1}(s)}{\tilde{i}_p(s)} & \frac{\tilde{i}_{sd2}(s)}{\tilde{i}_p(s)} \\ \frac{\tilde{i}_{sq1}(s)}{\tilde{i}_p(s)} & \frac{\tilde{i}_{sq2}(s)}{\tilde{i}_p(s)} \end{bmatrix}^{-1} \quad (5-8)$$

$$\mathbf{Z}_{Ldq}(s) = \begin{bmatrix} \frac{\tilde{v}_{d1}(s)}{\tilde{i}_p(s)} & \frac{\tilde{v}_{d2}(s)}{\tilde{i}_p(s)} \\ \frac{\tilde{v}_{q1}(s)}{\tilde{i}_p(s)} & \frac{\tilde{v}_{q2}(s)}{\tilde{i}_p(s)} \end{bmatrix} \begin{bmatrix} \frac{\tilde{i}_{Ld1}(s)}{\tilde{i}_p(s)} & \frac{\tilde{i}_{Ld2}(s)}{\tilde{i}_p(s)} \\ \frac{\tilde{i}_{Lq1}(s)}{\tilde{i}_p(s)} & \frac{\tilde{i}_{Lq2}(s)}{\tilde{i}_p(s)} \end{bmatrix}^{-1}$$

As mentioned in the last section, the frequency domain average method can enhance the signal SNR to improve the measurement accuracy. Due to the possible asynchronous sampling of the signal, the average method by Welch [108] is used in this paper for data processing instead of

a direct average of the spectra. The method involves windowing and overlapping when cutting and calculating the spectra, which alleviates the leakage effect caused by asynchronous sampling.

5.1.3. Simulation of Proposed Approach

The proposed approach is simulated using Simulink. The circuit simulated is shown in Figure 5-4.

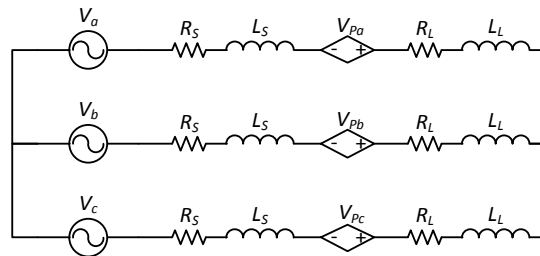


Figure 5-4: Simulation circuit

A three-phase fixed-frequency (60 Hz) voltage source feeds a three-phase R-L load through some small resistors and inductors representing the bus impedances. The perturbation is generated using ideal controlled voltage sources. The voltage sources are better for the high-impedance load-side measurement, which is the measurement target in this simulation. The circuit parameters are given in Table 5-1.

Table 5-1 Simulation circuit parameters

Source voltages (rms per phase)	266 V
Source resistance	0.01 Ω
Source inductance	10 μH
Load resistance	7 Ω
Load inductance	460 μH
Peak injection voltage (per phase)	4 V
Measurement frequency range	1 Hz – 1 kHz

To test the performance of the proposed approach, white noises with -20 dB/Hz power spectra density are added to the three phase source, which produces the voltage signal SNR to about 0 dB. The impedance extraction using different procedures are compared. The procedures are listed below:

1. Single chirp injection for the whole frequency range, DFT based spectrum calculation is used
2. Single chirp injection for the whole frequency range; correlation method is used
3. Frequency range is split equally into 10 segments; single chirp injection for each segment; correlation method is used.
4. Frequency range is split equally into 10 segments; 10 chirps are repeated for each segment, correlation method and average technique are used.

The extracted impedances Z_{dd} terms of extracted impedances are compared in Figure 5-5.

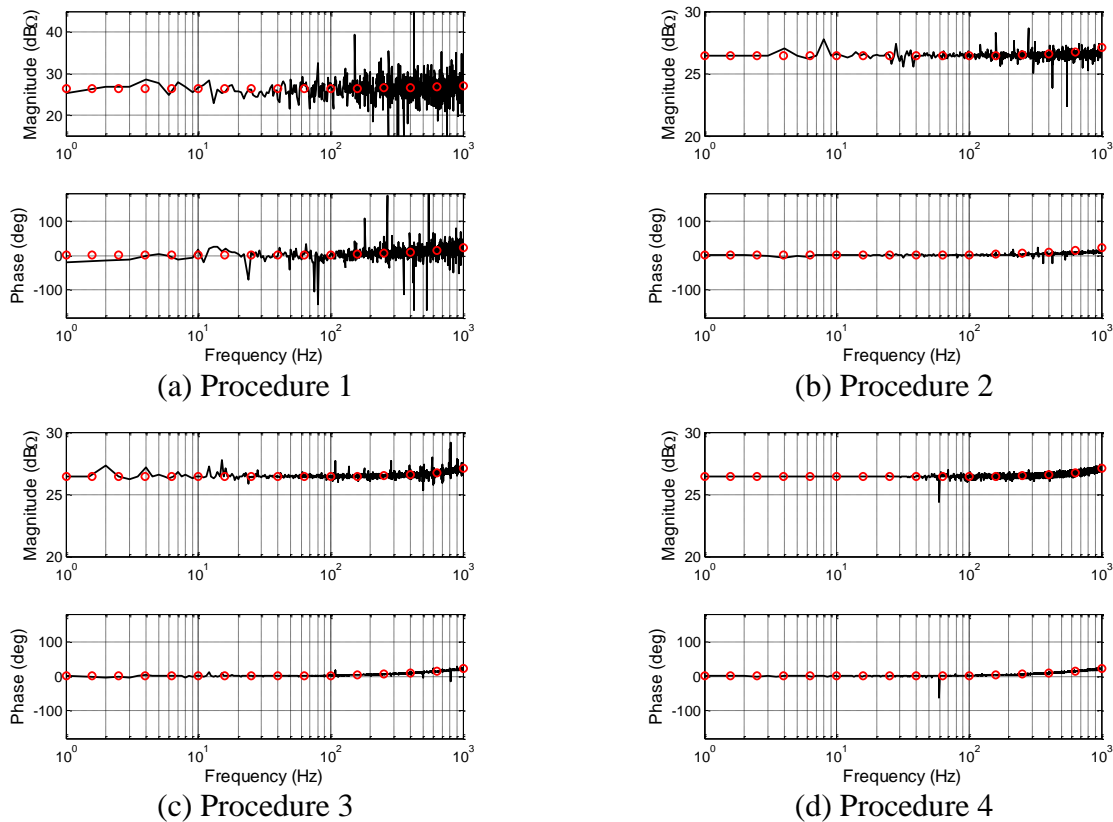


Figure 5-5: Comparison of impedances extracted by different procedures (Black solid lines: simulation result; red circles: analytical values)

As can be seen from Figure 5-5a-d, frequency range split and frequency domain average techniques further reduces the noise in the results. With all the techniques applied, the proposed approach produces good results even with 0 dB SNR.

5.2. Measurement System Architecture Design

5.2.1. Measurement System Requirement

Before the design of a system, a few basic requirements are specified, which may affect the design results. As described in Chapter 1, the system impedance is most useful in small systems. The system power rating varies between a few hundreds of kilo-watts to a few mega-watts. The following design is based on a low power prototype used in the lab which is rated at 100 kW.

System voltage: 190 V ~ 460 V ac line to line.

System current: 12 A ~ 125 A per phase.

Frequency range: from less than 1 Hz to 1 kHz.

Although designed for low power, the scalability is kept in mind during the design. The final target is to work in a system rated at 36 MW with a voltage level of 13.8 kV.

5.2.2. Measurement System Partitioning

The impedance measurement system can be divided into several blocks. Figure 5-6 shows the partitioning of the system. The blocks within the dashed line constitute the impedance measurement system. The measurement system is connected to the power system bus at the point to be measured as shown at the bottom of the figure. The operator interacts with the measurement system through the human interface unit shown at the top of the figure.

The partitioning of the blocks is made based on the functions. During the implementation, several function blocks may be combined into one physical unit. The detail functions of the blocks are described in the following sections.

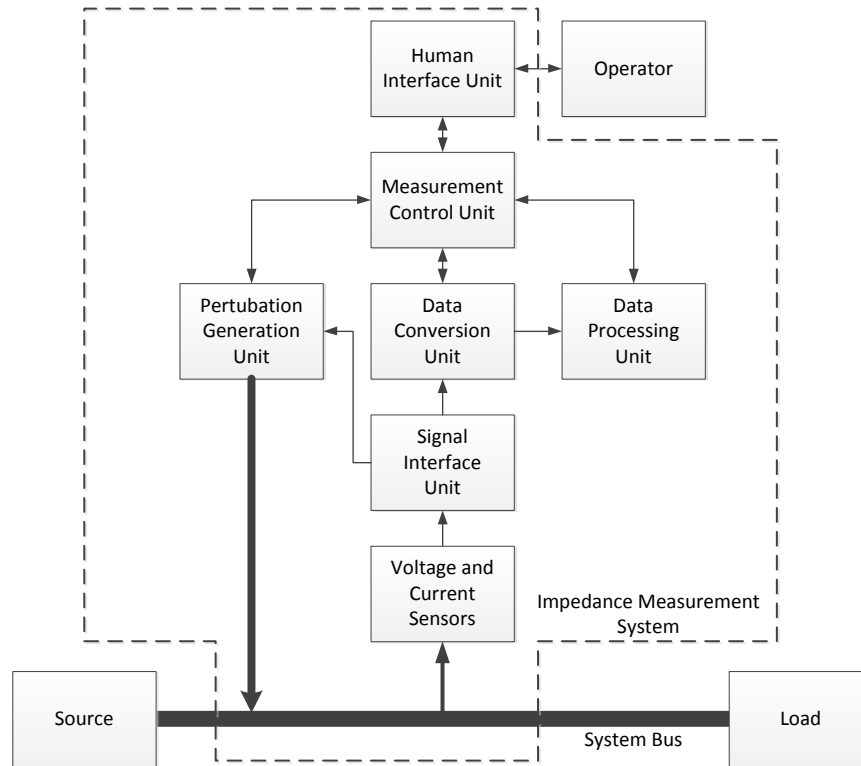


Figure 5-6: Impedance Measurement System

5.2.3. Perturbation Injection Unit

The perturbation injection unit (PIU) creates a small disturbance in the system to be measured. According to experience gained at CPES, 1% to 5% of nominal power, which the power bus is rated at, is usually required to obtain satisfying results. For a high power system, the perturbation power is still at a significant level. Thus, switching converters are preferred compared to linear amplifiers because of its high efficiency. Since the perturbation signals are at frequencies different from the fundamental one, the power converter does not generate active power. Although it requires the unit to be capable of handling high power, the energy consumed by the unit is only limited by the converter losses.

To cover the wide range of frequencies, including very low ones, it is preferred to avoid transformer at the output stage of the unit. To be able to measure the system with a wide range of source and load impedance ratios, both shunt injection and series injection should be implemented as mentioned in Chapter 3. Thus, the unit should be able to handle full system voltage or current depending on whether shunt or series connection is in use.

Considering the availability and the flexibility, a three-phase full-bridge converter is selected to work at the specified voltage level of 460 V.

C. Shunt Injection Mode

Shunt injection mode injects current perturbation into the system. One suitable topology for this purpose is the boost rectifier shown in Figure 5-7 – a three phase Voltage Source Converter (VSI) connected to the system via the three phase boost inductors shown as L in the figure. The VSI regulates the injected currents using a current loop control.

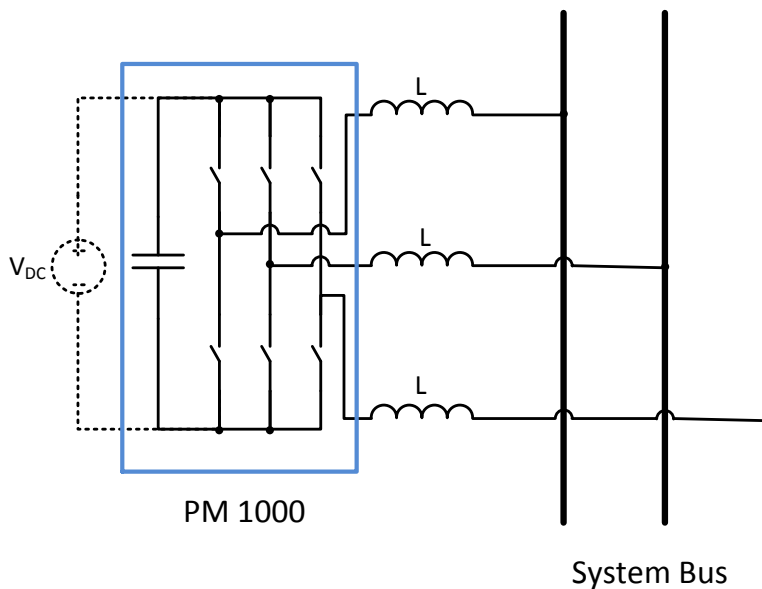


Figure 5-7: Shunt injection circuit using VSI

Since the shunt injection circuit does not need to generate DC current in d-q coordinates, there is no active power output transferred from the dc side to the ac side of the VSI. Thus, the dc voltage source, shown with a dashed line in Figure 5-7, can be omitted. Only a properly designed capacitor is required to support the dc bus voltage, together with a dc voltage loop feedback, as used in any Active Front End (AFE) or Active Power Filter (APF). Indeed, the behavior of this circuit is quite similar to a shunt APF. The difference is that instead of injecting only line frequency harmonic currents, the injected current frequency spectrum covers all the frequencies

to be measured. As in any APF, the injection circuit absorbs some small active power only due to converter losses.

While injecting the perturbation current at the measurement frequency, switching frequency current and its harmonic are also injected into the system if the circuit in Figure 5-7 is used. Since the current injected is only a small fraction of the nominal current, the effect of the current ripple in the measurement accuracy may be relevant. In any case, as any VSI connected to a power grid, an additional filter is needed before it is connected to the system bus.

D. Series Injection Mode

In ac systems, the source impedance is usually much smaller than the load impedance. Perturbing the system using shunt mode, most of the injected current flows into the low impedance source side. The high impedance load side is not disturbed enough for good measurement accuracy.

A workaround is to use the series injection mode. Instead of injecting perturbation current, voltage perturbation is used. Using this provision, most of the injected power flows to the high impedance load side. The disadvantage of the series injection mode is that it is harder to be connected into the system. For shunt injection, the perturbation generation has only three terminals that can be connected to the junction point where the impedances need to be measured. But for series injection, the system bus has to be broken into two parts at the point to be measured to insert the perturbation voltage source. Albeit this disadvantage, series injecting is still the best solution to measure the high impedance load side.

Figure 5-8 shows the circuit to implement series injection into the system using VSI. The VSI output is filtered by a second order LC filter. The filter removes switching frequency components and its harmonics. Then the voltage is applied to the system through three isolation transformers. Besides isolation, transformers are also used to increase the current capability of the perturbation injection unit since it has to sustain the full system current. The unit is usually capable of generating high voltage. But the current rating is only part of the system current. Although transformerless design should be used to measure the frequencies very close to the line frequency in d-q coordinates, over-sized transformers can still be used at the designed power level of 100 kVA to measure to only a few hertz away from the line frequency.

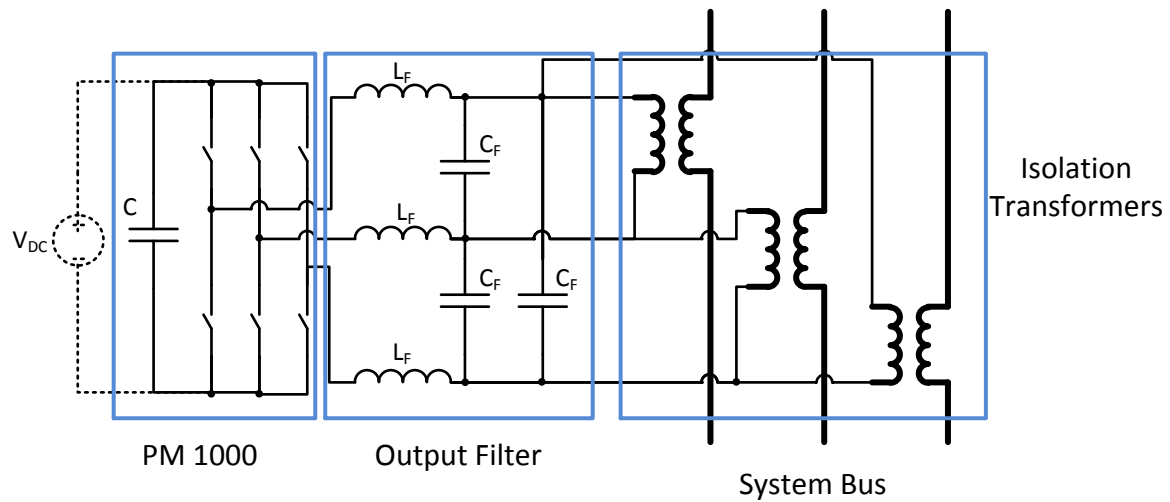


Figure 5-8: Series injection circuit using VSI

As far as the active power generation is concerned, the same reasoning reported for the shunt injection holds true. Thus, the dashed voltage source can be omitted and the dc-link voltage is controlled by a feedback loop

E. Perturbation injection unit Controller

Besides the requirement of the power stage, a digital controller should also be included in the perturbation generation unit. The controller communicates to the other units and controls the power stage to inject required disturbance into the system. The control tasks include: 1) identifying the system phase angle, 2) generating perturbation signal reference, and 3) controlling the power stage to generate perturbation which follows the reference.

The VSI switching frequency is usually designed to be at least 20 kHz depending on the semiconductor devices used. Double update is preferred to achieve a higher control bandwidth. The controller should also be able to talk to the other parts of the system to receive commands and send the perturbation reference out for further use.

5.2.4. Sensor Selection

Voltage and current sensors convert the high level of voltages and currents from the system into a lower level that can be handled by widely used operational amplifiers based analog signal conditioning circuits.

The perturbation signal and its response are usually of only a few percentages of the full system voltages or currents. But the sensors have to deal with the full system voltage and current. Thus they should have excellent accuracy. Moreover, the sensors that measure different phase should match each other very well. Otherwise, additional frequencies are generated after the signals are transformed into d-q coordinates.

Another key parameter of the sensors is the bandwidth. The sensors should be able to convert all the frequencies of interest linearly. For the design target, the frequency range is from sub-hertz to 1 kHz. Since the low end of the range is in the sub-hertz range, sensors that are capable of handling the frequency range from dc to 1k Hz are required. To keep the flatness of the transfer function of the sensors, the bandwidth stated in the datasheet, which is usually -1 dB point or -3 dB point, should be much higher than the highest measurement frequency 1 kHz.

It is hard to build sensors in-house to exceed the performance of the ones designed and manufactured by the specialized companies. Therefore, the sensors are just selected from those that are commercially available.

5.2.5. Signal Interface Unit

The signal interface unit provides an interface between the data conversion unit and the physical signals. The signals obtained from the sensors are prepared to be readily used by the data conversion unit. Its most important functions include amplifying, attenuating, offsetting, and filtering the signal. While processing the signal, the most important point is to keep the distortion and noise introduced by the circuits as low as possible. While a change in the signals is unavoidable, the circuit should keep the change the same for all the three phases. The output signals of the data conversion unit are also processed so that they are ready to connect to other components. These parts of the functions are mainly buffering the signals.

All the sensors' outputs are connected to the signal interface unit. The unit processes the signals using an analog circuit to prepare them to be sampled. Since the analog circuit performs

much better than the digital signal processing on the dynamic range and the sampling of the signal brings aliasing in frequency domain. Thus, the amplification, attenuation, and anti-aliasing filtering of the signal have to be implemented by analog circuits.

Figure 5-9 shows a diagram of the proposed signal conditioning function implementation. The signals from the sensors are buffered by the input stage. Then the signals are either notch filtered or directly sent to the next multiplexer stage. The notch filter is designed to filter out the fundamental frequency components of the signal to fully use the ADC resolution. But the filter characteristic becomes very different due to the component variation when the frequency goes close to the center frequency. This is not acceptable. Thus the notch filter is only used when the measured frequencies are far enough away or the multiplexers feed the next stage directly from the buffer stage. Then the signals are passed through a low pass filter for anti-aliasing purposes. Finally, the output stage enhances the driving capability to pass the signals through a cable to the data conversion unit.

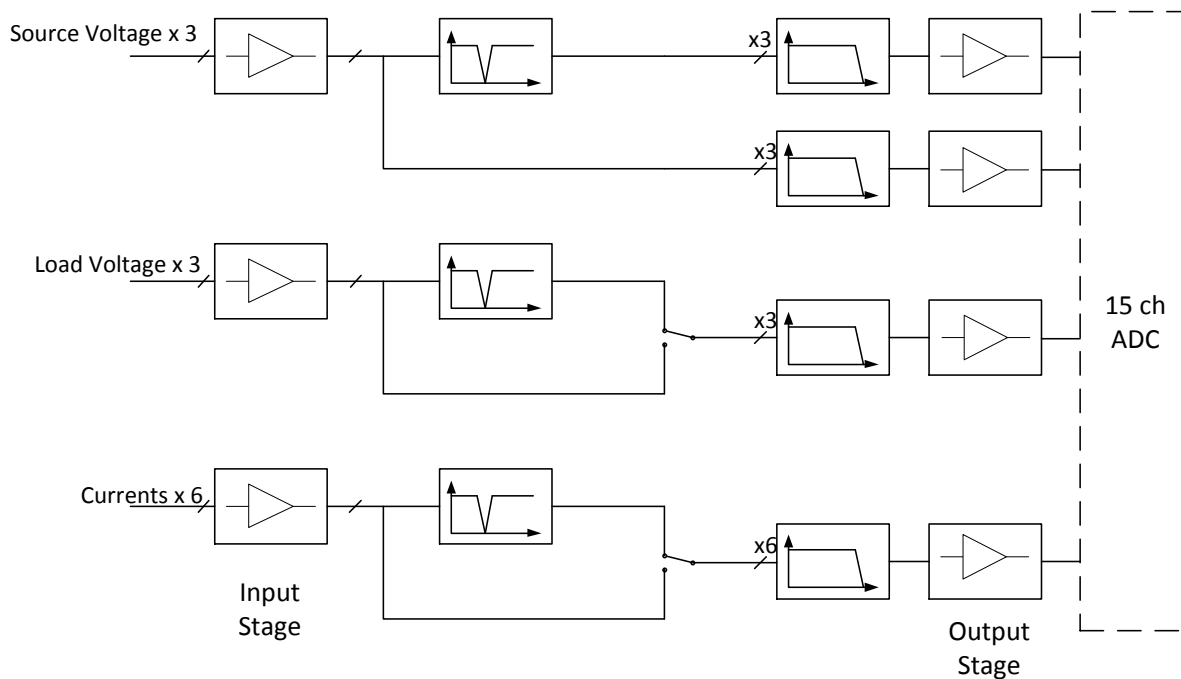


Figure 5-9: Signal conditioning circuit block diagram

5.2.6. Data Conversion Unit

The data conversion unit converts between digital signals from a host computer and the analog signals from the signal interface unit. All the voltage and current information has to be digitalized for the algorithm to extract the impedance, which is the most important function of this unit. Some other real time tasks may also need to be done in this unit, such as the system phase tracking, and down sampling filter when oversampling is applied. Hence, the unit should also provide enough calculation power.

One parameter of this unit is the sampling frequency. It should be high enough to avoid losing signal information, which is more important when the sampling frequency is not synchronous with the perturbation frequency. Taking into account that the highest frequency of interest is only 1 kHz, 1000 samples per period, which is one mega sample per second, is easily achievable.

Another more critical parameter is the analog-to-digital converter resolution. Since the amplitude of the injected signal may be lower than one percent of the fundamental signal while the frequency could be very close to the fundamental. Under these conditions, an intensive signal processing is required in order to extract the perturbation signal accurately and, at the same time, the ADC resolution should be high enough to capture the necessary information due to the existing noise in the measurement system. The use of higher resolution ADC may not necessarily increase the accuracy of the measurement. Increasing the resolution by oversampling is sometimes preferred because it reduces the influence of the noise.

A PXI platform based computer is selected to be the unit. PXI (PCI eXtensions for Instrumentation) is a rugged PC-based platform used for measurement and automation systems. PXI combines PCI electrical-bus features with the rugged, modular, Eurocard packaging of CompactPCI and then adds specialized synchronization buses and key software features. PXI is both a high-performance and low-cost deployment platform for measurement and automation systems [109]. The PXIe specification improves the performance of the original PXI platform by adopting the PCIe bus in addition to the PCI bus. The communication bandwidth is boosted from 132MB/s to 500MB/s per device, per direction. It also increases the system synchronization clock frequency from 10 MHz to 100 MHz.

5.2.7. Data Processing Unit

After the raw data is collected, it needs to be processed to calculate the desired impedances. The most critical challenge in this unit is the algorithm selection and development. Since the task can be done off-line and there is no strict limit on time consumption, the requirement on hardware is very flexible. The final decision is made for easy development and easy communication with the other units.

The data processing unit extracts the system impedances from the raw data collected by the data conversion unit. Intensive digital signal processing algorithms can be applied at this stage. Since no strict timing is required, the widely available personal computer is the choice for this unit. It offers enough calculation power with very low cost. The hard drive of several tera-bytes provides plenty of storage of the measurement data for later review. Well-designed software, such as MatLAB provides a wide selection of signal processing function libraries and speeds up the software design procedure.

5.2.8. Measurement Control Unit

The measurement control unit receives the commands from the human interface unit and coordinates all the above units to do the measurements. Its function is to communicate with all the units plus a little timing and logical control.

The key requirement of the unit is the interface that talks to different units. Since the perturbation injection unit and data conversion unit both have Ethernet ports. Ethernet is good choice for the interface. It can provide a high bandwidth which is necessary to pull the digitalized signal from the data conversion unit. The physical layer of the connection can also be changed to optical fiber instead of twisted copper wires if a high isolation voltage is required for the perturbation generation unit. Although excellent communication performance is required, the control task itself is simple. It just includes a few time sequence and logical controls, which can be implemented using many kinds of hardware. To simplify the hardware design, the same pc used for data processing unit is chosen. Measurement control is designed to be a part of the software in the PC. By this way, the communication between the measurement control unit and the data processing unit is strongly simplified.

5.2.9. Human Interface Unit

The human interface unit provides the measurement results and the control of the whole system to the operator. The resulting storage and management functions are also classified into this unit. Although this function is not related to the measurement procedure, it is very useful that the operator can easily retrieve and review previous measurement results. Since this function is only utilized by the human interface unit, it is reasonable to integrate it into the same unit.

To simplify the operation, a graphical user interface (GUI) is proposed. The windows based computer is selected as the hardware platform due to the familiarity of its interface. The development suit used to provide the communication of the data acquisition from National Instrument also provides a library for user interface development. Since the human interface unit is based on a pc platform, it is reasonable to share the same computer with the data processing unit and measurement control unit. These units just run as different pieces of software.

The above three unit are detailed in the appendix.

5.2.10. System Architecture Summary

The system hardware architecture is summarized in Figure 5-10. The components within the blue box are the impedance measurement system.

The PC with software developed by MatLAB and LabWindows is the human interface. It also controls the measurement procedure and processes the digitalized signal to extract the impedance. The perturbation unit consist one VSI, an output filter, a controller and implements both series and shunt injection into the system. The perturbation and responses are sensed by the voltage and current sensors then processed by the signal interface unit. The PXI platform computer samples the processed signals from the signal condition circuit, finishes the real time task and then sends the data out for final processing.

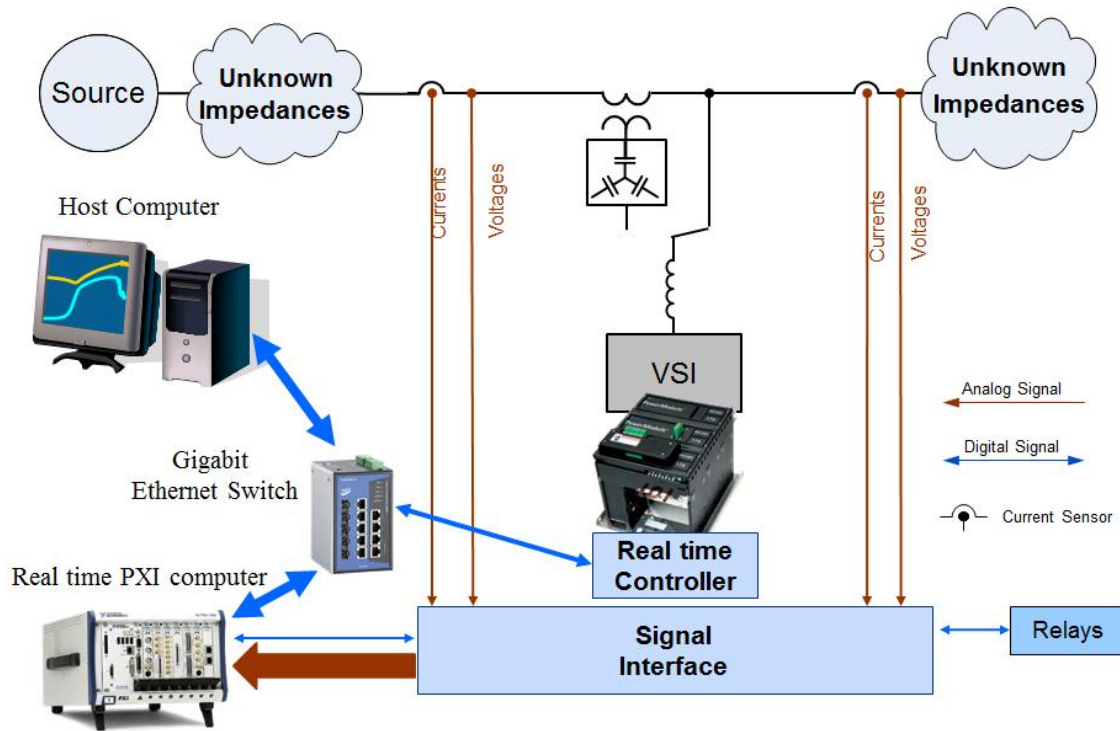


Figure 5-10: System architecture diagram

Figure 5-11 shows a more detailed signal flow diagram including the connections between the hardware controllers and the internal software communication flow. There are three pieces of controller hardware in the system: a Windows based pc, a PXI computer running a real time operating system, and the embedded controller in the VSI, which is a part of the perturbation generation unit. A measurement procedure includes:

- The human interface unit imposes the start command.
- The measurement control unit initializes the perturbation unit through Ethernet and communicates the start command to the PXI computer.
- The VSI controller samples the system voltages and tracks the system phase through a PLL. After the PLL is locked, the output voltages or currents are controlled to follow the internally generated references by a closed-loop control.
- While the perturbation is injected into the system, the PXI computer tracks the system phase using the same PLL technique and then filters and down-samples the acquired signals. Together with the phase information from the PLL, the obtained voltage and current information are sent to the host PC via Ethernet.

- The recorded data are firstly saved on the hard drive. Then the processing algorithm reads the data and calculates the impedances. Finally, the extracted impedances are presented to the operator through human interface.

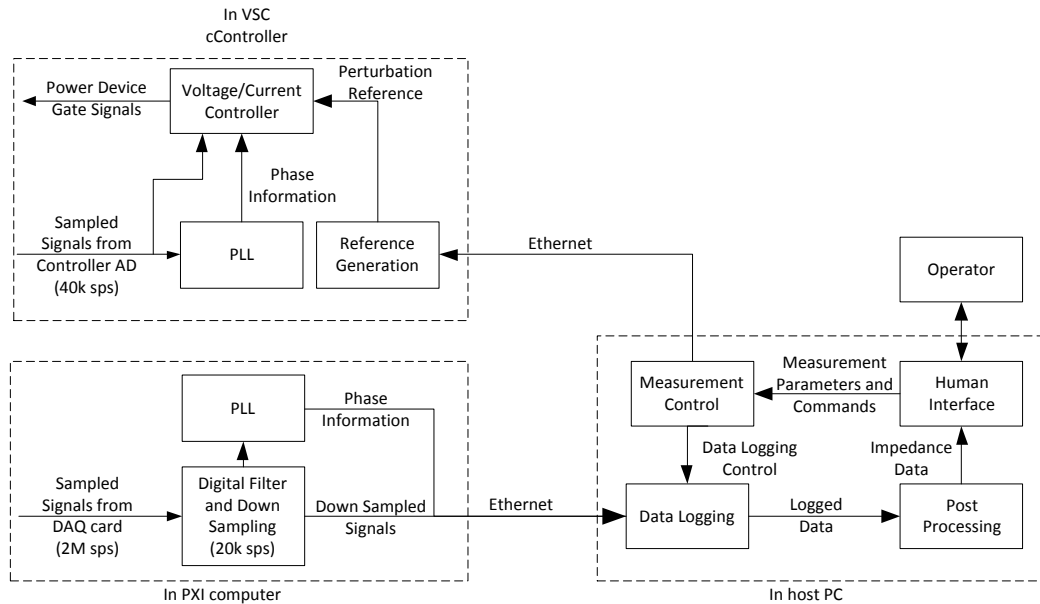


Figure 5-11: System signal flow diagram

5.3. System Scalability

Among the abovementioned function blocks, only the perturbation generation unit and the sensor interface should be scaled for the measurements on the high-power systems (36 MW). Thus, when the system voltage and current go up, two main things in the measurement system need to be increased: perturbation power and isolation.

To keep the disturbance magnitude measurable, the power injected into the system should be kept at the same relative percentage used in the low-power case. Thus, the power rating of the perturbation generation unit should increase in proportion to the power of system to be measured.

For the medium power converters, multilevel topologies are usually the most appropriate solution due to the device availability and performance requirement.

Isolation is another issue when the system voltage raises. The isolation requirement is mainly on the components that directly interact with the system bus including the sensors, perturbation generation power stage and the auxiliary power supplies for the power stage. In the current phase

of design, they are selected from the commercially available components. The parts that may require custom design will be studied later.

The last point is the protection. It is extremely important to implement reliable protection when working in a medium power system to avoid damage and ensure safety. Since the protection may be much different than that of the low power prototype; it is not studied at this phase of design.

5.3.1. Scaling Up of Perturbation Injection Unit

The perturbation generation is one of the two units that need to be changed when the system power increases. The power rating of the unit increases proportionally to the system power. For the 36 MW high power design, the system voltage increase from 460 V to 13.8 kV and the system current increases from 125 A to 1.5 kA. To maintain a similar switching frequency to the low power prototype, a similar IGBT module based converter should be used instead of the GTO or IGCT based high power converters. Thus the topology of the converter needs to be changed to provide the required perturbation power.

For the shunt mode injection, the converter should withstand the system's full voltage 13.8 kV while injecting about 5% of the system current which is 75 A. The common IGBT module can easily run at 75 A current level, but the block voltage is much less than enough to directly build a converter running with 13.8 kV voltage. Transformers can be used to solve the problem, but it is not suitable for outputting very low frequency, which is necessary. Therefore, a multilevel converter is proposed to raise the voltage capability of the converter.

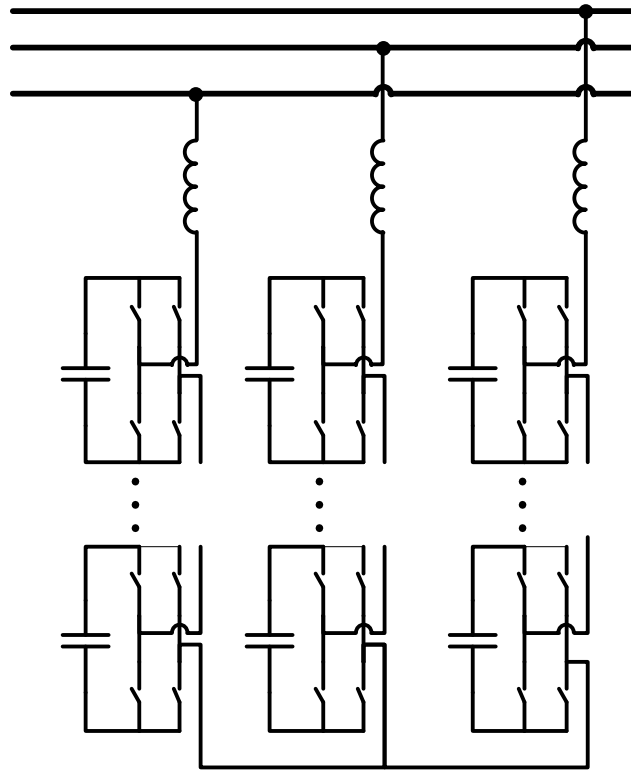


Figure 5-12: Topology for shunt injection at full voltage

Figure 5-12 shows the proposed cascaded H-bridge topology where several H-bridge inverters are connected in series at the ac side. Each converter provides only part of the system voltage and the string of the H-bridge ensures the nominal voltage for one phase. The topology is selected for its robustness, easy control and flexibility, since extra modules can easily be added to extend the output voltage. PM 1000 modules can still be used to construct the converter of this topology. Each phase needs at least twelve modules to sustain the 13.8 kV voltages if 690V output modules are used. That is 36 modules in total. One disadvantage of this topology is the requirement of many isolated DC sources, but there is no active power output demand for this application. Thus, all the DC bus capacitors can be just left floating and controlled by voltage loop feedback. The control algorithm can be developed using the existing results for the same topology used as an APF [110].

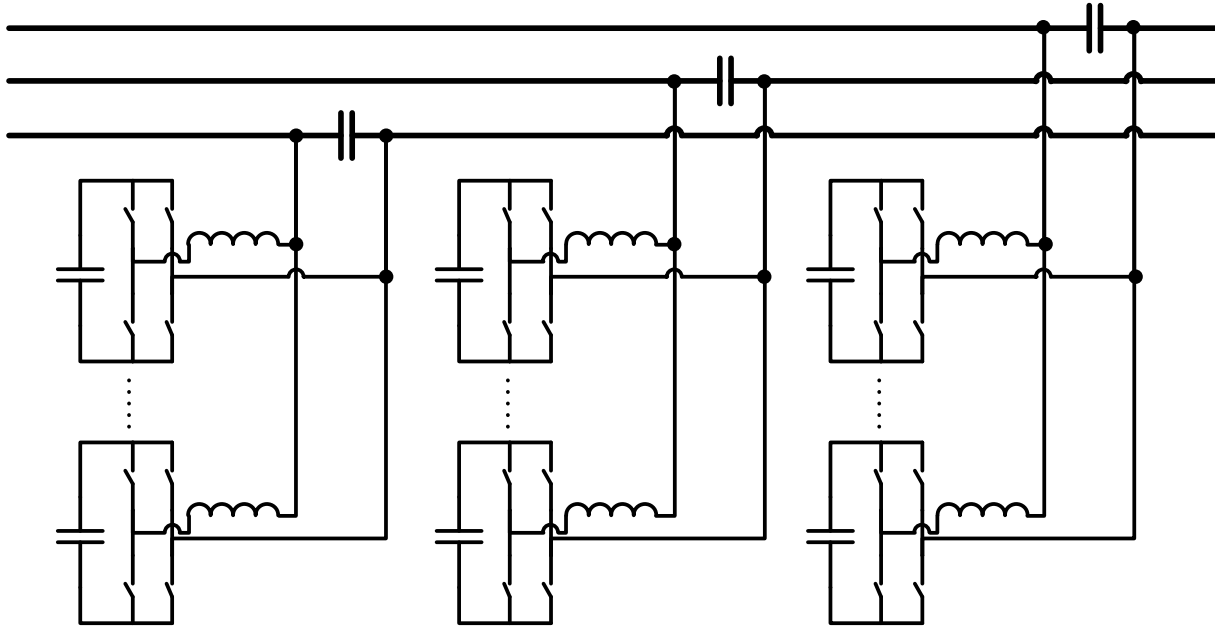


Figure 5-13: Topology for series injection at full current

For the series mode injection, the converter only needs to generate 5% of the system phase to neutral voltage which is about 400V. The voltage is still within the capability of a two level VSI built using IGBTs. But the converter needs to carry 1500A full system current. Hence, several converters are used in parallel to increase the current capability. Another requirement is that transformers should be avoided. In this case, the topology used in transformerless DVR [111] is selected. An H-bridge inverter with floating DC bus capacitor and LC output filter build up the isolated voltage source for perturbation. But there is no need to cascade the H-bridges as stated in the paper, since the required output voltage is much lower. Instead of increasing output voltage, output current needs to be boosted. Paralleling converters with interleaving control [112] is also a good choice. Figure 5-13 shows the proposed topology proposed for a series injection for a full power system applying interleaving to the transformerless DVR in [111]. By interleaving between the paralleled converters, not only is the output current enlarged, but also the equivalent switching frequency is increased. The increase of the equivalent switching can reduce the switching frequency ripple and raise the control loop bandwidth, which can both benefit our system. A common issue in an interleaved system is that there is loop current between different converters. This issue can be easily solved by separating the DC buses of

each converter as shown in Figure 5-13. The reason why this solution can be used is that no active power is demanded.

5.4. Experimental Results

To test the performance of the equipment, various impedances are measurement. The results are compared with impedances obtained via other approaches when available.

5.4.1. Passive Impedance Measurement Result

Passive impedances are first measured. The impedances are also measured by an Agilent 4194A precision impedance analyzer out of the system phase by phase. Then the impedances are transferred into the *dq* frame using the method described in the previous section to compare with the measurement result obtained by the equipment.

The first load measured is a simple three phase resistor load back. The measurement setup is shown in Figure 5-14. And the result comparison given in Figure 5-15.

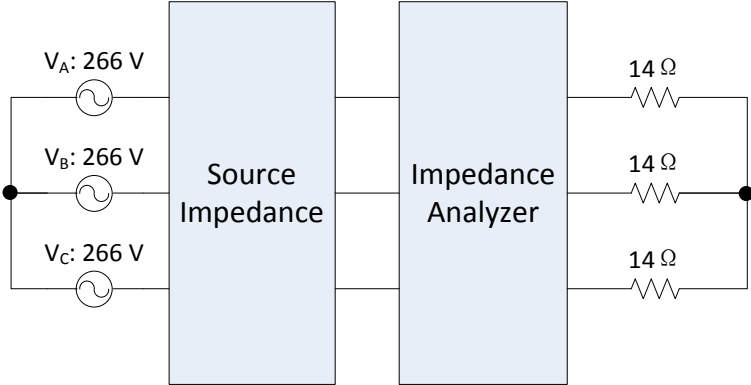


Figure 5-14: Measurement setup of R load

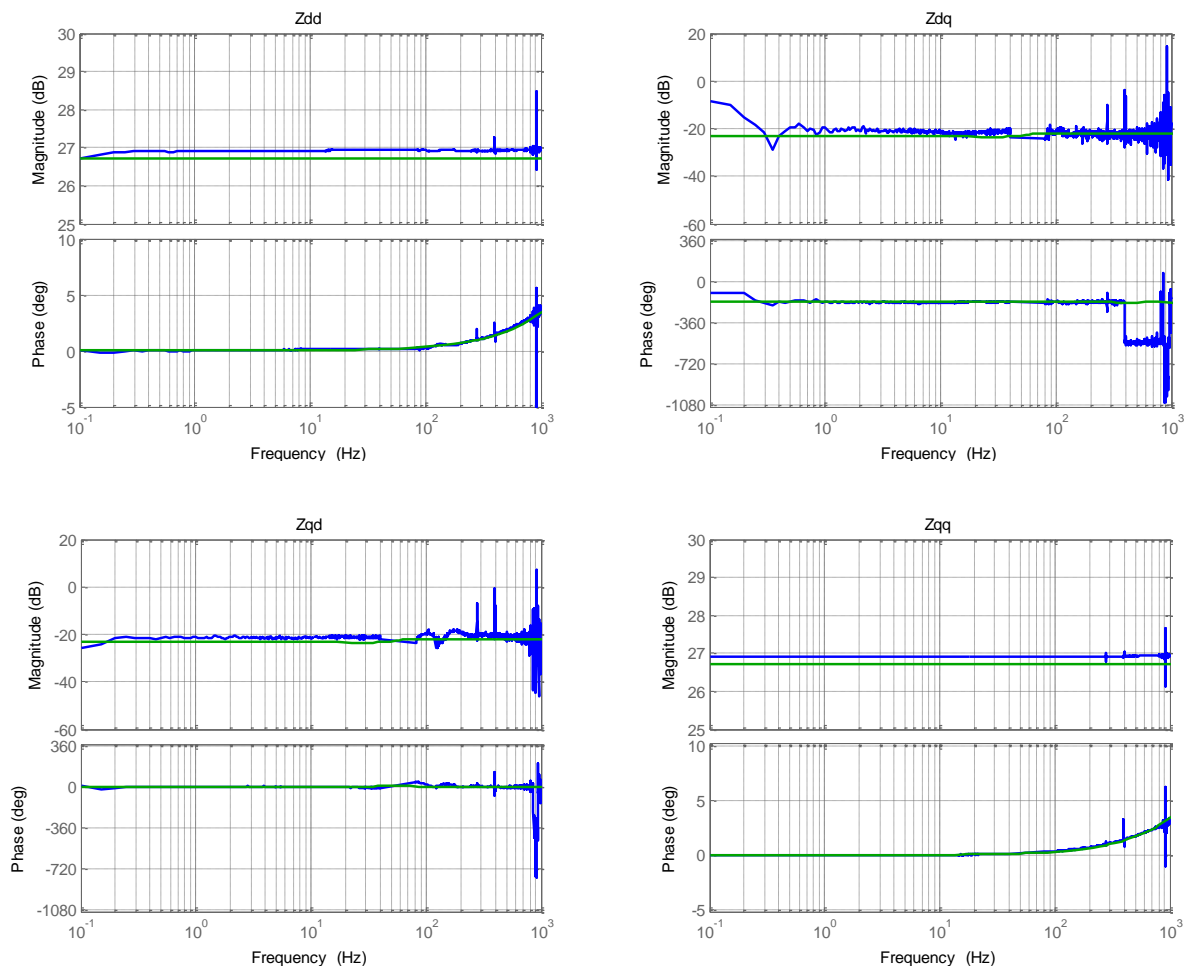


Figure 5-15: Resistive load impedance measurement result using design equipment (blue curve) and Agilent equipment (green curve)

The impedances shown in Figure 5-15 shows good match in the sub-hertz to one kilo-hertz range. The scales of the four figures are different. They are zoomed in so that the difference between the two results can be easily seen. There are a few differences between the results. There are several spikes shown on the blue curve because of the existence of voltage or current in the system to be measured at these specific frequency points. The magnitude differences in Z_{dd} and Z_{qq} are because of the change of the load bank resistance. The Agilent measurement is conducted with no current flowing through the load bank. But while the load bank is measured in the system, about sixteen amps of current goes through the resistors, which causes the temperature to increase by more than one hundred degree Celsius. The resistance increases together with the temperature. At high frequencies, Z_{dq} and Z_{qd} shows disagreement from the

results measured by Agilent equipment. This is because at a higher frequency, the injected perturbation drops due to the controller transfer function gain decrease. A smaller response level reduces the measurement accuracy. The reason why they only appear on Z_{dq} and Z_{qd} is these two terms are much smaller than the main terms (nearly 60 dB). The relative error becomes larger when the absolute value goes smaller. At very low frequencies (below 0.5 hertz), the measurement results are also suspicious, this is because the frequency reaches into the DC bus voltage controller of the perturbation generation device. The controller attenuates the perturbation reference to output gain. Less excitation causes the error as in the high frequency ranges.

Inductors are added before the load bank to increase the cross-coupling terms. The test setup and parameters are given in Figure 5-16:

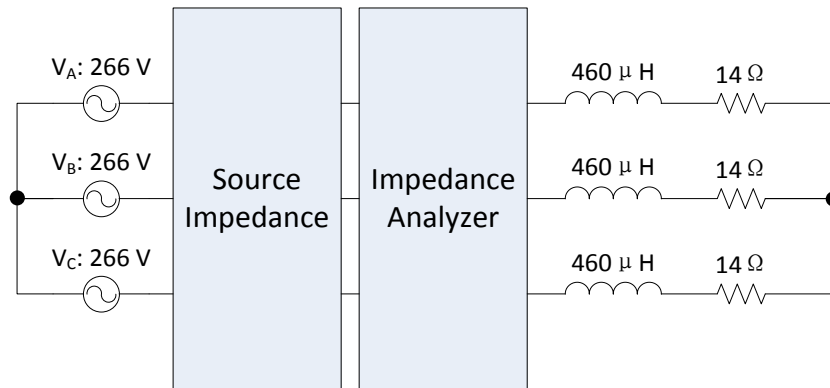


Figure 5-16: Measurement setup of RL load

The measurement result is also compared with the Agilent impedance analyzer's result. Figure 5-17 shows the comparison. The graphs show similar offset in Z_{dd} and Z_{qq} . They also have spikes in the measurement results at similar frequencies. But the error on Z_{dq} and Z_{qd} at high frequencies is reduced a lot. This is because the magnitudes of the two terms are enlarged compared with the resistive only load. Therefore the relative errors are reduced as expected.

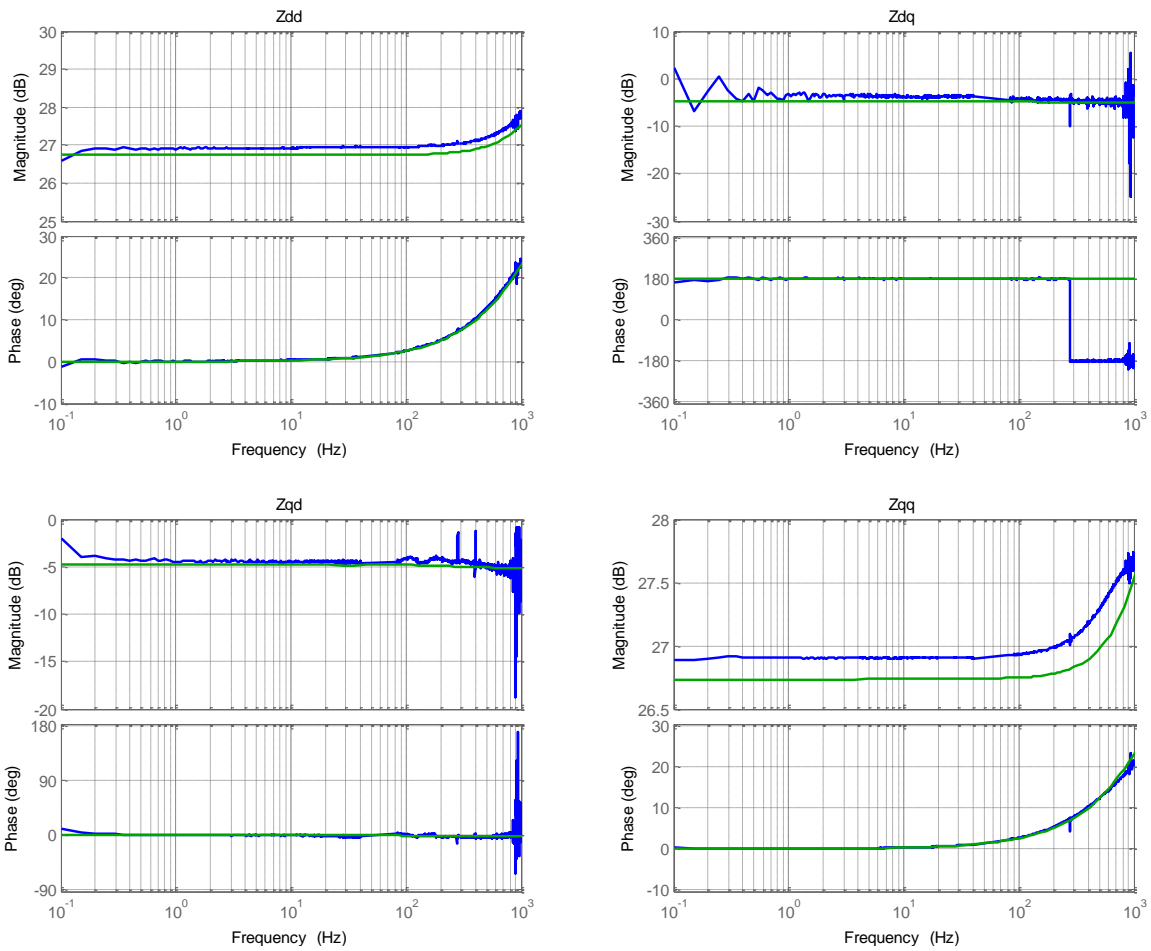


Figure 5-17: Resistive and inductive load impedance measurement result using design equipment (blue curve) and Agilent equipment (green curve)

5.4.2. Commercial Power Supply Impedance Measurement Result

During the measurement of passive impedance, the source side impedance is also measured in the same setup. Figure 5-18 shows the measurement result in previous two setups.

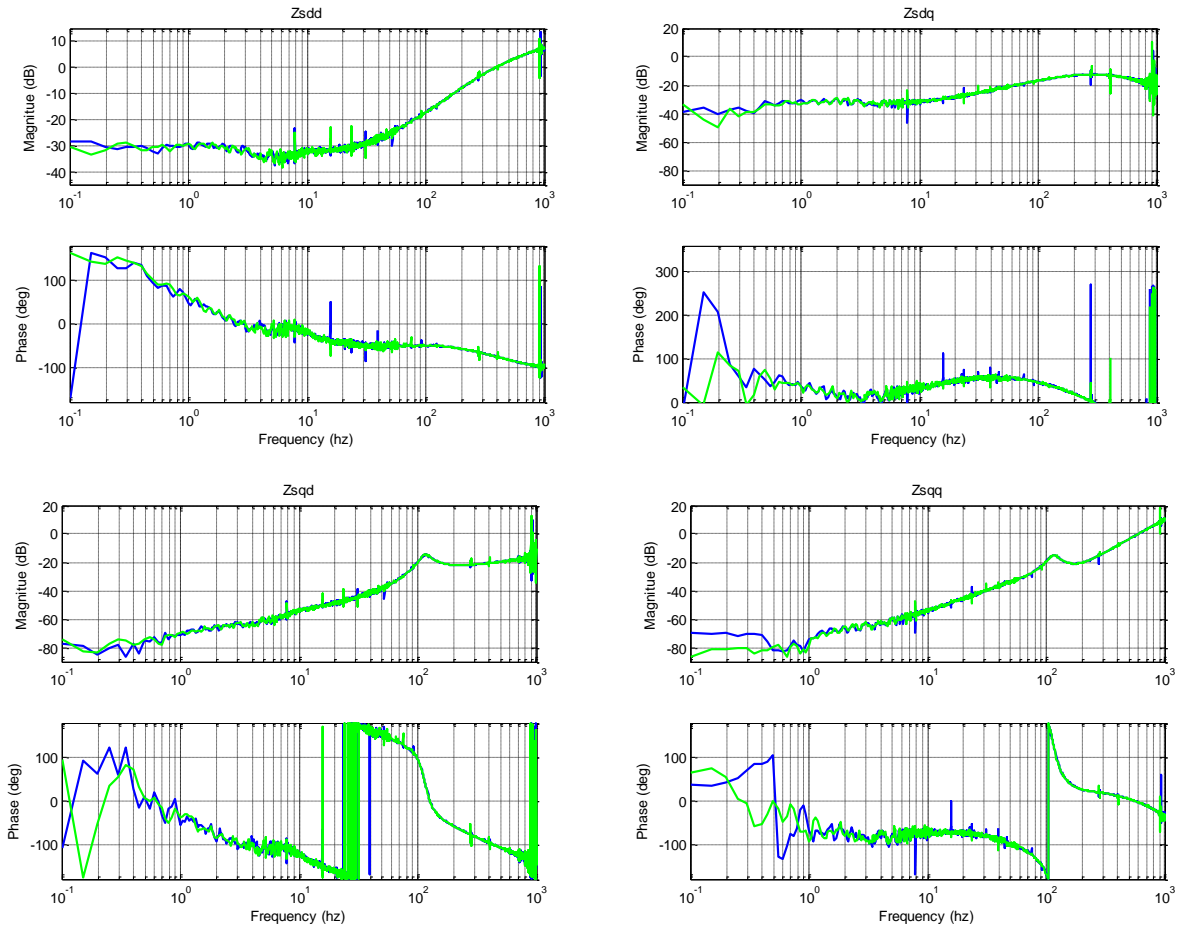


Figure 5-18: Impedance measurement of the commercial power supply (blue curve: measured with resistive load; green curve: measured with resistive-inductive load)

The two groups of measured impedances show good agreement from one-hertz to one kilo-hertz range. This is because the operating points of the two setups stay very similar. Although extra inductors are added, the influence on impedance at the fundamental frequency – 60 Hz – is so small that can be neglect. At very low frequency, the measurement shows suspicious results, which are caused by the same reason as the previous measurement.

Although there is no model or parameters to compare, the results do show reasonable value and trends. All the impedances are small, which is required to be a good voltage source. They also increase with the frequency showing the decrease of controller open loop gain.

5.4.3. Diode Rectifier Impedance Measurement Results

To test the performance on a non-linear load, a six-pulse diode rectifier is built. The setup and the parameters are shown in Figure 5-19. Figure 5-20 gives out the measured impedance result using blue curves.

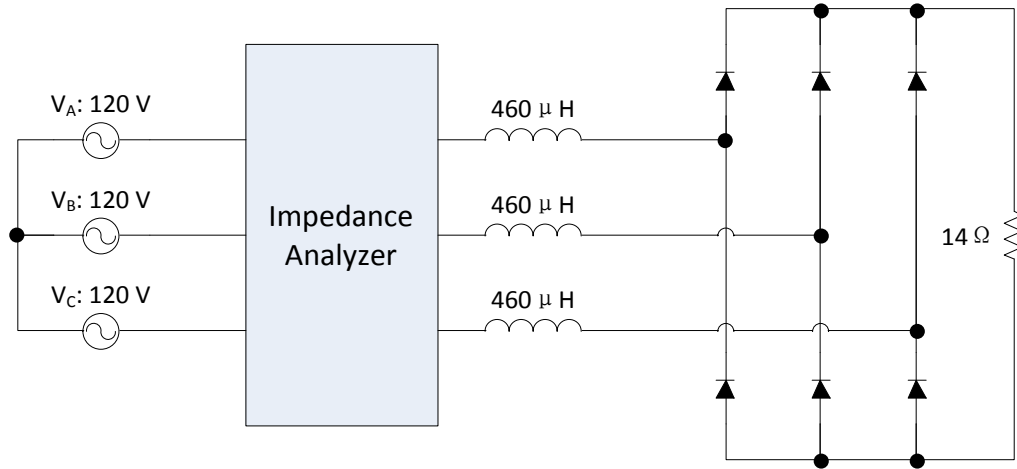


Figure 5-19: Diode bridge measurement setup

For comparison, the green dots show impedances extracted from a switching simulation model using a sinusoidal injection signal. The comparison shows a good match between the measurement and simulation results. A few spikes can be found in the curves. They are caused by the existing frequency component in the system. The average concept on the switching converter is valid up to half of the switching frequency. Thus all the results are shown up to 180 Hz which is the half of the diode bridge switching frequency.

The average concept on the diode bridge is considered to be valid up to half of the switching frequency [113, 114]. Thus all the results are shown up to 180 Hz, which is half of the diode bridge switching frequency.

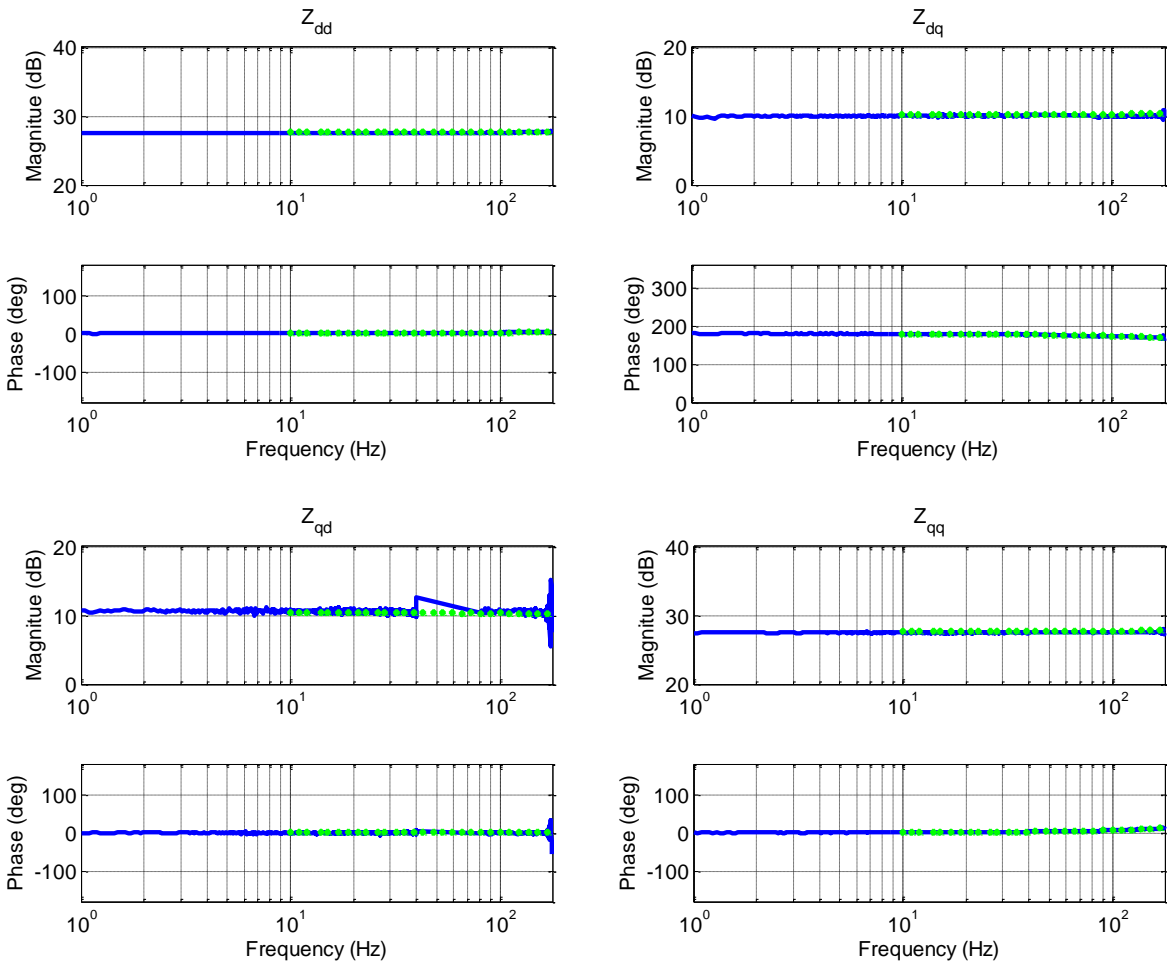


Figure 5-20: Diode bridge impedance measurement (blue curve) and simulation (green dots) result

A twelve pulse rectifier shown in Figure 5-21 is also measured. But the result is not compared with the simulation due to inaccurate modeling of the transformer used in the rectifier. The measurement result is shown in Figure 5-22.

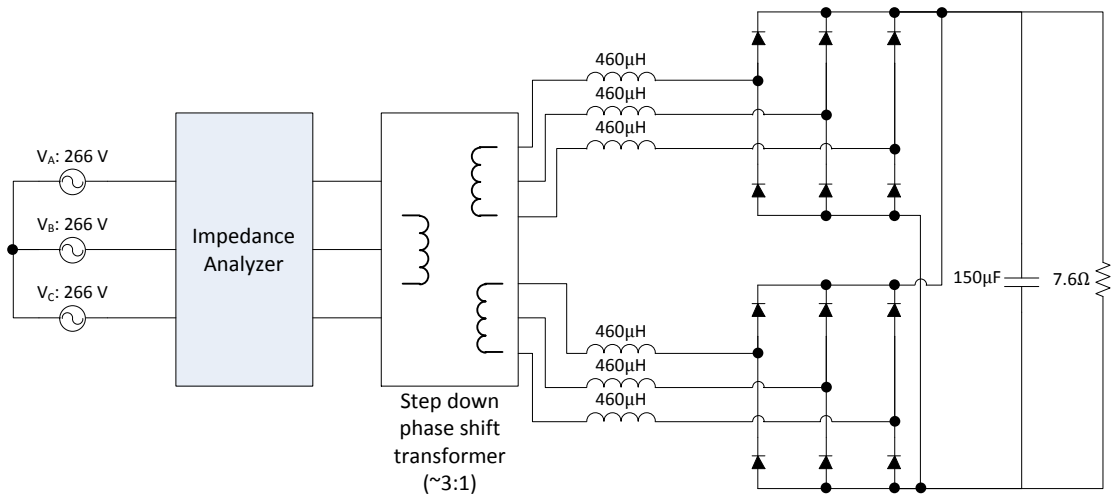


Figure 5-21: Measurement setup of twelve-pulse diode rectifier

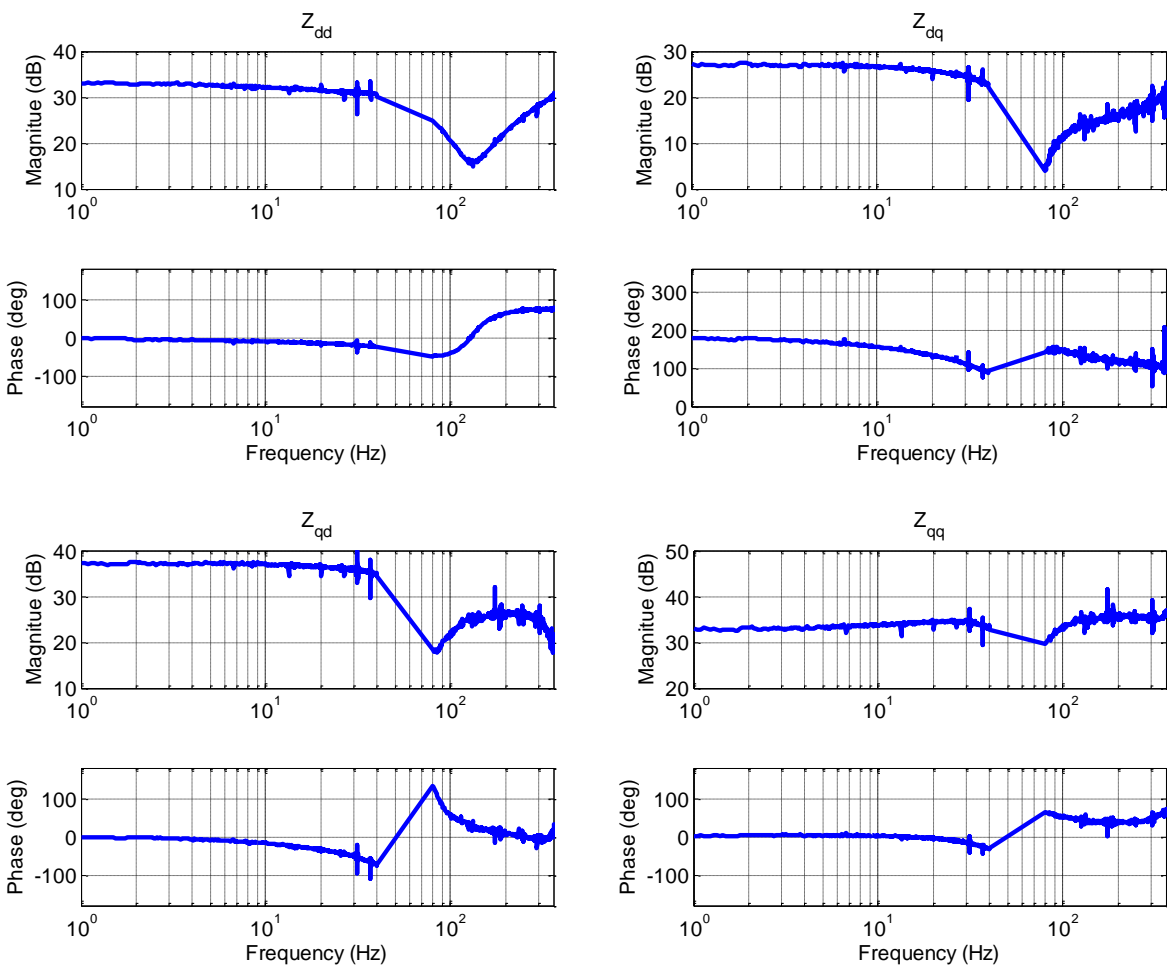


Figure 5-22: 12-pulse diode bridge impedance measurement result

5.5. Conclusion

The system architecture is designed in this chapter. The system is first divided into several function units. Then comments are made on the design or selection of each of the units. The software architecture and the signal flow are also designed in this chapter. The algorithm is also changed to better suit the targeted specifications. While the architecture is designed to be used on a low power prototype, the scalability is also discussed. An equipment is built according to the proposed architecture. The equipment is tested with various impedances. Two sets of passive impedance are measured. They show good match to the independent measurement made by the Agilent precision impedance analyzer. The reason for the difference between the results are discussed. The source impedances of the lab power supply are also presented, although not much discussion is made due to the lack of knowledge about the source inside information. Two diode rectifiers are measured to test the performance of the equipment on non-linear loads. The measured results are compared to the simulation results and shows an acceptable agreement when an accurate model is available. The equipment displays good performance on all the loads tested within a one hertz to one kilo hertz range.

Chapter 6. Conclusion and Future Work

6.1. Summary

This work presents the development of an impedance analyzer system to measure impedances of a three-phase AC power system in synchronous coordinates.

After the review of literature in Chapter 2, some error sources are identified in Chapter 3. The effect of nonidentical transfer functions for three-phase signal-processing circuits and the PLL on the measurements is derived in this chapter. The possible solutions to improve performance are also discussed. First, an improvement on the previous architecture is attempted in Chapter 4. The main contribution in this part is the connection change of the current injection amplifiers and the rearrangement of the measurement procedure. Some hardware tuning is also performed to further improve the performance.

Due to the limitation of previous architecture, a new, improved architecture is proposed in Chapter 5. A chirp signal is introduced into the three-phase AC system impedance measurement. Chirp signals have a low crest factor as a sine signal. It has a controllable spectrum that can spread across the frequency to be measured. Thus the measurement speed can be increased, which is useful for measuring at very low frequencies. Series injection is also found to be necessary in order to obtain good measurement at all source and load impedance combinations. Thus it is added into the improved architecture. The functions in each subsystem are rearranged, which makes the interface simple and saves communication bandwidth. An equipment is built using the proposed algorithm and architecture. The equipment is tested with various impedance. The test results show the implemented impedance analyzer is capable of identifying source and load impedances in the lab setup. The passive component impedances are correctly identified as compared to third-party equipment measurement results. The input impedances of a six-pulse diode rectifier and the output impedances of the lab power supply at different operating points are also obtained. Although there are no known correct results to compare, the measured impedances show a reasonable level and trend.

6.2. Conclusions

A three-phase impedance analyzer is developed. The equipment is validated measuring passive loads and tested with active loads. During the development of the system, the importance of the series injection is identified and emphasized. The series injection is first implemented in literature in the measurement of three-phase impedances. The influence of PLL on impedance measurement is studied. It shows potential compensation of the effect which means PLL with higher bandwidth could be used in the system without affecting the measurement accuracy. The effect of different transfer functions of three phase signal processing circuits is analyzed. It shows that the average of the transfer functions can be used to obtain the correct measurement. Chirp signal is introduced into the three-phase system impedance measurement. It shortens the measurement time. To leverage the power spectrum density drop caused by spreading the energy across the whole spectrum. A series of chirp signals are used. The data processing procedure from response signal to impedance is formalized. It includes the spectrum identification of the response signals, transfer function extraction from perturbation signal to response signals, and the final impedance calculation.

6.3. Future Work and Improvements

6.3.1. High Power High Bandwidth Injection Device Design

To scale the impedance analyzer to be used in higher power systems, a high power injection device is required. Some possible power stage topology is discussed in the dissertation. However, the control and other details of the implementation is not included, since it still requires significant effort. Other possible power stage topologies and injection devices can also be investigated.

6.3.2. Error Analysis

The error analysis in this dissertation focuses on systematical errors. Each stage in the measurement path is modeled by a group of transfer functions, which captures only the linear

part. The nonlinear behavior of the components should be further analyzed. Moreover, the various random errors and their propagation can be further studied to improve the knowledge of the measurement accuracy.

References

- [1] Middlebrook, R. D., “Input Filter Considerations in Design and Application of Switching regulators”, *IEEE Industry Applications Society Annual Meeting 1976 Record*, pp. 366-382, 1976.
- [2] Middlebrook, R. D., “Design Techniques for Preventing Input-Filter Oscillations in Switched-Mode Regulators”, *Proceedings of PowerCon 5, the Fifth National Solid State Power Conversion Conference*, May 1978.
- [3] C. Rivetta, G. A. Williamson, and A. Emadi, “Constant power loads and negative impedance instability in sea and undersea vehicles: statement of the problem and comprehensive large-signal solution,” in *Electric Ship Technologies Symposium, 2005 IEEE*, 2005, pp. 313–320.
- [4] Jian Sun, “AC power electronic systems: Stability and power quality,” in *Control and Modeling for Power Electronics, 2008. COMPEL 2008. 11th Workshop on*, 2008, pp. 1–10.
- [5] J. A. Weimer, “Electrical power technology for the more electric aircraft,” in , *AIAA/IEEE Digital Avionics Systems Conference, 1993. 12th DASC*, 1993, pp. 445 –450.
- [6] Kamiar J. Karimi, “The role of power electronics in more electric airplanes (MEA),” presentation at *2006 IEEE Control and Modeling for Power Electronics (COMPEL) Workshop*, July 2006.
- [7] J. A. Weimer, “The role of electric machines and drives in the more electric aircraft,” in *Electric Machines and Drives Conference, 2003. IEMDC'03. IEEE International*, 2003, vol. 1, pp. 11 – 15 vol.1.
- [8] J. Sun, “Analysis and design of single-phase PFC converters for airborne systems,” in *The 29th Annual Conference of the IEEE Industrial Electronics Society, 2003. IECON '03*, 2003, vol. 2, pp. 1101 – 1109 Vol.2.
- [9] N. Doerry and K. McCoy, “Next generation integrated power system: NGIPS technology development roadmap,” DTIC Document, 2007.
- [10] T. J. McCoy, “Trends in ship electric propulsion,” in *2002 IEEE Power Engineering Society Summer Meeting*, 2002, vol. 1, pp. 343 –346 vol.1.
- [11] J. V. Meer, A. Bendre, S. Krstic, and D. Divan, “Improved ship power system - generation, distribution, and fault control for electric propulsion and ship service,” in *2005 IEEE Electric Ship Technologies Symposium*, 2005, pp. 284 – 291.
- [12] T. J. McCoy and J. V. Amy, “The state-of-the-art of integrated electric power and propulsion systems and technologies on ships,” in *IEEE Electric Ship Technologies Symposium, 2009. ESTS 2009*, 2009, pp. 340 –344.

- [13] A. Emadi and S. S. Williamson, "Modern Automotive Power Systems: Advancements into the Future," in *Power Electronics and Motion Control Conference, 2006. EPE-PEMC 2006. 12th International*, 2006, pp. 1762-1768.
- [14] A. Emadi, A. Khaligh, C. H. Rivetta, and G. A. Williamson, "Constant power loads and negative impedance instability in automotive systems: Definition, modeling, stability, and control of power electronic converters and motor drives," *IEEE Transactions on Vehicular Technology*, vol. 55, pp. 1112-1125, Jul 2006.
- [15] A. Emadi, M. Ehsani, and J. M. Miller, *Vehicular electric power systems : land, sea, air, and space vehicles*. New York: Marcel Dekker, 2004.
- [16] J. M. Carrasco, L. G. Franquelo, J. T. Bialasiewicz, E. Galvan, R. C. P. Guisado, M. A. M. Prats, J. I. Leon, and N. Moreno-Alfonso, "Power-Electronic Systems for the Grid Integration of Renewable Energy Sources: A Survey," *IEEE Transactions on Industrial Electronics*, vol. 53, no. 4, pp. 1002 –1016, Jun. 2006.
- [17] F. Blaabjerg, Z. Chen, and S. B. Kjaer, "Power electronics as efficient interface in dispersed power generation systems," *IEEE Transactions on Power Electronics*, vol. 19, no. 5, pp. 1184 – 1194, Sep. 2004.
- [18] N. Hatziargyriou, H. Asano, R. Iravani, and C. Marnay, "Microgrids," *IEEE Power and Energy Magazine*, vol. 5, no. 4, pp. 78 –94, Aug. 2007.
- [19] D. Boroyevich, I. Cvetkovic, D. Dong, R. Burgos, F. Wang, and F. Lee, "Future electronic power distribution systems a contemplative view," in *2010 12th International Conference on Optimization of Electrical and Electronic Equipment (OPTIM)*, 2010, pp. 1369 –1380.
- [20] M. Reza, D. Sudarmadi, F. A. Viawan, W. L. Kling, and L. Van Der Sluis, "Dynamic Stability of Power Systems with Power Electronic Interfaced DG," in *Power Systems Conference and Exposition, 2006. PSCE '06. 2006 IEEE PES*, 2006, pp. 1423 –1428.
- [21] M. Reza, P. H. Schavemaker, J. G. Slootweg, W. L. Kling, and L. van der Sluis, "Impacts of distributed generation penetration levels on power systems transient stability," in *IEEE Power Engineering Society General Meeting, 2004*, 2004, pp. 2150 –2155 Vol.2.
- [22] J. G. Slootweg and W. L. Kling, "Impacts of distributed generation on power system transient stability," in *2002 IEEE Power Engineering Society Summer Meeting*, 2002, vol. 2, pp. 862 –867 vol.2.
- [23] S. Rosado, R. Burgos, S. Ahmed, F. Wang, and D. Boroyevich, "Modeling of power electronics for simulation based analysis of power systems," in *Proceedings of the 2007 summer computer simulation conference* San Diego, California: Society for Computer Simulation International, 2007
- [24] Xiaogang Feng, Jinjun Liu, and F. C. Lee, "Impedance specifications for stable DC distributed power systems," *Power Electronics, IEEE Transactions on DOI - 10.1109/63.988825*, vol. 17, no. 2, pp. 157–162, 2002.

- [25] S. Vesti, T. Suntio, J. A. Oliver, R. Prieto, and J. A. Cobos, “Impedance-Based Stability and Transient-Performance Assessment Applying Maximum Peak Criteria,” *IEEE Transactions on Power Electronics*, vol. 28, no. 5, pp. 2099–2104, May 2013.
- [26] C. M. Wildrick, F. C. Lee, B. H. Cho, and B. Choi, “A method of defining the load impedance specification for a stable distributed power system,” *IEEE Transactions on Power Electronics*, vol. 10, no. 3, pp. 280–285, May 1995.
- [27] S. D. Sudhoff, S. F. Glover, P. T. Lamm, D. H. Schmucker, and D. E. Delisle, “Admittance space stability analysis of power electronic systems,” *Aerospace and Electronic Systems, IEEE Transactions on DOI - 10.1109/7.869516*, vol. 36, no. 3, pp. 965–973, 2000.
- [28] L. Harnefors, M. Bongiorno, and S. Lundberg, “Stability analysis of converter-grid interaction using the converter input admittance,” in *Power Electronics and Applications, 2007 European Conference on*, 2007, pp. 1–10.
- [29] Jian Sun, “Small-Signal Methods for AC Distributed Power Systems—A Review,” *Power Electronics, IEEE Transactions on DOI - 10.1109/TPEL.2009.2029859*, vol. 24, no. 11, pp. 2545–2554, 2009.
- [30] J. Liu, X. Feng, F. C. Lee, and D. Borojevich, “Stability margin monitoring for DC distributed power systems via perturbation approaches,” *IEEE Transactions on Power Electronics*, vol. 18, no. 6, pp. 1254–1261, Nov. 2003.
- [31] Y. Qiu, L. Xiao, N. Zhang, and Z. Yao, “Stability of three-phase grid-connected inverters,” in *Power Electronics and Applications (EPE 2011), Proceedings of the 2011-14th European Conference on*, 2011, pp. 1–9.
- [32] P. Dang, J. Petzoldt, and T. Ellinger, “Stability analysis of multi-parallel APF systems,” in *Power Electronics and Applications (EPE 2011), Proceedings of the 2011-14th European Conference on*, 2011, pp. 1–8.
- [33] J. He, Y. W. Li, D. Bosnjak, and B. Harris, “Investigation and Active Damping of Multiple Resonances in a Parallel-Inverter-Based Microgrid,” *IEEE Transactions on Power Electronics*, vol. 28, no. 1, pp. 234–246, Jan. 2013.
- [34] M. Cespedes and J. Sun, “Methods for stability analysis of unbalanced three-phase systems,” in *2012 IEEE Energy Conversion Congress and Exposition (ECCE)*, 2012, pp. 3090–3097.
- [35] Zhonghui Bing, K. J. Karimi, and Jian Sun, “Input Impedance Modeling and Analysis of Line-Commutated Rectifiers,” *Power Electronics, IEEE Transactions on DOI - 10.1109/TPEL.2009.2025333*, vol. 24, no. 10, pp. 2338–2346, 2009.
- [36] Jian Sun, Zhonghui Bing, and K. J. Karimi, “Input Impedance Modeling of Multipulse Rectifiers by Harmonic Linearization,” *Power Electronics, IEEE Transactions on DOI - 10.1109/TPEL.2009.2033067*, vol. 24, no. 12, pp. 2812–2820, 2009.

- [37] Jian Sun and K. J. Karimi, "Small-signal input impedance modeling of line-frequency rectifiers," *Aerospace and Electronic Systems, IEEE Transactions on*, vol. 44, no. 4, pp. 1489–1497, 2008.
- [38] A. MacFarlane and I. Postlethwaite, "The generalized Nyquist stability criterion and multivariable root loci," in *Int. Jour. of Control*, vol. 25, pp. 81-127, Jan. 1977.
- [39] A. MacFarlane, *Frequency-Response Methods in Control Systems*. IEEE Press, Inc., New York 1979.
- [40] I. Postlethwaite and A. MacFarlane, "A complex variable approach to the analysis of linear multivariable feedback systems," in A.V. Balakrishnan and M. Thoma, *Lecture Notes in Control and Information Sciences*, no.12, Springer-Verlag, Berlin 1979.
- [41] A. MacFarlane, *Complex Variable Methods for Linear Multivariable Feedback Systems*. Taylor & Francis Ltd., London 1980.
- [42] A. MacFarlane, "Return-difference and return-ratio matrices and their use in analysis and design of multivariable feedback control systems," in *Proc. IEE*, no. 117, pp.2037-2049, 1970.
- [43] A. MacFarlane and J. Belletrutti, "The characteristic locus design method," in *Automatica*, no. 9, pp. 575-588, 1973.
- [44] H. Rosenbrock, *Computer-Aided Control System Design*. Academic Press Inc, New York 1974.
- [45] J. Layton, *Multivariable Control Theory*. Peter Peregrinus Ltd., England 1976.
- [46] H. Nyquist, "Regeneration theory," *Bell Syst. Tech. Journ.*, vol. 11, pp. 126–147, Jan. 1932.
- [47] W. Evans, "Control system synthesis by root locus method," *AIEE Trans.*, vol. 69, pp. 66–69, 1950.
- [48] M. Stojic, and D. Siljak, "Generalization of Hurwitz, Nyquist and Mikhailov stability criteria," *IEEE Trans. on Aut. Control*, vol. 10, no. 3, pp. 250–254, July 1965.
- [49] W. Brockett, and J. Willems, "Frequency domain stability criteria—Part I," *IEEE Trans. on Aut. Control*, vol. 10, no. 3, pp. 255–261, July 1965.
- [50] W. Brockett, and J. Willems, "Frequency domain stability criteria—Part II," *IEEE Trans. on Aut. Control*, vol. 10, no. 4, pp. 407–413, Oct. 1965.
- [51] N. Munro, *Modern Approaches to Control System Design*. Peter Peregrinus Ltd. & IEE, New York and London 1979.
- [52] M. Safonov, *Stability and Robustness of Multivariable Feedback Systems*. The MIT Press, MA 1980.

- [53] I. Postlethwaite, J. Edmunds, and A. MacFarlane, "Principal gains and principal phases in the analysis of linear multivariable feedback systems," *IEEE Trans. on Aut. Control*, vol. 26, no. 1, pp. 32–46, Feb. 1981.
- [54] M. Smith, "Matrix fractions and strict system equivalence," *Int. Jour. of Control*, vol. 34, no. 5, pp. 869–883, 1981.
- [55] M. Smith, "On the generalized Nyquist stability criterion," *Int. Jour. of Control*, vol. 34, no. 5, pp. 885–920, 1981.
- [56] M. Smith, "Multivariable root-locus behaviour and the relationship to transfer-function pole-zero structure," *Int. Jour. of Control*, vol. 34, no. 5, pp. 885–920, 1981.
- [57] S. Hiti, "Modeling and control of three-phase PWM converters," Blacksburg, VA: Virginia Polytechnic Institute and State University, 1995., 1995.
- [58] S. Hiti, V. Vlatkovic, D. Borojevic, and F. C. . Lee, "A new control algorithm for three-phase PWM buck rectifier with input displacement factor compensation," *IEEE Transactions on Power Electronics*, vol. 9, no. 2, pp. 173–180, Mar. 1994.
- [59] M. Belkhat, "Stability criteria for AC power systems with regulated loads," West Lafayette, IN: Purdue University, 1997.
- [60] Z. Liu, J. Liu, W. Bao, Y. Zhao, and F. Liu, "A novel stability criterion of AC power system with constant power load," in *Applied Power Electronics Conference and Exposition (APEC), 2012 Twenty-Seventh Annual IEEE*, 2012, pp. 1946–1950.
- [61] R. Burgos, D. Boroyevich, F. Wang, K. Karimi, and G. Francis, "On the Ac stability of high power factor three-phase rectifiers," in *Energy Conversion Congress and Exposition (ECCE), 2010 IEEE*, 2010, pp. 2047-2054.
- [62] R. Burgos, D. Boroyevich, F. Wang, K. Karimi, and G. Francis, "Ac stability of high power factor multi-pulse rectifiers," in *Energy Conversion Congress and Exposition (ECCE), 2011 IEEE*, 2011, pp. 3758-3765.
- [63] D. Crevier and A. Mercier, "Estimation of Higher Frequency Network Equivalent Impedances by Harmonic Analysis Natural Waveforms," *Power Apparatus and Systems, IEEE Transactions on*, vol. PAS-97, no. 2, pp. 424–431, 1978.
- [64] M. Sumner, B. Palethorpe, D. W. P. Thomas, P. Zanchetta, and M. C. Di Piazza, "A technique for power supply harmonic impedance estimation using a controlled voltage disturbance," *Power Electronics, IEEE Transactions on*, vol. 17, no. 2, pp. 207–215, 2002.
- [65] M. L. Gasperi, "AC power line impedance monitoring method and system," U.S. Patent 716427516-Jan-2007.

- [66] J. P. Rhode, A. W. Kelley, and M. E. Baran, "Complete characterization of utilization-voltage power system impedance using wideband measurement," *Industry Applications, IEEE Transactions on*, vol. 33, no. 6, pp. 1472–1479, 1997.
- [67] N. Ishigure, K. Matsui, and F. Ueda, "Development of an on-line impedance meter to measure the impedance of a distribution line," in *Industrial Electronics, 2001. Proceedings. ISIE 2001. IEEE International Symposium on*, 2001, vol. 1, pp. 549–554 vol.1.
- [68] M. Sumner, B. Palethorpe, D. Thomas, P. Zanchetta, and M. C. Di Piazza, "Estimation of power supply harmonic impedance using a controlled voltage disturbance," in *Power Electronics Specialists Conference, 2001. PESC. 2001 IEEE 32nd Annual*, 2001, vol. 2, pp. 522–527 vol.2.
- [69] M. Nagpal, W. Xu, and J. Sawada, "Harmonic impedance measurement using three-phase transients," *Power Delivery, IEEE Transactions on*, vol. 13, no. 1, pp. 272–277, 1998.
- [70] A. Knop and F. W. Fuchs, "High frequency grid impedance analysis with three-phase converter and FPGA based tolerance band controller," in *Compatibility and Power Electronics, 2009. CPE '09.*, 2009, pp. 286–291.
- [71] M. B. Harris, A. W. Kelley, J. P. Rhode, and M. E. Baran, "Instrumentation for measurement of line impedance," in *Applied Power Electronics Conference and Exposition, 1994. APEC '94. Conference Proceedings 1994., Ninth Annual*, 1994, pp. 887–893 vol.2.
- [72] J. P. Rhode, A. W. Kelley, and M. E. Baran, "Line impedance measurement: a nondisruptive wideband technique," in *Industry Applications Conference, 1995. Thirtieth IAS Annual Meeting, IAS '95., Conference Record of the 1995 IEEE*, 1995, vol. 3, pp. 2233–2240 vol.3.
- [73] M. L. Gasperi, D. L. Jensen, and D. T. Rollay, "Method for AC Powerline Impedance Measurement," *Industry Applications, IEEE Transactions on DOI - 10.1109/TIA.2008.926189*, vol. 44, no. 4, pp. 1034–1037, 2008.
- [74] J. Xie, Y. X. Feng, and N. Krap, "Network Impedance Measurements for Three-phase High-voltage Power Systems," in *Power and Energy Engineering Conference (APPEEC), 2010 Asia-Pacific*, 2010, pp. 1–5.
- [75] N. Hoffmann and F. W. Fuchs, "Online grid impedance estimation for the control of grid connected converters in inductive-resistive distributed power-networks using extended kalman-filter," in *2012 IEEE Energy Conversion Congress and Exposition (ECCE)*, 2012, pp. 922–929.
- [76] M. Cespedes and J. Sun, "Online grid impedance identification for adaptive control of grid-connected inverters," in *2012 IEEE Energy Conversion Congress and Exposition (ECCE)*, 2012, pp. 914–921.

- [77] K. Matsui, N. Ishigure, and F. Ueda, "On-line impedance meter to measure the impedance of a distribution line using inverter," in *Industrial Electronics Society, 2001. IECON '01. The 27th Annual Conference of the IEEE*, 2001, vol. 2, pp. 1230–1236 vol.2.
- [78] M. L. Gasperi, D. L. Jensen, and D. T. Rollay, "Power line parameter analysis method and system," U.S. Patent 752639228-Apr-2009.
- [79] B. Palethorpe, M. Sumner, and D. W. P. Thomas, "Power system impedance measurement using a power electronic converter," in *Harmonics and Quality of Power, 2000. Proceedings. Ninth International Conference on*, 2000, vol. 1, pp. 208–213 vol.1.
- [80] A. de Oliveira, J. C. de Oliveira, J. W. Resende, and M. S. Miskulin, "Practical approaches for AC system harmonic impedance measurements," *Power Delivery, IEEE Transactions on*, vol. 6, no. 4, pp. 1721–1726, 1991.
- [81] D. Martin, E. Santi, and A. Barkley, "Wide bandwidth system identification of AC system impedances by applying perturbations to an existing converter," in *Energy Conversion Congress and Exposition (ECCE), 2011 IEEE*, 2011[68]1, pp. 2549–2556.
- [82] Y. L. Familant, K. A. Corzine, J. Huang, and M. Belkhat, "AC Impedance Measurement Techniques," in *Electric Machines and Drives, 2005 IEEE International Conference on*, 2005, pp. 1850–1857.
- [83] Y. L. Familant, "AC impedance measurement techniques in power systems," University of Wisconsin, Milwaukee, 2006.
- [84] J. Huang and K. A. Corzine, "AC impedance measurement by line-to-line injected current," in *Industry Applications Conference, 2006. 41st IAS Annual Meeting. Conference Record of the 2006 IEEE*, 2006, vol. 1, pp. 300–306.
- [85] S. Cobreces, F. Huerta, D. Pizarro, F. J. Rodriguez, and E. J. Bueno, "Three-phase power system parametric identification based on complex-space recursive least squares," in *Intelligent Signal Processing, 2007. WISP 2007. IEEE International Symposium on*, 2007, pp. 1–6.
- [86] Peng Xiao, G. Venayagamoorthy, and K. Corzine, "A Novel Impedance Measurement Technique for Power Electronic Systems," in *Power Electronics Specialists Conference, 2007. PESC 2007. IEEE*, 2007, pp. 955–960.
- [87] Peng Xiao, G. K. Venayagamoorthy, and K. A. Corzine, "Impedance Identification of Integrated Power System Components using Recurrent Neural Networks," in *Electric Ship Technologies Symposium, 2007. ESTS '07. IEEE*, 2007, pp. 48–52.
- [88] Peng Xiao, G. K. Venayagamoorthy, and K. A. Corzine, "Combined Training of Recurrent Neural Networks with Particle Swarm Optimization and Backpropagation Algorithms for Impedance Identification," in *Swarm Intelligence Symposium, 2007. SIS 2007. IEEE*, 2007, pp. 9–15.

- [89] Y. A. Familiant, Jing Huang, K. A. Corzine, and M. Belkhat, “New Techniques for Measuring Impedance Characteristics of Three-Phase AC Power Systems,” *Power Electronics, IEEE Transactions on*, vol. 24, no. 7, pp. 1802–1810, 2009.
- [90] Jing Huang, K. A. Corzine, and M. Belkhat, “Online Synchronous Machine Parameter Extraction From Small-Signal Injection Techniques,” *Energy Conversion, IEEE Transactions on*, vol. 24, no. 1, pp. 43–51, 2009.
- [91] Jing Huang, K. A. Corzine, and M. Belkhat, “Small-Signal Impedance Measurement of Power-Electronics-Based AC Power Systems Using Line-to-Line Current Injection,” *Power Electronics, IEEE Transactions on*, vol. 24, no. 2, pp. 445–455, 2009.
- [92] V. Valdivia, A. Lázaro, A. Barrado, P. Zumel, and C. Fernández, “Impedance identification method of three-phase balanced voltage source inverters based on load current steps,” in *Control and Modeling for Power Electronics (COMPEL), 2010 IEEE 12th Workshop on*, 2010, pp. 1–7.
- [93] G. Francis, “An Algorithm and System for Measuring Impedance in D-Q Coordinates,” Virginia Tech, Blacksburg, 2010.
- [94] G. Francis, R. Burgos, D. Boroyevich, F. Wang, and K. Karimi, “An algorithm and implementation system for measuring impedance in the D-Q domain,” in *Energy Conversion Congress and Exposition (ECCE), 2011 IEEE*, 2011, pp. 3221–3228.
- [95] V. Valdivia, A. Lázaro, A. Barrado, P. Zumel, C. Fernández, and M. Sanz, “Impedance Identification Procedure of Three-Phase Balanced Voltage Source Inverters Based on Transient Response Measurements,” *Power Electronics, IEEE Transactions on DOI - 10.1109/TPEL.2011.2141687*, vol. 26, no. 12, pp. 3810–3816, 2011.
- [96] Williams, Michael Lamar, “Method for measuring stability margin at a node of a polyphase power grid,” U.S. Patent 7508224.
- [97] L. Harnfors, M. Bongiorno, and S. Lundberg, “Input-Admittance Calculation and Shaping for Controlled Voltage-Source Converters,” *Industrial Electronics, IEEE Transactions on DOI - 10.1109/TIE.2007.904022*, vol. 54, no. 6, pp. 3323–3334, 2007.
- [98] V. Valdivia, A. Lázaro, A. Barrado, P. Zumel, C. Fernández, and M. Sanz, “Black-box modeling of three phase voltage source inverters based on transient response analysis,” in *Applied Power Electronics Conference and Exposition (APEC), 2010 Twenty-Fifth Annual IEEE*, 2010, pp. 1279–1286.
- [99] S. Ahmed, Z. Shen, P. Mattavelli, D. Boroyevich, M. Jaksic, K. Karimi, and J. Fu, “Small-signal model of a voltage source inverter (VSI) considering the dead-time effect and space vector modulation types,” in *2011 Twenty-Sixth Annual IEEE Applied Power Electronics Conference and Exposition (APEC)*, 2011, pp. 685–690.
- [100] Zhiyu Shen, M. Jaksic, S. Ahmed, P. Mattavelli, and D. Boroyevich, “Parametric study of dead time effect on three phase AC output impedance of Voltage Source Inverter (VSI),”

- in *Proceedings of the 2011-14th European Conference on Power Electronics and Applications (EPE 2011)*, 2011, pp. 1–8.
- [101] S. Müller and P. Massarani, “Transfer-Function Measurement with Sweeps,” *Journal of Audio Engineering Society*, vol. 49, Jun. 2001, pp.
- [102] G. Stan, J. Embrechts, and D. Archambeau, “Comparison of Different Impulse Response Measurement Techniques,” *Journal of Audio Engineering Society*, vol. 50, Apr. 2002, pp. 249-262.
- [103] A. Barkley and E. Santi, “Online Monitoring of Network Impedances Using Digital Network Analyzer Techniques,” in *Twenty-Fourth Annual IEEE Applied Power Electronics Conference and Exposition, 2009. APEC 2009*, 2009, pp. 440 –446.
- [104] M. Sumner, B. Palethorpe, and D. W. P. Thomas, “Impedance measurement for improved power quality-Part 1: the measurement technique,” *Power Delivery, IEEE Transactions on*, vol. 19, no. 3, pp. 1442-1448, 2004.
- [105] S.-K. Chung, “A phase tracking system for three phase utility interface inverters,” *Power Electronics, IEEE Transactions on*, vol. 15, no. 3, pp. 431-438, 2000.
- [106] V. Kaura and V. Blasko, “Operation of a phase locked loop system under distorted utility conditions,” *Industry Applications, IEEE Transactions on*, vol. 33, no. 1, pp. 58-63, 1997.
- [107] B. Miao, R. Zane, and D. Maksimovic, “System identification of power converters with digital control through cross-correlation methods,” *Power Electronics, IEEE Transactions on*, vol. 20, no. 5, pp. 1093 – 1099, Sep. 2005.
- [108] P. Welch, “The use of fast Fourier transform for the estimation of power spectra: A method based on time averaging over short, modified periodograms,” *Audio and Electroacoustics, IEEE Transactions on*, vol. 15, no. 2, pp. 70-73, 1967.
- [109] <http://www.ni.com/pxi/whatis/>
- [110] Massoud, A.M., “Three-Phase, Three-Wire, Five-Level Cascaded Shunt Active Filter for Power Conditioning, Using Two Different Space Vector Modulation Techniques, ” *Power Delivery IEEE Transactions on*, Vol. 22, Issue 4, Oct. 2007
- [111] Li, B.H., “Transformerless dynamic voltage restorer, Generation,” *Transmission and Distribution, IEE Proceedings on*, Vol. 149, Issue 3, May 2002[110]
- [112] Zhang, Di, “Analysis and Design of Paralleled Three-Phase Voltage Source Converters with Interleaving”, Virginia Tech, 2010
- [113] Jian Sun and K. J. Karimi, “Small-signal input impedance modeling of line-frequency rectifiers,” *Aerospace and Electronic Systems, IEEE Transactions on*, vol. 44, no. 4, pp. 1489-1497, 2008.

- [114] Zhonghui Bing, K. J. Karimi, and Jian Sun, "Input Impedance Modeling and Analysis of Line-Commutated Rectifiers," *Power Electronics, IEEE Transactions on*, vol. 24, no. 10, pp. 2338-2346, 2009.
- [115] Justin S. Walraven, "Design of an Arbitrary Waveform Generator for Power System Perturbation," Virginia Tech, Blacksburg, 2011.

Appendix A. Design and Implementation of the Measurement Equipment

A.1. Perturbation Injection Unit

The perturbation generation unit is actually an arbitrary waveform generator, although it is used mainly to generate chirp signals in dq frame. Table A-1 outlines the specifications of the unit.

Table A-1: Performance and Hardware Specifications

Performance Mark/ Device Specified	Specification Value
Bus Power, Nominal	100 kW
Bus Voltage, line-to-line, Nominal	460 VAC RMS
Injection Power, min	1% of nominal Bus Power (1.0 kW)
Injection Power, max	5% of nominal Bus Power (5 kW)
Frequency Range of Interest	.1-1000 Hz
Injection Modes	Shunt and Series

The detail design procedure is described in [115]. Here only some important information is captured.

A.1.1. Power Stage Design

A PEBB converter American Superconductor PM1000 is used for both shunt and series injection. The converter is overrated for the application, which reduces the change of fault damage during the development. Thus, the semiconductor device selection and thermal design is not included. The main concern for the power stage design focuses on the passive components.

For shunt injection, the circuit in Figure A-1 is used. The components values are listed in Table A-2.

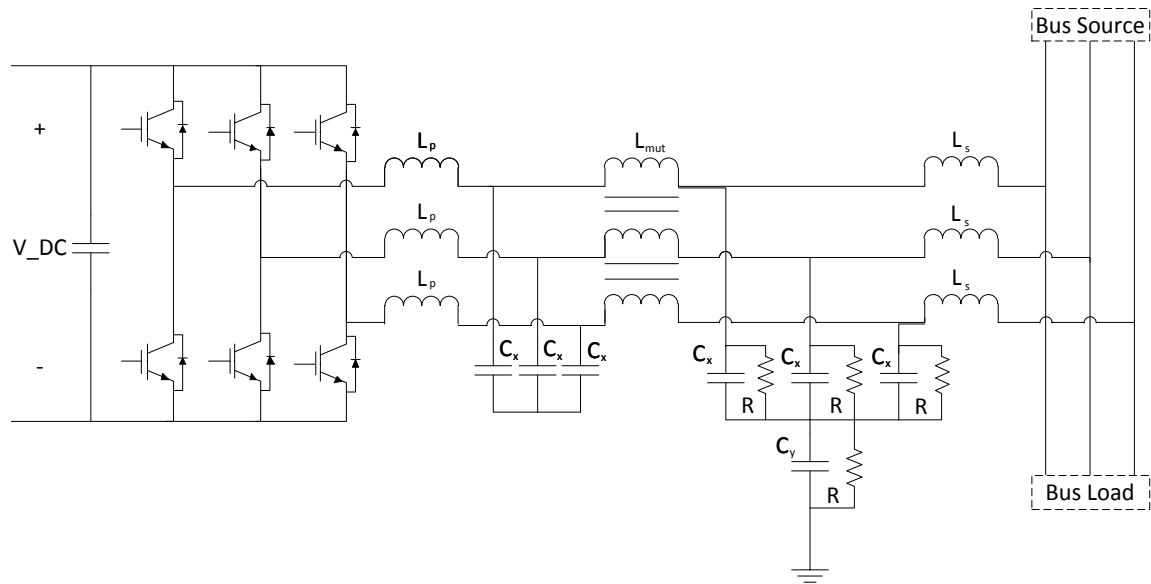


Figure A-1: Complete Shunt Injection Power Stage

Table A-2: Shunt Injection Power Stage Schematic Component Values

Component	Value
L_p	2.5mH
L_s	.5mH
L_m	3.5mH
C_x	2 μ F
C_y	1 μ F
R	1M Ω

The design uses a τ shape filter to remove the switching frequency components in the injected current. It also features an EMI filter to attenuate mainly the common mode noise generated by the converter. The differential mode capacitors in the EMI filter is reused to be the filter capacitor in the τ shape filter.

For series injection, the circuit in Figure 1-2 is used. Most of the passive components are reused, except the inductors connected to the bus, which are removed. Transformers are also added for isolation. The specification of the transformers are given in Table A-3.

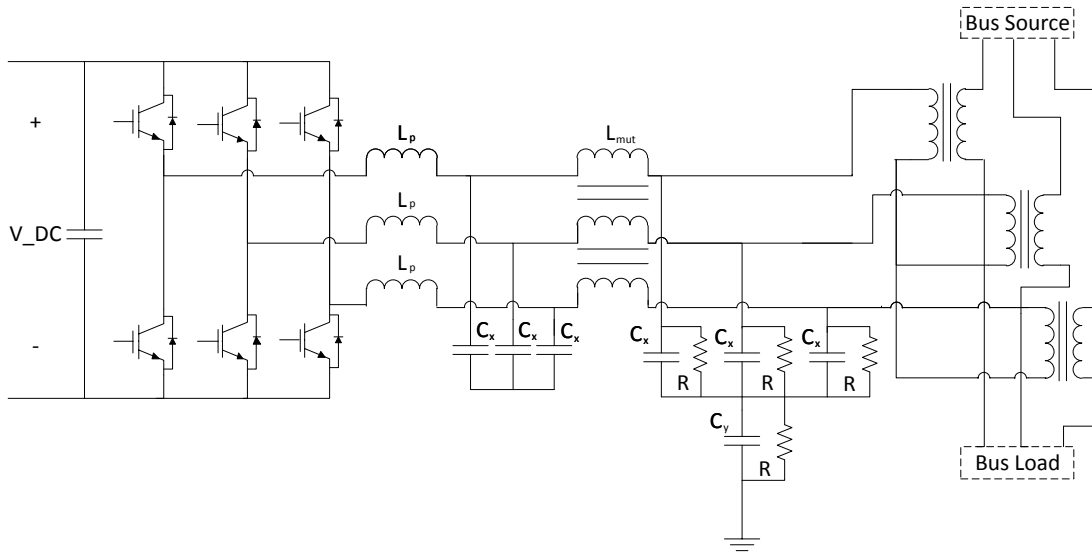


Figure A-2: Series Injection Power Stage

Table A-3: Series Injection Transformer Specifications

Specification	Value
Turns Ratio, Primary: Secondary	10:1
Primary Windings Maximum RMS Voltage	200V
Secondary Windings Maximum RMS Voltage	20V
Primary Windings Maximum RMS Operating Current	20A
Secondary Windings Maximum RMS Operating Current	200A
Overall Dielectric Strength to Ground	650.5V min
Lowest Frequency of Continuous Operation	40Hz

The converter runs open loop for series injection. Due to the existence of the filter impedances, the injection voltage sources shown in Figure 3-15 are no longer close to ideal. The filter impedances behave as the output impedance of the voltage sources in Figure 3-15. As the injection frequency increases, the leakage inductances of the transformer start to dominant and the voltage sources are no longer close to ideal. The unit, however still works well as a perturbation source.

A.1.2. Control Loop Design

The control block diagram of the unit is shown in Figure A-3. The controller is switched between the closed-loop current control for shunt connection shown in green blocks and the open-loop voltage control for series injection shown in blue blocks. For both injection modes, a DC bus voltage controller is shared.

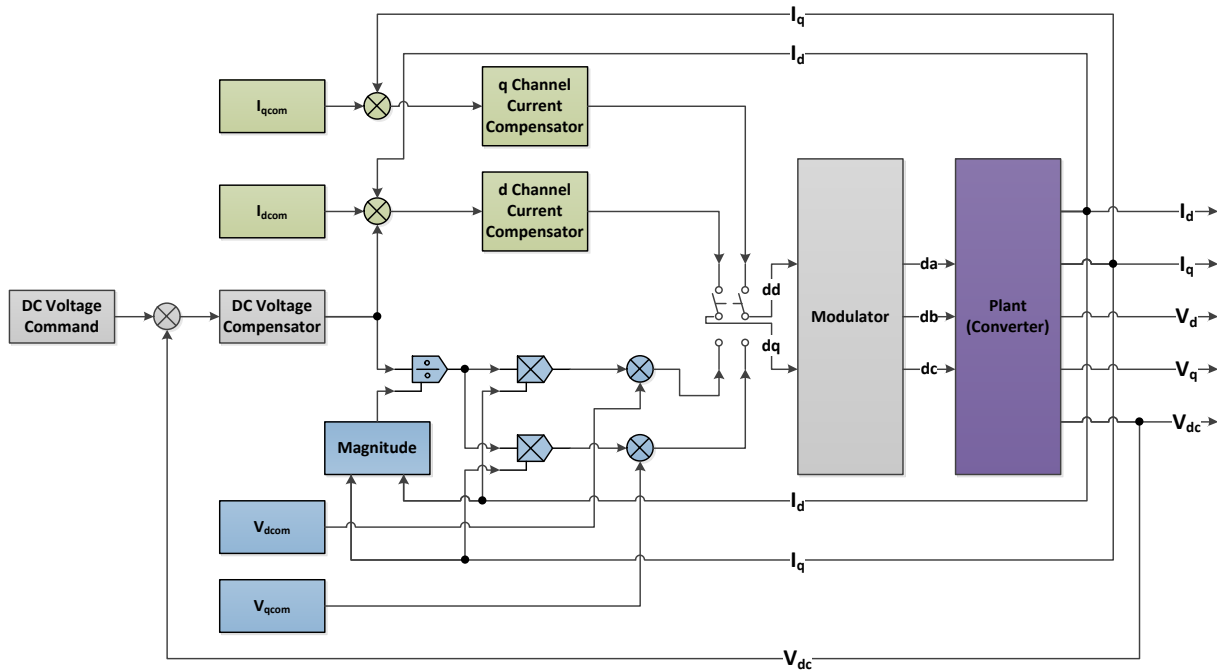


Figure A-3: PIU controller block diagram

A.1.3. Hardware Characteristics

A.1.3.1. Injection Spectrum

Figure A-4 gives out the injected current spectrum when the shunt connection is used. From this it can be seen that the requirement for a nearly flat spectrum between 1 Hz to 1 kHz is achieved. But at the frequencies below 1 Hz, the spectrum departs from the ideal chirp signal spectrum. This is because the dynamic of the DC bus voltage controller. The controller bandwidth can be further decreased to reduce this influence. But the DC bus capacitance needs to be increased accordingly.

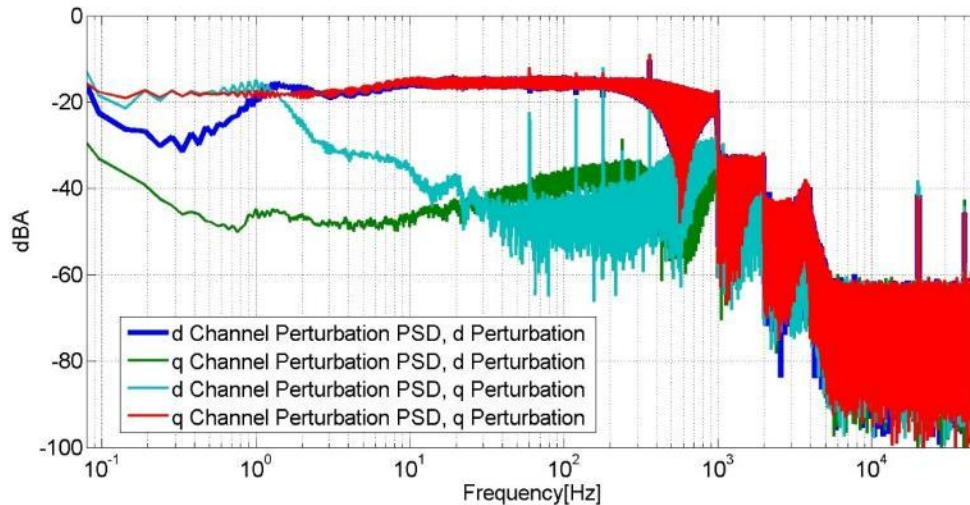


Figure A-4: d and q Perturbation Current Power Spectral Densities as a Result of a d and q Perturbation

A.1.3.2. Injection Capability

Although targeted at the specifications given at the beginning of this section, the practical design issues limit the injection capability. Figure 5-144 graphically describes these limits.

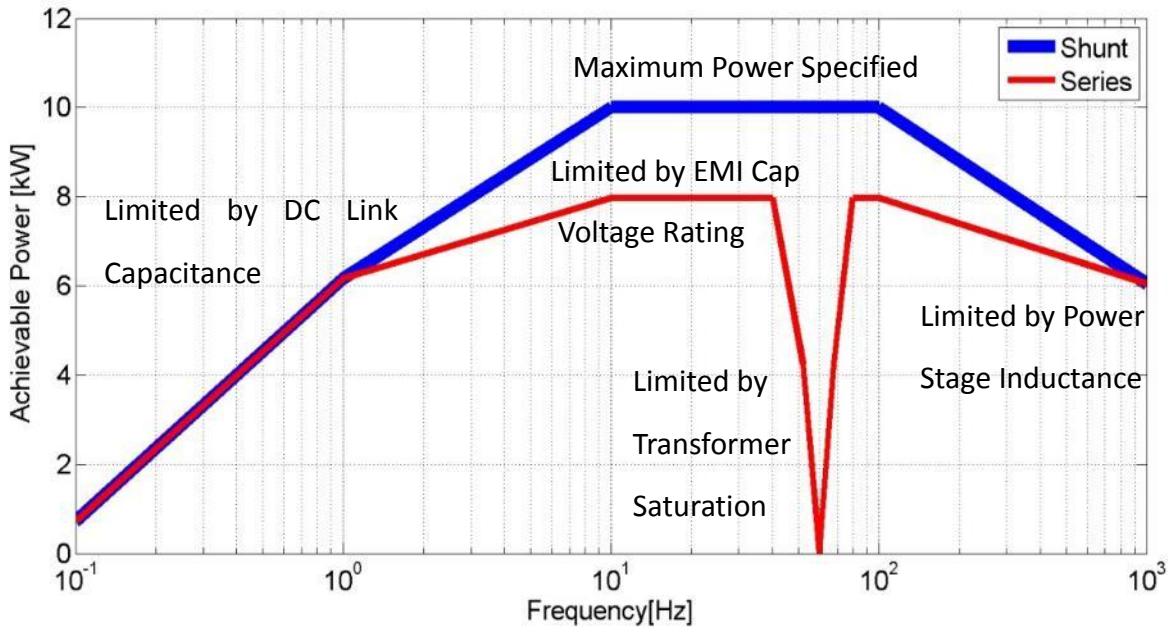


Figure A-5: Achievable Perturbation Power as a Function of Frequency

It can be seen from the figure that transformerless design with huge DC link capacitance or even DC bus power supply is preferred for a more uniform perturbation generation capability at all frequency points.

A.2. Signal Interface Unit

The signal interface unit connects the digital computer to the sensors and the relays. It conditions the signals and drives the relays. The unit implements four functions: analog input, analog output, digital input, digital output. Some other auxiliary components also exist in the unit to support these four functions. Figure A-6 shows the block diagram of the unit.

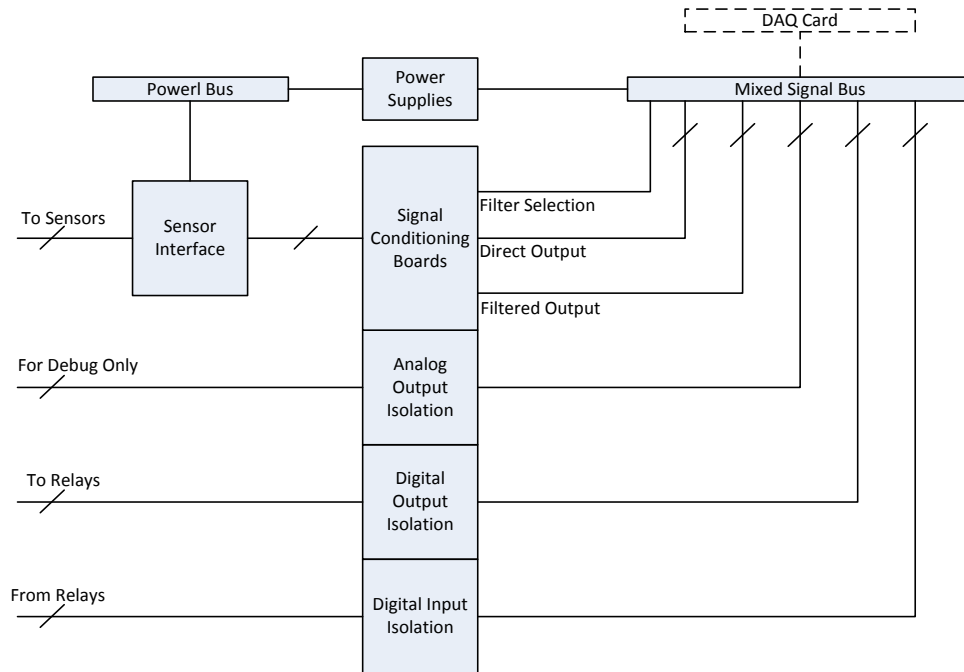


Figure A-6: Signal interface unit block diagram

Each of the four main functions has one kind of dedicated PCB card to implement the requirement. Each card provides a certain amount of channels for the required function. Several cards of the same function are integrated into the unit to obtain the necessary amount of channels. All of the card are plugged in the mixed signal bus to aggregate the signals and connect them to the PXI computer, which controls everything. Power supply of all the cards is also distributed on the bus board.

A.2.1. Analog Input

The analog input part of the SIU connects to the sensors. The unit processes the signals using analog circuits to prepare them to be sampled. Since an analog circuit performs much better than the digital signal processing on the dynamic range and the sampling of the signal brings aliasing in frequency domain. Thus, the amplification, attenuation, and anti-aliasing filtering of the signal have to be implemented by analog circuits. Besides the signals from the sensors, a synchronization signal from the PIU is also connected to this part of the SIU. It is sampled

simultaneously with the sensors signals to synchronize the perturbation reference signals generated by the PIU and the system response feedback from the sensors.

As shown in Figure 5-9, the card has four stages. They are input buffer, notch filter, multiplexer, anti-aliasing filter, and output buffer.

A.2.1.1. Input Stage

The main function of the input stage is the impedance adjustment. The following filter circuits need a low output impedance from the previous stage. But the signals from the sensors usually do not meet this requirement and prefer high impedance inputs. Thus, a high input impedance amplifier is used to match the requirement for both sides.

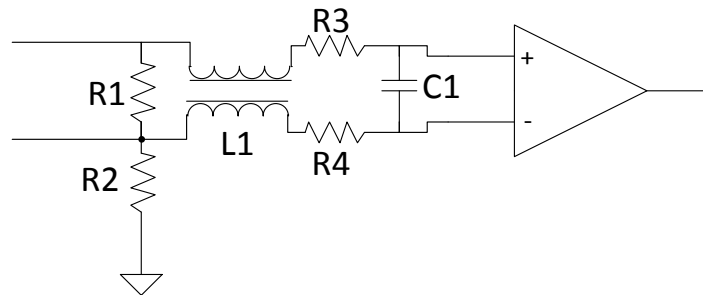


Figure A-7: Input stage circuit

Figure A-7 shows the implementation. R1 in the circuit provides the path for the differential mode current, while R2 is the path of the common mode current. The common mode choke attenuates the high frequency noise. The instrumentation amplifier itself can reject the low frequency common mode noise up to a few kilo hertz. R2, R4 and C1 form a low pass filter of differential mode to filter the noise.

A.2.1.2. Notch Filter Stage

The signals from the sensors include the information of both the system line frequency components and the perturbation frequency components, among which the line frequency component is dominant. If the signal is directly digitalized, many bits of the AD resolution are

used to represent the line frequency signal. Only a few bits are left to quantize the perturbation signal.

A solution to this problem is to filter out the line frequency and to amplify the perturbation signals to nearly the full scale of the AD input range. But this solution only works for the frequencies far enough away from the line frequency because it is hard to implement high-Q-factor analog filters with identical characteristics. When the frequency of interest is close to the line frequency, advanced digital signal processing is the only meaningful way to extract the perturbation information. Since the line frequency is much lower than the highest frequency of interest, over sampling technology can be applied to increase the equivalent ADC resolution.

To achieve narrow block bandwidth, eighth order filters are selected. The detail circuit is shown in Figure A-8. Since the line frequency may have a 3% variation, the filter is designed to attenuate the frequency components within 3% of the line frequency by at least 40 dB and to pass the frequency components 5Hz away from the line frequency with attenuation less than 0.02dB. The real components only have limited value to be selected from. They also have a tolerance band which means the values only sit within a certain range instead of being exactly the value as marked. The real achieved transfer functions are affected by these factors and are far from ideal.

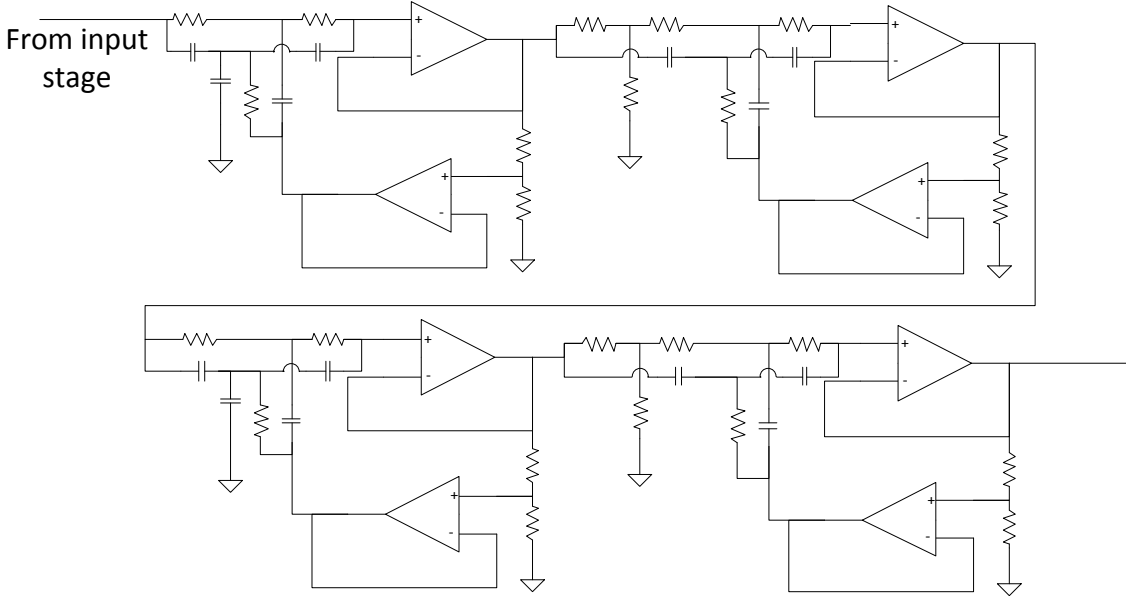
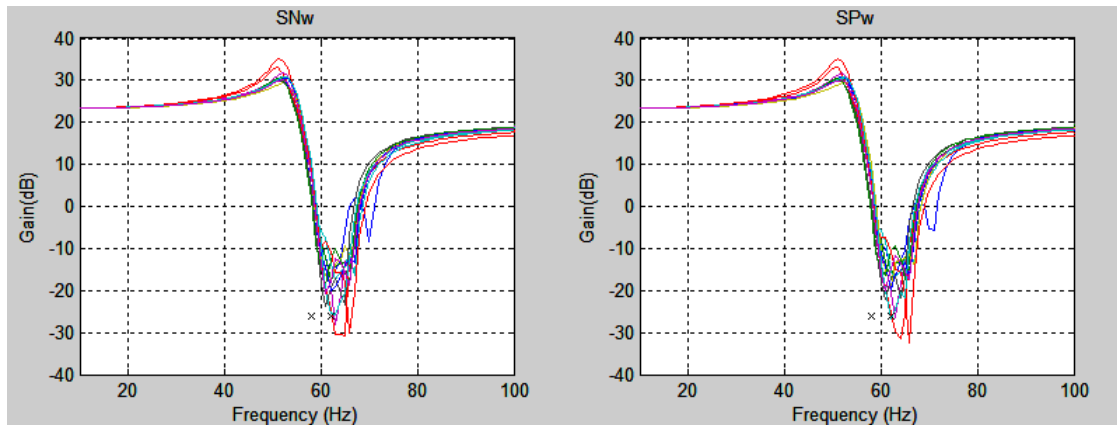


Figure A-8: Notch filter stage circuit

Figure A-9 shows the measured transfer function of the board with a notch filter in path. Since the output is a differential signal, which does not have a common ground with the input signal as described latter, the transfer functions are measured from positive rail and negative rail of the signal separately. From the figure we can see the attenuation is smaller than the design because the attempt to increase the notch width, and the transfer functions varies between different board. Hence we can see from the measurement result that, the notch filter can only be used for the measurement frequency range beyond 200 Hz.



(a) Positive rail

(b) Negative rail

Figure A-9: Transfer function of the signal conditioning card with 60 Hz notch filter in the path

A.2.1.3. Multiplexer Stage

Trying to use more of the AD input scale, several sets of the signal processing circuit are used for different frequency ranges. The notch filters reducing line frequency are used when the measurement frequency is above a certain frequency in d-q coordinates, which means the frequency components are several hertz away from the line frequency in abc coordinates. For the other frequencies to be measured, only a buffer is added to lower the output impedance.

The selection between these sets of circuits is made by several multiplexers controlled by the measurement control unit. The multiplexer is digital controlled analog switches made by MOSFETs.

While switching between the sets of the signal processing circuit, system voltages are always required to obtain the phase information. Thus a bypass path for the source voltages is designed. No matter which set of circuit is used; the source voltages are passed through a buffer then directly fed to the next stage.

A.2.1.4. Anti-aliasing Filter Stage

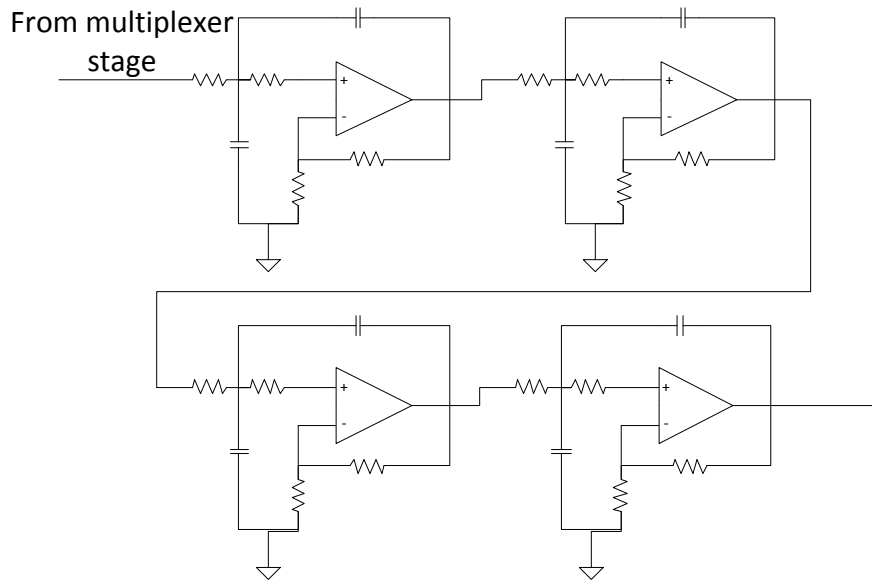


Figure A-10: Anti-aliasing filter stage circuit

When a signal is sampled and analyzed in the frequency domain using the discrete Fourier transform (DFT) technique, the frequency components that are higher than the Nyquist frequency (half of the sampling frequency) appear to be between the dc and the Nyquist frequency. There is no way to distinguish them from the real low frequency components digitally. Thus, an analog low pass filter is usually added before the sampling to attenuate the components beyond Nyquist frequency.

While attenuating the high frequency components, the lower frequency components of interest should not change. This can be achieved by setting the filter cut-off frequency high enough so that the useful frequencies are way below. Or a very steep filter should be used, the gain of which stay nearly constant below the cut-off frequency and drops immediately when reaching the cut-off frequency. Both of these provisions are adopted when designing the anti-aliasing filter. Since the sampling frequency is 2 MHz for the data conversion unit, the

corner frequency is set to 100 kHz, which is 100 times the highest interested frequency and an eighth order filter is used. Less than 0.001 dB attenuation at 1 kHz and more than 100 dB attenuation at 1 MHz are achieved.

A.2.1.5. Output Stage

A differential connection is less sensitive in picking up noise than the single ended one. Thus it is selected to transfer the signal from the signal interface unit to the data acquisition unit. Since the signal is in single ended form within the signal conditioning card, a final output stage is added to convert the signal to differential mode.

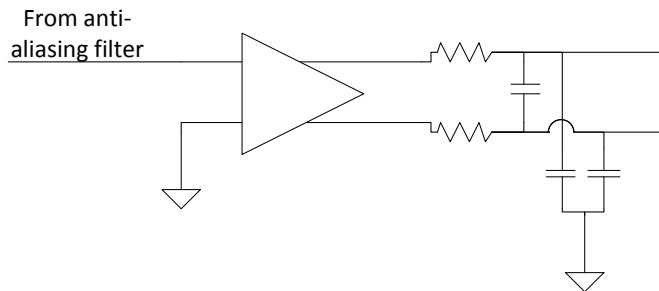


Figure A-11: Output stage circuit

The circuit shown in Figure A-11 is implemented for this purpose. The negative input of differential amplifier ADA4922-1 is connected to ground of the single ended signal. The positive input of the amplifier is fed by the previous anti-aliasing filter output attenuated to 50% by the resistor divider. The amplifier has a gain of two in this configuration. Thus the output of it is $\pm 10V$ with 0V common mode. Thus each line varies between -5V and +5V so that the maximum allowable input range of the data acquisition card is used. A low pass passive filter is added after the output of the amplifier. It filters both common mode and differential mode signal. The cut off frequency is set to 300 kHz to reduce the high frequency noise possibly generated by the amplifier without affecting the useful signals which are below 1 kHz.



Figure A-12: Picture of the signal conditioning card

Figure A-12 shows a picture of the populated signal conditioning card. The signals are sent to the card via the golden SMB on the left of the picture. At the right side of the connector is the input stage. Above the input stage is the power supply circuit of the card. The two rows of IC below the input stage are the operational amplifiers of the notch filters. The passive components of the filter are at the back of the card. Below the filter area are the multiplexer and the output stage of the card.

A.2.2. Analog Output

There is no mandatory requirement for the analog output function. But it is very useful during the debug stage. It can be used to monitor the state of the unit and some internal variables in the code which do not exist in the physical world. The DAQ card selected has digital to analog conversion (DAC) function integrated. So the interface unit just needs to bring them out for easy access. Since the analog output may be connected to equipment which may be grounded at a different point from the impedance analyzer rack, an isolation of the signal is preferred to prevent unnecessary ground loops, especially for common mode noise propagation.

The detail block diagram of the card is shown in Figure A-13. The key components of the card are two isolation amplifier ISO124 from Texas Instrument. They provide the isolation of 1500 V rms for analog signals up to 50 kHz bandwidth

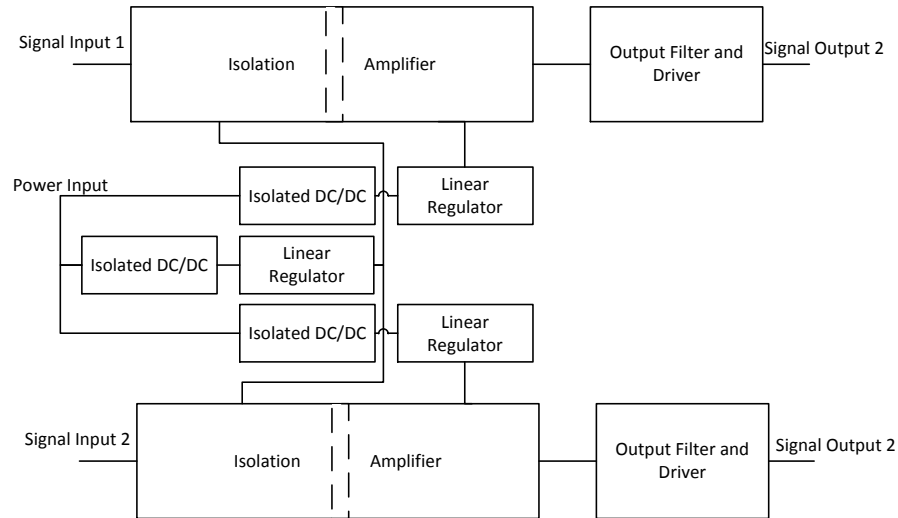


Figure A-13: Function diagram of analog output isolation card

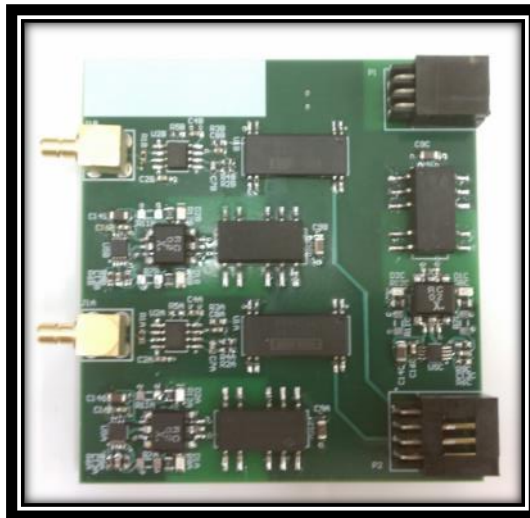


Figure A-14: Picture of the analog output isolation card

Figure A-14 shows the assembled analog output card. There is a third isolated DC/DC converter shown at the middle of right side of the card. This converter is added because the

ISO124 requires $\pm 15V$ for its operation. All the cards connected to the mixed signal bus are powered by $\pm 12.6V$ supplies. The converter here boosts the voltage up for the normal operation of the ISO124.

A.2.3. Digital Output

The digital output card is used to drive other components works from different power rail or easily introduce noise. In the impedance analyzer, it drives two indicators that are powered from the 120V power rail. All the relays that change the power part configuration are also driven by the isolated digital output card.

Figure A-15 shows the function diagram of one channel on the card. Its key components is an opto-couplers with TRIAC output. The input side of the optocoupler is driven by a digital signal buffer on the card which just repeats the state of the digital signals from the DAQ card while boosting its driving capability to ± 16 mA. The outputs of the optocoupler are directly wired to the connector. They work as AC switches for voltage up to 600 V.

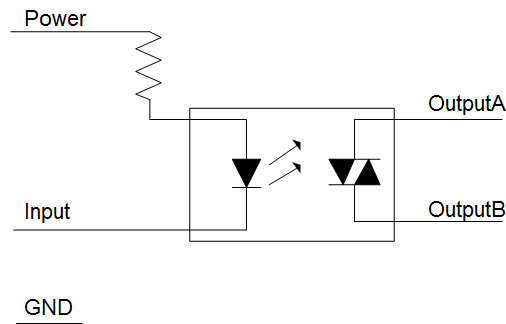


Figure A-15: Function diagram of one channel on digital output isolation card

The picture of the whole digital output isolation card is shown in Figure A-16. There are twenty-four channels on a single card. They are connected through the two connectors on the left of the picture.

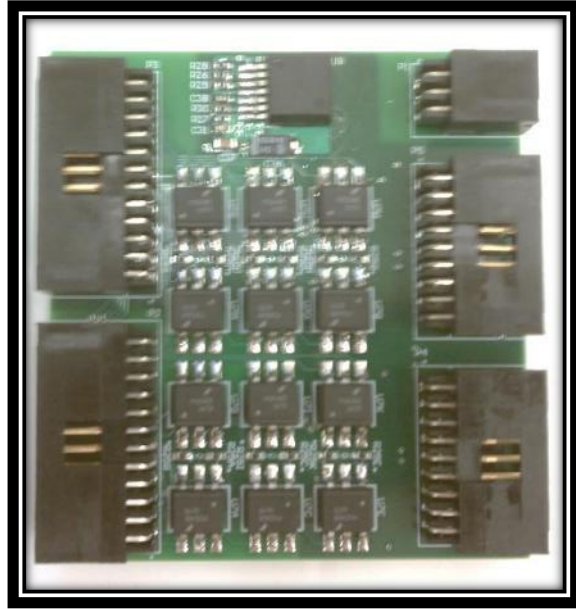


Figure A-16: Picture of the digital output isolation card

A.2.4. Digital Input

The digital input card provides the isolation for the input digital signals. In the impedance analyzer, it provides the state feedback from the relays. So the control unit can check the relay state after it commands the relay to act. It is important to have this feature for the relays configuring power part of the analyzer. If the circuit starts to work without the relays in the right position, they might be damaged.

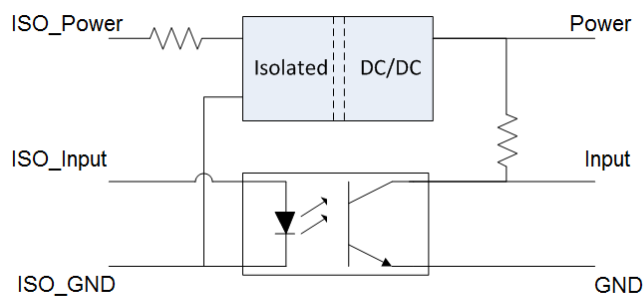


Figure A-17: Function diagram of one channel on digital input isolation card

Figure A-17 shows how a single channel works on the digital input card. The key component is still optocoupler. It is connected in the reverse direction of the digital output card. The input side of the optocoupler requires power to work. To work with switches with no power like relays, an isolated DC/DC converter is provided for each channel. All the DC/DC converters are independent from each other. So the channels can be used with circuit at different potentials within the isolations range of both optocouplers and the DC/DC converters. Figure A-18 shows the picture of the populated digital input card having 16 channels on it.

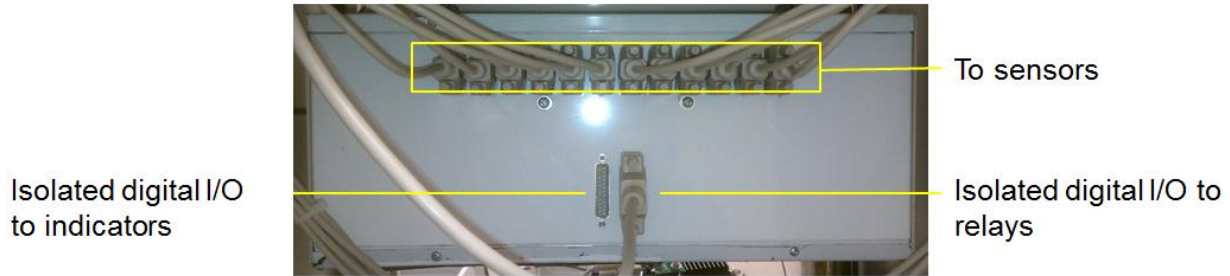


Figure A-18: Picture of the digital output isolation card

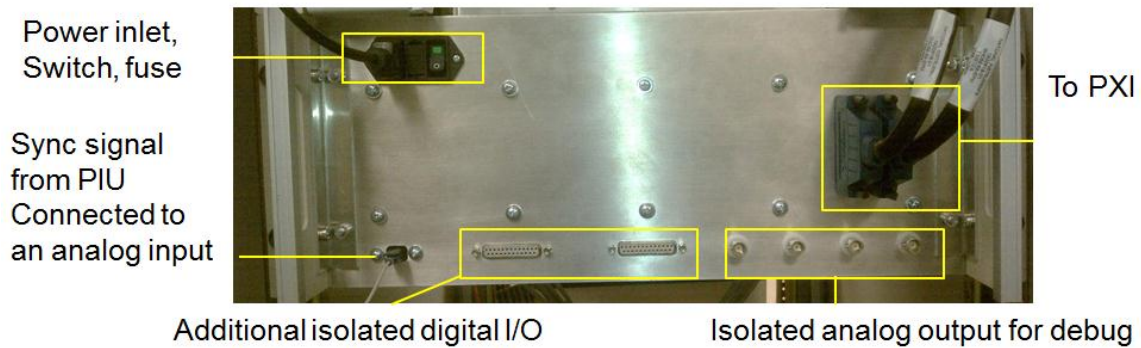
A.2.5. Unit Assembly

All the parts described in the previous sections are assembled in a case to be a single unit. A 4U height 19 inches wide chassis is selected to be easily mounted into the cabinet together with other components. The chassis is full metal and will be grounded through the mounting rack to provide shield to radiative EMI noise.

The connectors to the components interacting with the high power part of the equipment are located at the front side as shown in Figure A-19(a). All twelve sensors, relays and the indicators are connected via the connectors here.



(a) Front view



(b) Rear view

Figure A-19: Picture of the assembled signal interface unit

Figure A-19(b) shows the rear view of the SIU. It has all the other connectors. At the left bottom part of the picture, a small optofiber connection is shown. It connects to the thirteenth signal conditioning card. So the synchronization signal from PIU can be sampled simultaneously with the sensor signals connected to the other twelve signal conditioning cards.

A.3. Data Conversion Unit

A.3.1. Hardware Selection

As mentioned in Chapter 5, the hardware platform uses a PXI infrastructure computer. Such a computer usually contains three components: chassis, controller, and the extension card providing detail functions.

A.3.1.1. PXI chassis

The PXI chassis is the backbone of your PXI system. It provides the power, cooling, and communication buses of PCI and PCI Express for the controller and modules.



Figure A-20: PXI chassis – PXIe-1082

Figure A-20 shows the chosen chassis – PXIe-1082. It is an eight-slot chassis. A high-bandwidth backplane is provided by the chassis to meet a wide range of high-performance test and measurement application needs. The chassis accepts PXI Express modules in every slot and supports standard PXI hybrid-compatible modules in up to four slots. It also provides very accurate synchronized reference clock which is 100 MHz with an accuracy of ± 25 ppm, less than 3 ps jitter, and a maximum slot-to-slot skew of 100 ps.

A.3.1.2. Embedded Real Time Controller

The PXI chassis can accept two types of controllers: embedded controller and remote controller. The embedded controller is a module plugged into the chassis. The remote controller could be a desktop, workstation, server, or laptop computer and connected to the PXI chassis through a connection kit.

A dedicated embedded controller running a real-time operating system is selected for this application. Embedded controllers eliminate the need for an external PC, therefore providing a complete system contained within the PXI chassis. A real time operating system has to be used to provide a predictable execution time in micro seconds scale which is required by the algorithm to track the system phase.



Figure A-21: Real time controller – PXIe-8133

The NI PXIe-8133RT shown in Figure A-21 is selected. It has a 1.73 GHz quad-core Intel Core i7-820 processor. The tasks can be either explicitly assigned to run on specific cores of the processor or automatically distributed by the real-time operating system.

A.3.1.3. Data Acquisition Card

The data acquisition card is the key component of the unit in our design. It digitalizes the analog signal for the controller to use. Six currents and six voltages are measured to extract the impedance. To avoid phase shift between the signals, all of them need to be sampled simultaneously. Besides these twelve signals, three source voltages without filtering are also sampled separately for the system phase tracking purpose. Another channel is assigned to sample the synchronization signal from PIU. Thus a total of sixteen channels are required. AD conversion resolution is another important parameter of the card. A higher resolution helps to improve the measurement accuracy. But due to the noise control capability in the custom built signal conditioning board, 16 bits is the upper limit. Only oversampling can be applied to increase the equivalent resolution. Thus a very high sampling rate is anticipated.



Figure A-22: Data acquisition card – PXIe-6368

The NI PXIe-6368 card is chosen based all the requirements above. It can sample 16 differential analog inputs simultaneously at 2 MS/s. All the analog inputs have 16 bits resolution with 3.066 mV accuracy when the maximum input range $\pm 10V$ is selected. Besides all the analog

inputs, there are 48 digital I/O lines and 4 analog outputs provided. The digital IOs are used for auxiliary control in this project. The analog outputs are not used except for debugging purposes. Figure A-22 shows the PXIe-6368 card.

A.3.2. Software Design

The main task of the data acquisition unit is to digitalize the analog signal from the sensors and send them to the measurement control unit for further usage. Beside this, the control of digital input and output channels and the digital to analog output are also implemented by this unit. Other than the signal input and output control, the unit also conducts some real time control and signal processing task. All the data and control commands are sent and received through the TCP/IP protocol over the Ethernet connection.

Figure A-23 shows a block diagram of the software functions. To maximize the data through-output, the software is designed to run in multi threads. The threads are distributed between four physical CPU cores that the PXI computer provides. A thread is shown in the diagram as a blue box. A black box in the diagram represents a certain software function. Each of them is a group of code implementing certain functions while providing an interface for other parts of the code to access the function. The thick lines in the figure are the data flows including analog and digital input and output information. The thin lines in the figure are the control commands indicating how each of the function block should behave. The arrows on the lines describe the information directions. The detail of each function block is discussed in the following sections.

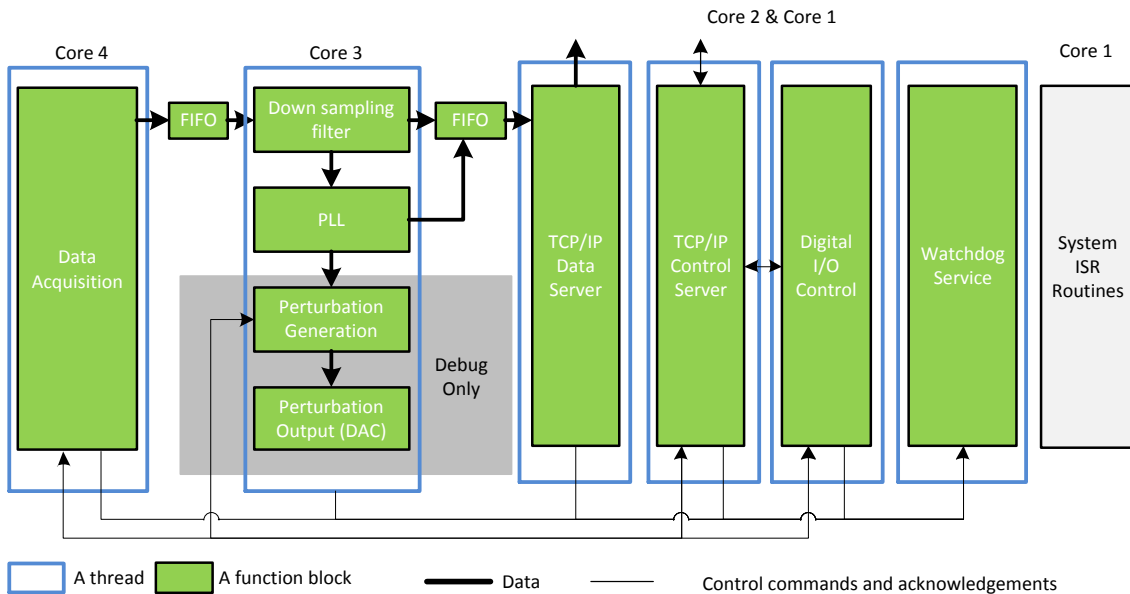


Figure A-23: Software function block diagram of the data acquisition unit

A.3.2.1. Data FIFO

Since the program is designed in a multi-threads way, the data transfer between different threads need to be carefully processed. If more than one thread tries to access the data at the same time, the data may be corrupted. FIFO represents first in first out. It is a common data structure to pass data from one thread to another. The data are put into the FIFO by one thread. Other threads can read from FIFO later at their own convenient time. While reading data, the data put into the FIFO first come out first.

To improve the efficiency, a custom FIFO is designed. The FIFO is designed using a circular buffer. The circular buffer is a chain of the data buffer as shown in Figure A-24. It contains two pointers which point to the previous block and the next block. A groups of buffers are chained using these two pointers in to a loop as shown in Figure A-25. From each block, the previous and the next blocks in the chain can be found using the pointers.

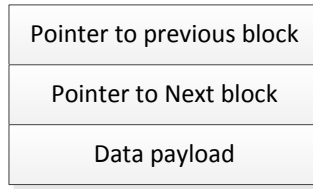


Figure A-24: FIFO data block

A reading pointer and a writing pointer are kept for the whole loop buffer. When there are data available from the writer thread, it puts the data according to the write pointer. Then the write pointer is moved to the next data block. When the pointer is moving, the FIFO is locked so that only this thread can access the pointer positions. It checks to see if the write pointer has passed the read pointer. If the write pointer passes by, it means that some data are overwritten before they are read. A counter for monitoring overflow is increased at this condition. Then the access of the FIFO is released to all the threads. Reading data uses similar procedure.

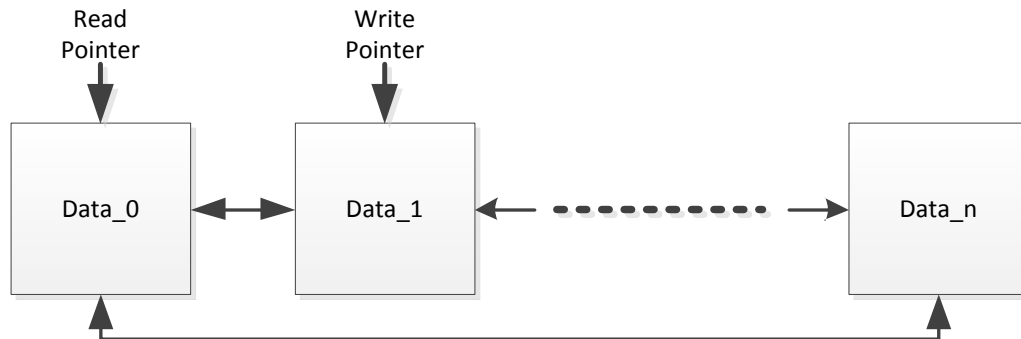


Figure A-25: FIFO circular buffers

The efficiency is improved by allowing reading and writing data of the FIFO to happen at the same time. Only the pointer modification is limited to the operation by a single thread.

A.3.2.2. **Data Acquisition**

Data acquisition is executed by the DAQ card. National Instrument provides the drivers for all of its hardware products. The control of the card is simplified by invoking the drivers. Even more, it provides the DAQ-mx framework to further simplify the data acquisition tasks.

Compared to the old frameworks of National Instrument, the DAQ-mx has the capability of being used by multiple threads which is necessary for the design. Therefore, the DAQ-mx is used all through the interfacing with the DAQ card.

The data acquisition control includes: setting the analog to digital conversion channel, sampling frequency and reading the sampled data into memory. All of these tasks are fulfilled by calling NI DAQ-mx API functions.

Although the DAQ-mx framework provides excellent functions, its efficiency is not very high due to its flexible nature. Thus all the functions are put on a dedicated CPU core, so that they are not disturbed by other threads. The data acquisition takes more than seventy percent of the CPU time by itself. Besides the CPU time on the core assigned to the thread, the driver also needs some extra time on the first core of CPU which is hard-coded in the operating system. The time is spent on interrupt service routines. Running at 20 kHz interrupt frequency takes about seven percent of the CPU time on the first core.

As part of the reason for the low efficiency, the DAQ-mx not only moves the sampled data from the DAQ card buffer into the computer memory, it also scales and offsets the data, even if it is not required by the user. So the scaling and offsetting of the signal is set to be with in this thread to save the CPU time for other threads.

To avoid moving the same data several times, only pointers of data buffers are passed between different functions. The pointer to which the DAQ-mx writes the data is obtained from the FIFO between the data acquisition thread and signal processing thread. The data is put into the FIFO directly by the driver DMA (direct memory access) call without making a copy in the computer memory.

A.3.2.3. Signal Processing

The raw data from the DAQ card is first processed in the unit itself before being sent out.

For the analog to digital conversion runs at 2 Msps, the raw data rate is 768 Mbps. It requires a lot bandwidth to send the raw data out. The highest frequency of interest is about 1 kHz. A

sample rate of 2 kHz is enough to represent such signal. Over-sampling technique is used to increase the resolution of the analog-to-digital conversion. The sampling rate is set to 2 Msps. The technique samples the analog signals at a frequency significantly higher than twice the bandwidth of the signal being sampled. The sampled data are then averaged to obtain a lower sampling rate data flow. The background noise is reduced during the averaging. This averaging procedure can be conducted in the same unit to reduce the data to be transferred. The down-sampling filter is the first part of the signal processing task. It reads the raw data from FIFO and then calculates the average of every one hundred points. The output is a data flow of 20 kHz sampling frequency. The required data rate is reduced to 7.68 Mbps which is easily met by the Ethernet connection.

Another task that is suitable for real time processing is the signal phase identification. The phase of the system voltage is used for the *abc* to *dq* coordinates transformation. It must track the real phase very well, otherwise, the spectrum of the signals in *dq* frame will be changed. Since the real system may have frequency change during measurement, it is better to identify the phase information in real time instead of obtaining them using DFT during the post processing. The PLL is used for this purpose. The technique is also used in the control of the perturbation injection unit and described in detail in Chapter 3. Besides the voltage phase, the system frequency is also logged. So the harmonics of the system frequency can be skipped later in the measurement. The down-sampled data together with the phase and frequency information obtained by PLL are passed to the output FIFO of the module. They are sent out later by the TCP/IP servers.

A.3.2.4. TCP/IP Server

The TCP/IP server is in charge of the communication to the measurement control unit. It receives control commands, sends out acknowledgements and the acquired data. In the software, there are two separate server threads. One is dedicated to sending the acquired data. The priority of this thread is set to above normal to ensure its execution time, so no data is lost because the

buffer ran out between the sending intervals. While its response time is guaranteed to be within a few tens of milli-seconds, the response time of the control server could be a few seconds.

A.3.2.4.1. Control Server

The control server is a thread controlling everything in the unit according to the command received. It listens on TCP port 2011. To simplify the design, only one client is allowed at a time. All other attempts to connect are dropped. For this application, the Ethernet connection is used as only a single series connection. One and only one user can operate the equipment at a time. Thus the single client restriction does not sacrifice any usability.

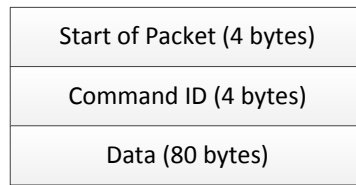


Figure A-26: Control command packet structure

The commands are received as data packets with the structure shown in Figure A-26. First, a hexogen number 0x5555AAAA indicates the start of the packet. Then a thirty-two bits integral number describes the content of the command. Finally, eighty bytes of space is reserved for the command parameters. The use of a data area is optional, but the structure is defined to be fixed length. So when the data area is not used, it still contains bit stream with no meaning.

After the successful execution of the command, the original command packet is sent back to the controller to acknowledge the command. Otherwise, an error is generated and an error report packet is sent to the host explaining the reason of the error.

A.3.2.4.2. Data Server

The data server is a separate thread to that sends the acquired data out. It listens on TCP port 2012. To ensure the data through-output, the task is implemented as simple as possible. Like the control server, only one client is allowed to simplify the design.

The thread reads data from the input FIFO where signal processing thread writes the data. If there is no client connected, the data are discarded. Otherwise, the data are sent out using the packet structure shown in Figure A-27.

Start of Packet (4 bytes)	
Sequence ID (4 bytes)	
Data (96 bytes)	Samples data (9 double numbers, 72 bytes)
	Phase (1 double number, 8 bytes)
	Angular speed (1 double number, 8 bytes)
	Sync signal (1 double number, 8 bytes)

Figure A-27: Data server packet structure

The packet has a fixed length. It starts with 4 bytes of data indicating the start of the packet and the packet type. A sequential ID is added before the real data. The start of the packet is hexogen number 0xAAAA5555. The sequential ID is a 32 bit integral number. It starts from zero for the first packet sent and is increased by one for each additional packet sent. Although TCP/IP protocol provides error detection and a data resending mechanism to ensure the data arrives to the target reliably, the data may still get lost when the program runs out of buffer and fails to read the data out from TCP/IP stack buffer. Thus this ID is provided to the program to detect the loss of data. After the fine tuning of the whole set of program, the data loss can be avoided in several hours of operation if a dedicated Gigabit Ethernet switch is used to connect the impedance analyzer rack to the host control computer. Sharing the connection with other computers may slow down the connection and cause data loss.

The real data payload is an array of twelve double precision floating point numbers, each of the number takes eight bytes of space. The first nine numbers are the sampled data. For shunt injection, they are three system voltages, three source side currents and three load side currents. For series injection, they are three system voltages, three source side voltages and three load side voltages. Then the phase and frequency information from PLL are added. They take eight bytes of space. At last, the sampled synchronization signal from the perturbation injection unit is added. It is less than one if the perturbation is being injected, or it stays at beyond five.

A.3.2.5. Digital I/O Control

In addition to the analog signal conversion and processing tasks, the unit also takes care of controlling and monitoring some digital signals. The function is implemented in the digital I/O control module.

The control of the output state is as simple as sampling the analog signal. It can be done by just calling the DAQ-mx API functions. The key task of this module is to monitor the digital input states.

The targeted output states are kept in an array. A thread is created to check the feedbacks from the relays controlled by the output channels. The feedbacks states are read every hundred milli-seconds. If the feedback is detected to be different from the target state, an error is reported to stop the unit operation. If any target state is required to be changed, the output state is first set according to the command, then the difference between the target and feedback of the channel is ignored for a small amount of time to allow the relay to act.

A.3.2.6. Watchdog Service

The watchdog service provides the interface for the software to access the hardware watchdog. A watchdog is a computer hardware or software timer that triggers a system reset or other corrective action if the main program, due to some fault condition, such as a hang, neglects to regularly service the watchdog. The intention is to bring the system back from the unresponsive state into normal operation.

The PXI computer has only one watchdog timer. It can reset the computer and put all of its output to a given state. But there are several different threads to be monitored. No matter which thread goes into fault condition, the watchdog should be triggered. Therefore, the watchdog should not be directly serviced by all the threads, which makes the watchdog only be triggered when all the threads stop servicing the watchdog.

An intermediate layer is provided by this software module. The module starts a separate thread to service the watchdog timer. The flow chart of the thread is shown in Figure A-28.

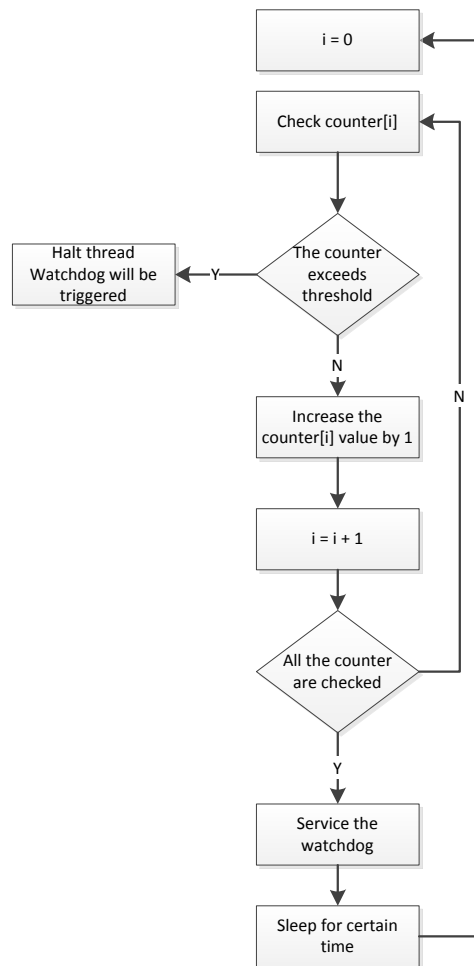


Figure A-28: Flow chart of the watchdog service thread

The software watchdog module keeps a group of counters, one for each thread to be monitored. It checks and increases all the counter at a certain time interval. If any of the counters exceeds a given threshold, the hardware watchdog will be triggered. Otherwise it services the watchdog to prevent it from triggering. If the thread itself fails, the hardware watchdog will also be triggered because of lack of servicing.

In all the threads to be monitored, the counters assigned to the thread are cleared to zero to avoid being increased beyond the threshold. The simultaneous operation of the counter is blocked by a mutex. So the increasing and the clearing operations are not affected by each other and are guaranteed to have the right value.

A.4. Software on Host Computer

There are several function units executing on the host computer which are controlled by the operator. They are the human machine interface (HMI), measurement control unit, data collecting and logging unit and data processing unit. Since these functions intensively interact with each other, they are discussed together here within this chapter.

Figure A-29 gives a summary of the software architecture on the host computer. According to the function, the software is divided into three programs: measurement control, result inspector and the index rebuilder.

The measurement control program is the kernel of the program set. The program includes all the function units for measurement control in the host computer. The user interface talks to the measurement control unit then the unit controls all the other units to conduct the measurement.

The result inspector is used to check the measurement result, which will be displayed automatically after the measurement. Although it is designed to be a standalone program, the user can also execute it without involving the measurement control program.

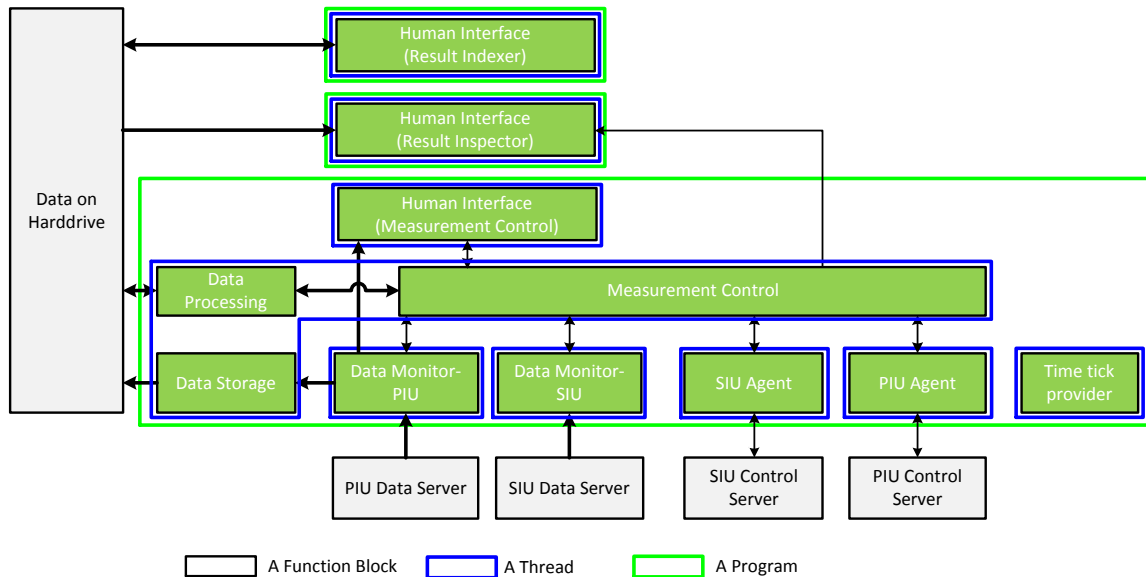


Figure A-29: Software architecture on host computer

The design of the Result Indexer and Result Inspector just follow a normal single thread windows program design procedure. Thus no design detail is discussed except accessing the mat format file which is introduced together with the data processing module. In this chapter, the interface and the function of all three programs are briefly introduced. Then the design of measurement control program is discussed in detail. The data post processing is described after that.

To speed up loading result summary and searching within the results, an index is used to save this information. A new record is added to the index after each measurement. The record contains measurement information and a pointer to the real files on the disk. But the management of the results is designed to be done via regular file explorer. When a result is moved, renamed or deleted, the index file is not updated. An error may occur or an existing result cannot be found in the result inspector if the index file is out of data. This simple program provides the function for updating the index file.

A.4.1. Introduction of HMI

For the user to interface with the system, a HMI has to be provided. The HMI can be implemented in two forms: the graphical user interface (GUI) and the command line interface (CLI). Both of these forms are used for this system. The GUI is usually easier for the operator to learn and use. It also displays the system states more vividly. Therefore GUI is designed for measurement control and viewing the results. The CLI is only used for a the simple function of updating the index file, which is only used occasionally. Figure A-30 shows an example of the GUI, which is a screen capture of the measurement control program.

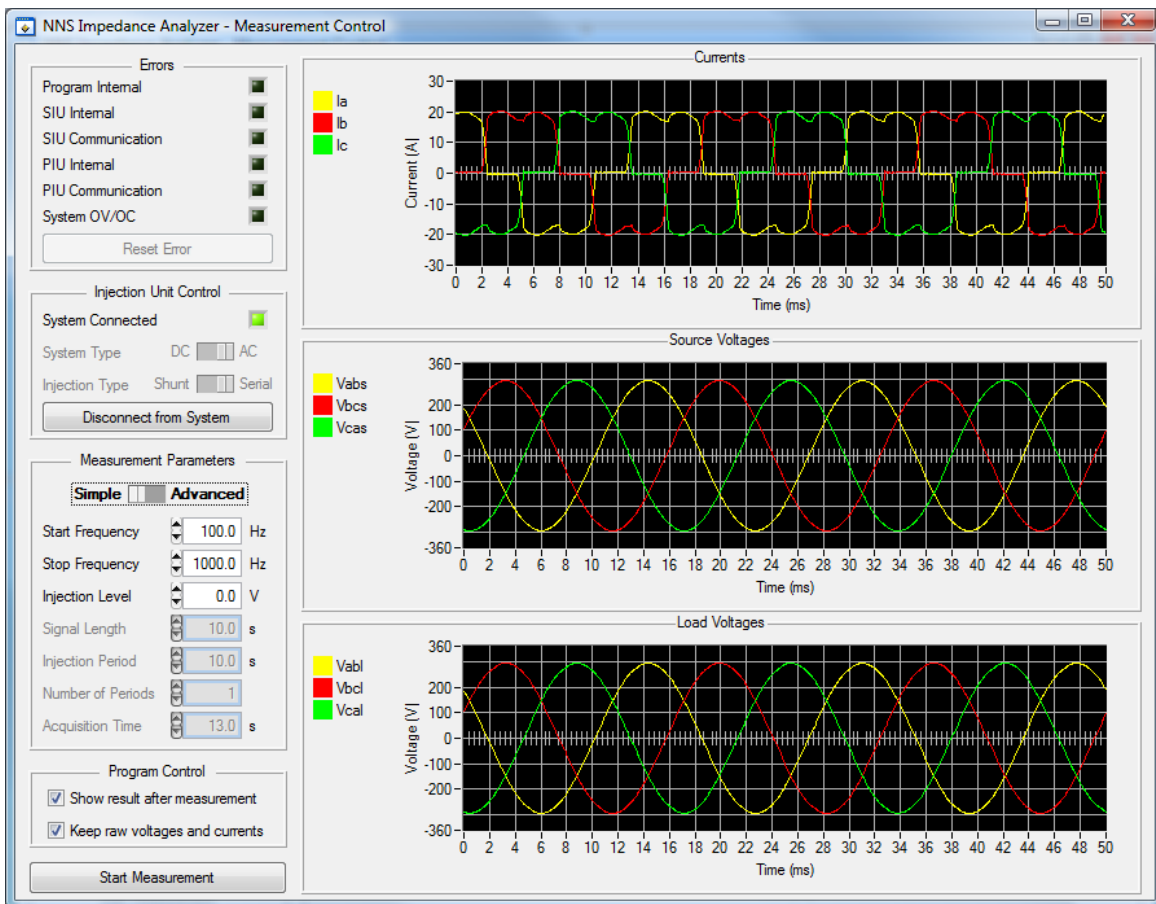


Figure A-30: Interface of the measurement control program

A.4.2. Software Design of Measurement Control

The measurement control is the key part of the software. To avoid any unnecessary block of the code execution and to improve the user interface response speed, the program is designed using the multi-thread technique. Each task that requires a fast response is put into a separate thread. As shown in Figure A-29, most of the tasks have their dedicated threads. A few tasks that always execute in order are combined into one thread. The implementation of the tasks are discussed below in this section. But before going into details of any task, some fundamental services need to first be explained.

A.4.2.1. Control Message Distribution Service

In a multi-thread environment, there must be a way for the threads to communicate with each other. The control message distribution service is designed for this purpose.

The service is designed based on message queues. The service is organized as a group of functions to read, write and manage the message queues. The actual message queues are maintained by the controlling threads. A message queue is a thread safe FIFO. The FIFO is only accessed by one thread at a time. A message is a data packet. The structure of it is shown in Figure A-31.

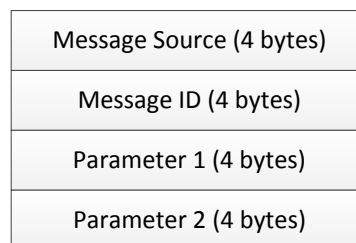


Figure A-31: Control message structure

The first part of the packet is the source of the message. After this comes the message ID, which indicates how a thread should react to the message. Two parameters can be sent together

within the message which are four bytes each. If more information needs to be passed, pointers to the real information can be passed.

Each of the controlling threads keeps its own message queue. The message is checked by a dead loop. The loop keeps running until the thread is terminated. If any new message is found in the queue, the loop calls the related function to complete the required action. Then the message is removed from the queue.

When a thread requires some action from another thread, it posts a message into the queue of the required thread. It can continue its work unit a reply message is found in its own message queue. Then it can determine the next step depending on the reply message.

A.4.2.2. *Time Tick Provider*

Time tick is another service that may be used by any of the tasks. Instead of being a group of functions, it runs in its own thread. The key component of the thread is an asynchronous timer. It wakes up every one tenth of a second and calls some functions. The functions are not part of the services. They are registered by the other tasks. If any task needs to invoke a certain function in a certain time interval, it can register the function with the time tick provider. The registered functions are organized as a chain. The functions will be called by the timer thread one by one when the timer is triggered. If the function has to be executed from the caller thread, the registered function could just simply put a message into the message queue of the caller thread.

A.4.2.3. *Data Collecting and Logging*

Data collecting is the most time sensitive task on the host computer. The embedded controller usually does not have a very large memory integrated. The sampled data can only be kept for a very short period of time. Then the new data will come out. It can either overwrite the old data or be dropped. Either way it causes the information loss. Thus the old sampled data has to be collected before the new data are generated. In the designed system, the period is a few milliseconds.

To guarantee no data loss, dedicated threads are assigned. There are two units sampling data at real time. The perturbation injection unit samples the perturbation reference. The data conversion unit samples all the voltages and currents. Two separate threads are allocated for these two data sources. These two threads are set to have a priority above normal. So they are not interrupted by any other threads and force other threads to pause execution when they need the CPU time. Thanks to the multi-core computers that we have now, these important threads can be really executed in parallel without interfering with each other.

To save the data collecting threads from maintaining their message queue, another thread is created to handle this task. The task runs the dead loop mentioned in the previous section and processes the messages. It communicates with the data collecting threads through a few shared variables which are simple and low overhead.

Part of the collected data are passed onto the GUI and displayed to the user. As shown in Figure A-30, the system voltage and current can be monitored directly on the GUI without using other equipment

The data collecting threads also log data into the given memory area when it is requested. The request is processed by the controlling thread using shared variables. The data logging in the data collecting thread is limited to put data into assigned memory. The final writing of the data onto the disk is completed in another thread – the measurement control thread which is introduced later. This is because the disk access is a time consuming task, it may slow down the data collecting thread considerably. Actually, the disk access is more efficient when working in burst mode. A batch of the data should be accumulated then put onto the disk at once. This is another reason to put the writing of data on hold until all the data are collected.

A.4.2.4. Agents of Perturbation Injection Unit and Data Acquisition Unit

There are two threads designed as agents of the perturbation injection unit and the data acquisition unit. These agent threads connect to the control servers in the units. The commands and responses are forwarded between the servers and the measurement control thread. There are

several reasons to create such a broker thread instead of letting the measurement control thread handle the communications:

- A unified interface can be provided to the measurement control unit. The protocol of the two units are a little bit different. The agent threads handle the protocol process and communicate with the measurement control thread using a message distribution service.
- The communication link state can be monitored by the agents. The agents keep sending a handshake packet. The link is considered to be broken if there is no response to the handshake packet in a certain time. An error will be generated and reported to the measurement control thread. The control thread can always consider the communication working.
- The server state is also monitored by the agent. If any command takes too long to execute or any error occurs during the execution, the agent tries to shut the unit safely and informs the control thread to stop safely other actions.

By offloading the monitoring work to the agent threads, the control thread can work more efficiently. It can continue other work after a command is issued to the agents.

A.4.2.5. Measurement Procedures Control

The measurement procedure control is conducted by the measurement control unit (MCU) in Figure A-29. It is designed to run as a simple state machine. Each measurement step has a corresponding state. The state is changed after a step is finished. To improve the reliability by reducing the conflicts between units, a single action is taken at a time. Besides the ongoing action, only some internal house-keeping work is conducted by the measurement control thread.

There are three main steps for the user to conduct a measurement: start the program, setup parameters, and start the measurement. The program only works during the two steps of the startup and the measurement. The measurement flow is detailed below:

A.4.2.5.1. Program Startup

The actions during startup are shown in the flow chart in Figure A-32. It first initializes the software frameworks on the host computer. Then the data conversion unit is connected to be able to operate the relays. The power to PIU is applied from the system to be measured by closing the relay for shunt injection. After the communication connection to PIU is created, the startup procedure is complete.

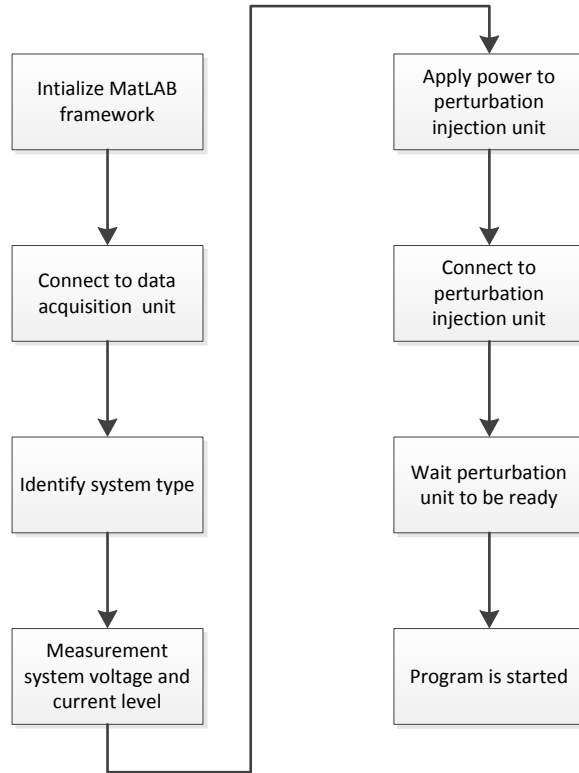


Figure A-32: Program flow chart during startup

A.4.2.5.2. Conducting Measurement

The measurement mode is shown in Figure A-33. Two perturbations are injected into the system in sequence. The response data are written to disk. The impedance calculation routine loads the data from disk and then calculates the impedance based on them. The raw data is then removed if the user does not select to keep them.

The detail steps of a perturbation are given in Figure A-34. Before anything else starts, the parameters set by user are collected and sent to the perturbation injection unit. Then the dc bus voltage is charged from the diode bridge output voltage to the working level. The connection to the system is switched at this point if a series injection is required. Then the data logging is started to ensure the capturing of the start part of the injection. The real injection is begun after the start of the data logging is confirmed.

The program waits until the required length data are logged into the buffer. The data logging time is enforced to be a few seconds longer than the injection time to guarantee that all the responses during the injection are captured. Then the perturbation injection unit is commanded to stop explicitly to initialize the house keeping work after injection if they have not been done yet. The system is then switched back to shunt connection to maintain the dc bus voltage using the diode bridge if a series injection is conducted.

The whole perturbation ends here. The injection unit is connected to the system in shunt. The semiconductor devices stop switching. Only the diode bridge still works to charge the dc bus capacitor when the voltage falls too low.

From the analysis in Chapter 5, if the chirp signal swept a large frequency range, the power distributed within a certain frequency range drops. Thus it is desirable to use a few short chirp signals for measurement, each covering a small range of frequency, instead of using a single chirp signal covering the whole range. The program is designed to be able to conduct the frequency split, measurement, and combine the results automatically.

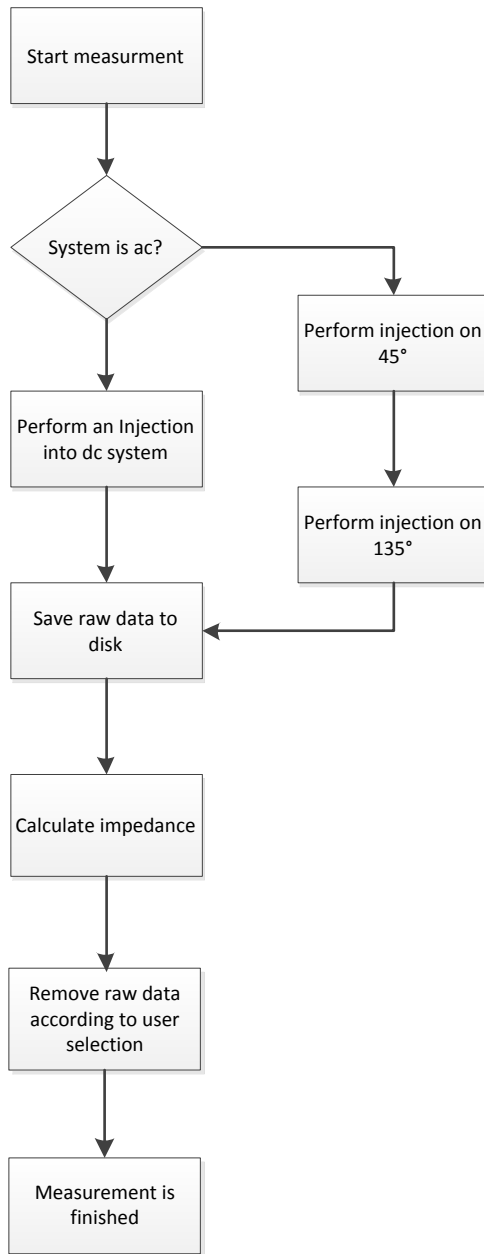


Figure A-33: Program flow chart during advance mode measurement

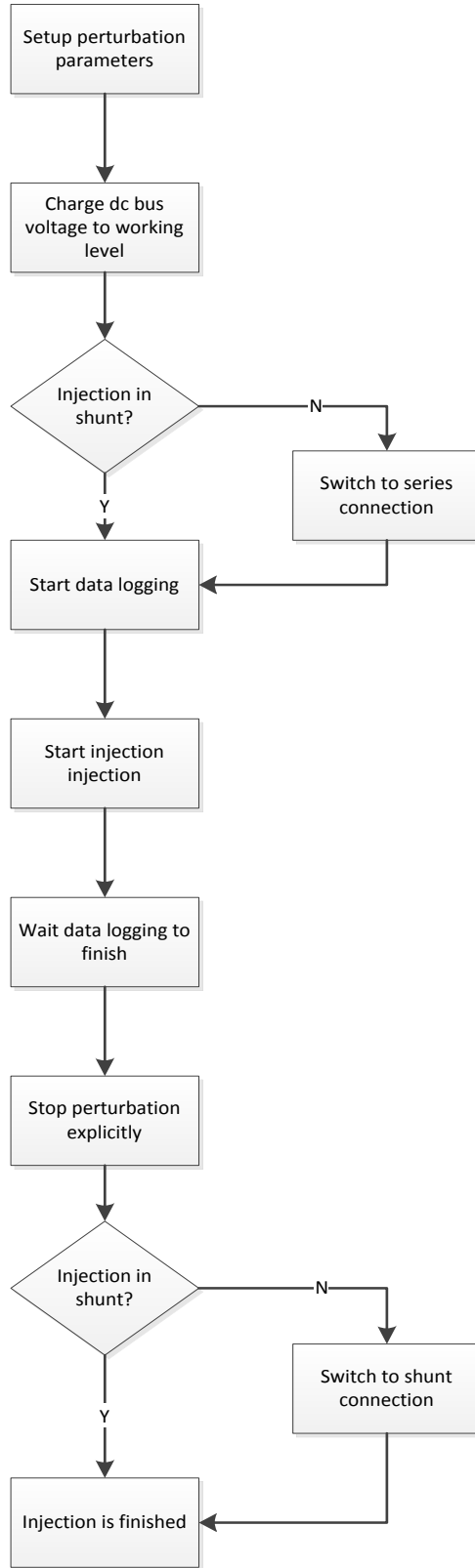


Figure A-34: Program flow chart during perturbation injection

A.4.3. Software Design of Data Post Processing

After the data are collected by the data logging unit, a digital signal processing algorithm needs to be applied to extract the impedance information. Instead of the C programming language used for all other parts of the software development, MatLAB functions are used for data processing. Although C is faster upon execution speed, the data collected are post processed here. Thus there is no constrain on code execution time. Except for the slower code execution, MatLAB provides an excellent platform and library for data processing, which saves the development time. The data format for storage is also selected to be the MatLAB standard ‘mat’ format. It can be easily imported into the MatLAB for further processing.

Since the data processing algorithm was previously described in Chapter 5, only some of the implementation details are discussed here.

A.4.3.1. Data Preparation

When the impedance extraction algorithm is discussed in Chapter 5, all the data are considered to be sampled synchronously. But in the real system, the data are sampled by two separate physical units without tight synchronization. All the control commands are also executed asynchronously. Besides the synchronization problem, the data are also collected in different formats. Therefore, a proper preparation is required before applying the algorithm.

There are two units sampling the data for impedance extraction. One is the data acquisition unit. It measures all the voltage and current responses to the perturbation and identifies the system phase angle in real time. Together with all these signals, a synchronization signal from the perturbation injection unit is sampled simultaneously. Due to the asynchronous execution of all the control commands, the data logging cannot be started at the exact time when the injection starts or ended at the time when the injection stops. Thus some extra sampling time is added before the injection starts and after the injection ends to ensure the capture of the whole response. The other unit that samples the data is the perturbation injection unit. It samples the perturbation reference which exists nowhere else in the system. The reference signal is used to reduce the

non-correlated noise. It is sampled only when the perturbation is being generated. The data from both these units are sampled at the same frequency of 20 kHz.

When the data from both units are loaded, all the voltage and current responses are transferred into *dq* coordinates using the phase angle provided together with them. Then the dc component which is usually a large value but out of the interested frequency range is removed. The reference signal then is aligned with all the other signals using the synchronization signal. The synchronization signal is a digital signal generated by the perturbation injection unit then sampled by the data acquisition unit as an analog signal. The value of the sampled signal is below one when the injection is active and near five before and after the injection. The edge during the transition between the two voltages is smoothed by the components in the transmission path. Thus the exact time is not well marked, but the error is within a few sampling points and is acceptable. The middle point of the reference signal is aligned to the middle point between the falling and rising edges of the synchronization signal. The next step is determining the perturbation duration by the length of the reference signal. Due to the precision of the fixed point number used in the perturbation injection unit controller, the real perturbation time may be a little different from the set value. Finally, all the signals are cut to length of the perturbation duration.

A.4.3.2. *Interface between MatLAB and C*

Interfacing between the MatLAB code and the C code includes two tasks. One is calling the MatLAB function to process data. The other is to access the data from the .mat files generated by MatLAB. MathWorks provides libraries and API to work with C program. The detail of the two tasks are described below.

A.4.3.2.1. *Calling MatLAB function from C code*

This task is done via MatLAB Compiler. It encrypts the script so that the code is not disclosed to the final user. Then the script is executed by a set of libraries called MatLAB compiler runtime (MCR). It is a subset of MatLAB runtime and can be distributed freely. A

series of functions is provided to form MatLAB variables which is later passed to the scripts. By using MatLAB variables as the parameters passed through the interfaces, the interface is made very flexible – nothing needs to be changed except the part forming the MatLAB variable when the interface variable needs to be changed, especially the structured variables are used. They wrap all the information under the same variable as different fields while keeping the top level variables number and name unchanged.

The MatLAB script is designed to work as a dynamically linked library (DLL). The MCR generates a DLL file which encapsulates all the MatLAB scripts and provides several interfaces for the C file to invoke the functions. A C file is also generated to further simplify the procedure. It aggregates the initialization and the cleanup functions.

A.4.3.2.2. Access MAT format files from C code

The mat file is in a private format of MathWorks. There is no document about the internal structure. However, MathWorks provides a set of libraries to access the file content. These libraries are already included in the MCR. Thus, accessing the mat file becomes a simple task with the help of these libraries.

To write to a mat file, a MatLAB variable needs to be created first. Since the variable contains not only raw data but also some other information used by MatLAB, the pointer to the memory for the raw data needs to be obtained first by calling a library function corresponding to the data type. Then the data can be directly fed into the allocated memory region. After that, the persistence of the variable is as simple as a calling of *matPutVariable* function. To read data from a mat file is just the reversed procedure. First the function *matGetVariable* is called. It returns a MatLAB variable. Then the pointer to real data needs to be obtained by the same function used when writing data. After the pointer is acquired, all the reading is the same as in normal C language.

A.5. System Assembly

All the above mentioned units are assembled in a cabinet for easy handling and use. Figure A-35 shows the finished equipment. All the internal components can be seen in these two pictures since transparent covers are used.

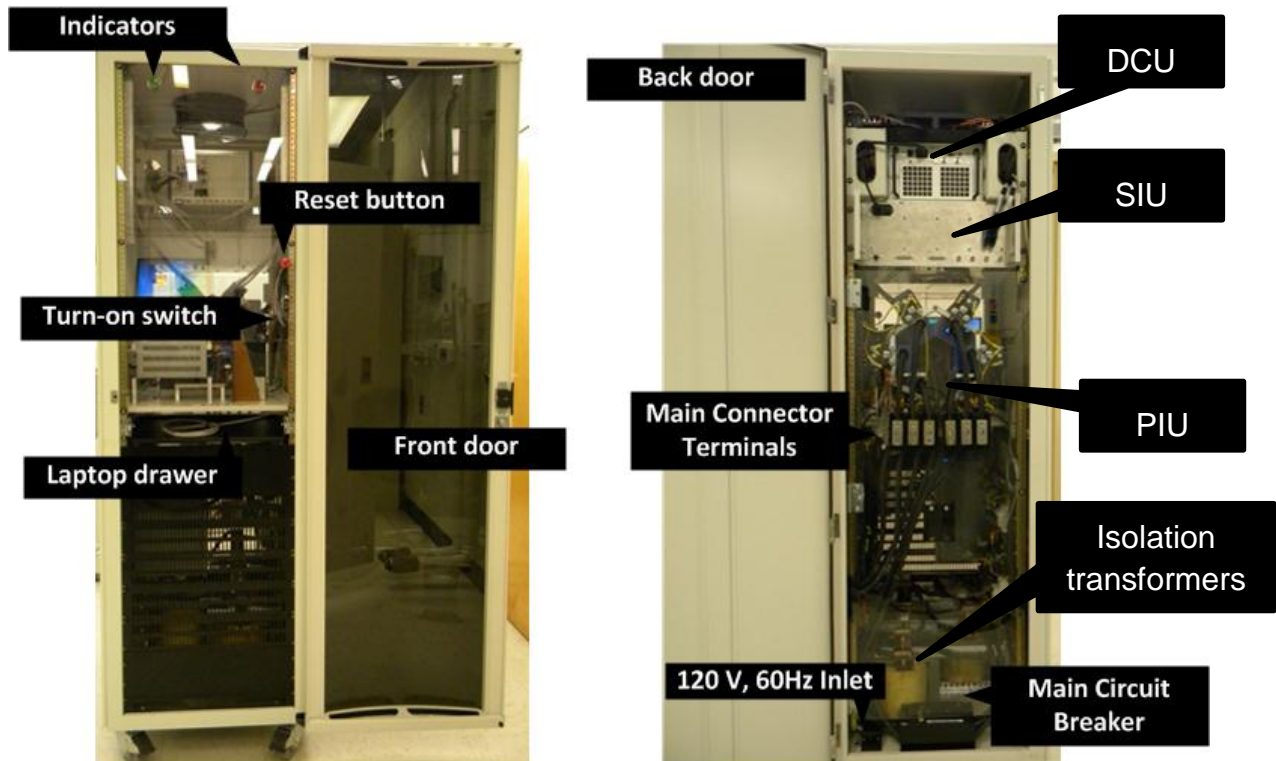


Figure A-35: The Impedance Analyzer's front and back views

A.6. Additional Reference

The appendix covers the main topics on the equipment implementation. More detailed documents can be found in the following internal reports:

1. Final report of Boeing Project: System Stability and Analysis—Phase III, Design and Construction of AC Impedance Analyzer, 2009.09

2. Final report of Newport News Shipbuilding project: Study and Development of an AC/DC Impedance Tester for Medium Voltage High Power Systems, Phase I: Feasibility Study & Demonstration, 2012.04

The original code and CAD files can be found as the electronic appendixes of the reports, which are on the delivery CDs.